



DEPARTAMENTO DE FÍSICA

Universidade de Coimbra

Dissertação de Mestrado em Engenharia Biomédica

ASSESSMENT OF HEMODYNAMIC PARAMETERS

NEW APPROACH TO THE USE OF PIEZOELECTRIC SENSORS

Elisabeth Sofia Borges Ferreira

Setembro de 2008

SUPERVISORS

Prof. Dr. Carlos M. Correia

Prof. Dr. Luís Requicha Ferreira



Centro de Electrónica e Instrumentação
Departamento de Física
FCTUC

IN COLLABORATION with

João Maldonado, MD



Instituto Investigação & Formação
Cardiovascular, S.A.

Eng.º José Basílio



Intelligent Sensing Anywhere

This report is made in fulfillment of the requirements of Project, a discipline of the 5th year of the Biomedical Engineering graduation.

ABSTRACT

Over the last years, several studies pointed out arterial stiffness as a major cause of cardiovascular risk. This hemodynamic parameter has been widely investigated and is normally associated with high blood pressure and aging. Measuring pulse wave velocity, *PWV*, is considered the standard method to assess the arterial stiffness. Nowadays, although this is well accepted by the medical/scientific community, the equipments available in the market are very expensive and difficult to operate, even by skilled personnel. These are the main reasons why these devices are still hard to find not only in medical offices but also in clinical/hospital unities. This context has been the main motivation to address the problem of finding new methods for the assessment of arterial stiffness and other associated hemodynamic parameters, as is the case of the augmentation index, *AIx*, ankle-arm index, *AAI*, and others.

This work was centred on the development of a new approach to the use of piezoelectric, *PZ*, sensors with related test and signal conditioning circuits as well as on the development of a software analysis tool. Tests with humans are also included, just to demonstrate that results are consistent and reproducible.

Different data acquisition and signal processing issues have also rose along the work and will be described in detail in due time. For the first, the NI USB 6210© has proved to be an adequate choice, while for the latter, the use of MatLab® provided the right environment as well as the short development cycles that a one year project requires.

Keywords

CARDIOVASCULAR DISEASES, ARTERIAL STIFFNESS, PULSE WAVE VELOCITY, AUGMENTATION INDEX, HEART RATE VARIABILITY, ARTERIAL PRESSURES, PIEZOELECTRIC SENSOR.

RESUMO

Nos últimos anos, diversos estudos realizados apontam a rigidez arterial como a maior causa de risco cardiovascular. Este parâmetro hemodinâmico tem sido amplamente investigado, aparecendo normalmente associado ao aumento da pressão arterial e ao envelhecimento. A medição da velocidade da onda de pulso, VOP, é considerada o método padrão para avaliar a rigidez arterial. Actualmente, apesar de este ser bem aceite pela comunidade médica/científica, os equipamentos que se encontram disponíveis no mercado são bastante onerosos e difíceis de operar, mesmo por profissionais da área. Pelas razões apontadas, é difícil encontrar estes aparelhos em consultórios médicos e em unidades clínicas/hospitalares. Foi esta a problemática que motivou o estudo de novos métodos para a determinação da rigidez arterial, bem como de outros parâmetros hemodinâmicos associados a esta, como é o caso do índice de aumentoção, Alx , índice braço-pé, IBP, entre outros.

Este trabalho centrou-se no desenvolvimento de novas perspectivas de utilização para sensores piezoeléctricos, com circuitos de acondicionamento de sinal e testes relacionados, assim como no desenvolvimento de uma ferramenta informática de análise. Foram também realizados testes em humanos, apenas com o objectivo de demonstrar que os resultados são consistentes e reprodutíveis.

Questões relacionadas com a aquisição e processamento de sinal, que futuramente serão descritas, foram igualmente levantadas e analisadas durante o trabalho. Em adiantamento, pode-se afirmar que, em primeiro, o módulo NI USB 6210© demonstrou ser uma boa opção e, por último, que o uso do programa MatLab® providenciou um ambiente de análise ideal, assim como as curtas rotinas desenvolvidas e requeridas para um ano de projecto.

Palavras-chave

DOENÇAS CARDIOVASCULARES, RIGIDEZ ARTERIAL, VELOCIDADE DA ONDA DE PULSO, COEFICIENTE DE AUMENTAÇÃO, VARIABILIDADE DA FREQUÊNCIA CARDÍACA, PRESSÃO ARTERIAL, SENSOR PIEZOELÉCTRICO.

ACKNOWLEDGEMENTS

The Project discipline was undoubtedly the most interesting and useful of my graduation, particularly because it has provided me the great chance to increase my knowledge in this area and to grow as a professional. For that, it is a pleasure to me to express my gratitude to everyone who made this work possible.

Foremost, I would like to thank my supervisors, Prof. Dr. Carlos Correia and Prof. Dr. Luís Requicha, for their support and aid along all this work. It is difficult to overstate my gratefulness to Prof. Dr. Carlos Correia, whose expertise, “powerful mind”, friendship and great capacity to explain things clearly and simply, enticed me to face the problems I found and incentivized me to appreciate the world of research. This work would not have been possible without the technical component supplied by Prof. Dr. Luís Requicha, who was always ready to rapidly and astutely develop the necessary hardware.

I want to show especial gratitude to Eng. Catarina Pereira, who was an external guide to me, giving continuous and accurate advices and sincere help.

I must thank all the members of the *Centro de Electrónica e Instrumentação* for their kindness and availability to give an essential *ingredient* to this work: their hemodynamic signals.

Thanks also to my uncle, Prof. Dr. Amadeu Borges, who was always ready to helping and advising me.

I cannot end without thanking my parents, Maria da Graça Ferreira and Duarte Ferreira, my brother, Abraão Ferreira, my boyfriend, João Oliveira, and my friend and work colleague, Patrícia Coimbra. Everyone was there when I needed; all gave me one of the things I appreciate much: friendship. I need to specifically thank my boyfriend who endured me even if I was really grumpy, bothered or sad.

To my parents, I have no way to reward the huge effort their actually making. To them I dedicate this work.

CONTENTS

Abstract	vi
<i>Resumo</i>	vii
Acknowledgements	ix
List of Figures	xv
List of Tables	xvii
1. INTRODUCTION	1
1.1 Motivation	1
1.2 Purposes	2
1.3 CEI Hemodynamic Research Team	2
1.4 Overview of the Dissertation	3
2. THEORETICAL BACKGROUND	5
2.1 Cardiovascular Physiology Concepts	5
2.1.1 Cardiac Cycle	5
2.1.2 Arterial pulse Wave	6
2.2 Arterial Stiffness and Its Assessment	10
2.2.1 Arterial Stiffness Increase and Cardiovascular Diseases	10
2.2.2 Arterial Stiffness Assessment	11
2.2.2.1 Pulse Wave Velocity	11
2.2.2.2 Augmentation Index	16
2.3 Heart Rate Variability	19
2.3.1 Definition and Physiological Meaning	19
2.3.2 Clinical Significance Meaning	21
2.3.3 Measurement	21
2.3.4 State of the Art	23
2.4 Piezoelectric Sensors	25
2.4.1 General Concepts	25
2.4.2 Physical Quantities Measured with <i>PZs</i>	26
2.4.3 Electrical Properties	26
3. PROCESS METHODOLOGY	29
3.1 Context	29
3.2 Acquisition System	30
3.2.1 Piezoelectric Single Probes	30
3.2.2 Acquisition Unit	32
3.2.3 Respiratory Signal	34
3.3 Experimental Trials	34
3.3.1 Data Acquisition	34

3.3.2 Data Processing	-----	-----	-----	-----	-----	-----	-----	-----	-----	35
3.4 To Retain	-----	-----	-----	-----	-----	-----	-----	-----	-----	36
4. INTEGRATION vs. DECONVOLUTION	-----	-----	-----	-----	-----	-----	-----	-----	-----	37
4.1 Motivation for the Experiment	-----	-----	-----	-----	-----	-----	-----	-----	-----	37
4.2 Deconvolution Method	-----	-----	-----	-----	-----	-----	-----	-----	-----	37
4.2.1 General concepts	-----	-----	-----	-----	-----	-----	-----	-----	-----	37
4.2.2 Experimental settings	-----	-----	-----	-----	-----	-----	-----	-----	-----	38
4.3 Integration Method	-----	-----	-----	-----	-----	-----	-----	-----	-----	40
4.4 Results	-----	-----	-----	-----	-----	-----	-----	-----	-----	41
4.4.1 <i>PZ Probe Impulse Response</i>	-----	-----	-----	-----	-----	-----	-----	-----	-----	41
4.4.2 Arterial Pulse	-----	-----	-----	-----	-----	-----	-----	-----	-----	42
4.5 Discussion	-----	-----	-----	-----	-----	-----	-----	-----	-----	42
5. PIEZOELECTRIC PROBE CALIBRATION	-----	-----	-----	-----	-----	-----	-----	-----	-----	45
5.1 Motivation for the Experiment	-----	-----	-----	-----	-----	-----	-----	-----	-----	45
5.2 Calibration Method	-----	-----	-----	-----	-----	-----	-----	-----	-----	45
5.2.1 Concept	-----	-----	-----	-----	-----	-----	-----	-----	-----	45
5.2.2 Procedures	-----	-----	-----	-----	-----	-----	-----	-----	-----	46
5.3 Carotid Signals	-----	-----	-----	-----	-----	-----	-----	-----	-----	48
5.4 Discussion	-----	-----	-----	-----	-----	-----	-----	-----	-----	51
6. SOFTWARE ANALYSIS TOOL	-----	-----	-----	-----	-----	-----	-----	-----	-----	53
6.1 General Performance	-----	-----	-----	-----	-----	-----	-----	-----	-----	53
6.2 Software Structure	-----	-----	-----	-----	-----	-----	-----	-----	-----	53
6.2.1 Master Routine	-----	-----	-----	-----	-----	-----	-----	-----	-----	53
6.2.2 Single Pulse Analysis	-----	-----	-----	-----	-----	-----	-----	-----	-----	54
6.2.3 Local List Analysis	-----	-----	-----	-----	-----	-----	-----	-----	-----	57
6.2.4 Global Analysis	-----	-----	-----	-----	-----	-----	-----	-----	-----	59
6.3 Software Background for some Software Routines	-----	-----	-----	-----	-----	-----	-----	-----	-----	61
6.3.1 <i>HR</i>	-----	-----	-----	-----	-----	-----	-----	-----	-----	61
6.3.2 <i>Aix</i>	-----	-----	-----	-----	-----	-----	-----	-----	-----	62
6.3.3 <i>PWV</i> from a Single Pulse	-----	-----	-----	-----	-----	-----	-----	-----	-----	62
6.3.4 <i>PWV</i> from Two Pulses	-----	-----	-----	-----	-----	-----	-----	-----	-----	64
6.3.5 <i>HRV</i> and Respiration Signal	-----	-----	-----	-----	-----	-----	-----	-----	-----	64
6.4 Software Short-Term Improvements	-----	-----	-----	-----	-----	-----	-----	-----	-----	64
7. RESULTS	-----	-----	-----	-----	-----	-----	-----	-----	-----	67
7.1 <i>Aix</i>	-----	-----	-----	-----	-----	-----	-----	-----	-----	67
7.2 <i>PWV</i> from a Single Pulse	-----	-----	-----	-----	-----	-----	-----	-----	-----	71
7.3 <i>PWV</i> from Two Pulses	-----	-----	-----	-----	-----	-----	-----	-----	-----	74
7.4 Comparison Results	-----	-----	-----	-----	-----	-----	-----	-----	-----	77
7.5 <i>HRV</i>	-----	-----	-----	-----	-----	-----	-----	-----	-----	78
7.6 <i>HR</i>	-----	-----	-----	-----	-----	-----	-----	-----	-----	81

8. DISCUSSION	-----	-----	-----	-----	-----	-----	-----	-----	-----	-----	83
8.1 Arterial Stiffness Related Parameters	-----	-----	-----	-----	-----	-----	-----	-----	-----	-----	83
8.2 <i>HRV</i> and Respiration Signal	-----	-----	-----	-----	-----	-----	-----	-----	-----	-----	86
8.3 <i>HR</i>	-----	-----	-----	-----	-----	-----	-----	-----	-----	-----	87
9. CONCLUSIONS	-----	-----	-----	-----	-----	-----	-----	-----	-----	-----	89
10. FUTURE WORK	-----	-----	-----	-----	-----	-----	-----	-----	-----	-----	91
10.1 Instrument Optimization	-----	-----	-----	-----	-----	-----	-----	-----	-----	-----	91
10.1.1 Piezoelectric Probes	-----	-----	-----	-----	-----	-----	-----	-----	-----	-----	91
10.1.2 Acquisition Unit	-----	-----	-----	-----	-----	-----	-----	-----	-----	-----	93
10.2 Software Optimization	-----	-----	-----	-----	-----	-----	-----	-----	-----	-----	93
10.3 Clinical Tests	-----	-----	-----	-----	-----	-----	-----	-----	-----	-----	93
References	-----	-----	-----	-----	-----	-----	-----	-----	-----	-----	95

LIST OF FIGURES

Figure 1 Heart physiology	6
Figure 2 Aortic pressure wave shape	7
Figure 3 Changes in the pressure wave shape due to different diseases	8
Figure 4 <i>PWV</i> measurement using the <i>foot-to-foot velocity</i> method	12
Figure 5 <i>PWV</i> values along the arterial tree	13
Figure 6 Complior® system	14
Figure 7 SphygmoCor® system	15
Figure 8 Graphic representation of <i>AIx</i>	16
Figure 9 <i>AIx</i> (%) against age	17
Figure 10 HEM 9000ai® system	18
Figure 11 Colin-Omron VP 2000® system	18
Figure 12 Heart rate variability	19
Figure 13 Heart rate and blood volume	20
Figure 14 <i>HRV</i> frequency domain measurement	23
Figure 15 HRVlive® software	24
Figure 16 HRVlive® hardware	24
Figure 17 Sensor based on the <i>PZ</i> sensor	25
Figure 18 Metal disks with <i>PZ</i> material	26
Figure 19 Schematic symbol and electronic model of a <i>PZ</i> sensor	27
Figure 20 Basic equivalent circuits of a <i>PZ</i> sensor (flat region)	27
Figure 21 High pass filter characteristic of a <i>PZ</i> sensor	28
Figure 22 General measurement system architecture	30
Figure 23 Initial <i>PZ</i> probe	30
Figure 24 Final <i>PZ</i> probe	31
Figure 25 Acquisition unit	32
Figure 26 NI USB-6210©	33
Figure 27 <i>Veroboard</i> circuitry – Charge amplification circuit	33
Figure 28 <i>NTC</i> respiration detection circuit	34
Figure 29 Results consistency	35
Figure 30 Schematic of the deconvolution process	38
Figure 31 Scheme of the experimental assembly for the <i>IR</i> acquisition	39
Figure 32 <i>Veroboard</i> circuitry - Buffer circuit	39
Figure 33 Influence of the integration points	40
Figure 34 <i>PZ</i> probe <i>IR</i>	41
Figure 35 Integration and deconvolution results	43
Figure 36 Input-output relationship of the <i>PZ</i> sensor	46
Figure 37 <i>Impulse response</i> (200V DC)	47
Figure 38 Integrated <i>impulse response</i>	48
Figure 39 Y-axis calibration in terms of displacement	48

Figure 40 Relationship between the maximum displaces and the systolic pressure	-----	----	50
Figure 41 Relationship between the maximum displaces and the pulse pressure	-----	----	50
Figure 42 First pop-up menu with a real carotid signal acquired for about 250s	-----	-----	54
Figure 43 Single pulse analysis pop-up menu and current pulse view	-----	-----	55
Figure 44 Integration and deconvolution windows	-----	-----	56
Figure 45 AIx determination windows	-----	-----	57
Figure 46 Local list analysis pop-up menu and normal average pulse	-----	-----	58
Figure 47 Operation pop-up menu for the local list analysis	-----	-----	58
Figure 48 Global analysis pop-up menu and analysing carotid signal	-----	-----	59
Figure 49 Operation pop-up menu for the global analysis	-----	-----	60
Figure 50 HRV and respiration signals (time domain)	-----	-----	60
Figure 51 HRV and respiration signals (frequency domain)	-----	-----	61
Figure 52 Main branches of the arterial tree	-----	-----	63
Figure 53 Comparison of AIx values obtained using the integration and the deconvolution methods (mean column of tables VIII and XIX)	-----	-----	69
Figure 54 Mean AIx versus average pulse AIx (for the integration method)	-----	-----	69
Figure 55 Mean AIx versus average pulse AIx (for the deconvolution method)	-----	-----	70
Figure 56 Relationship between mean AIx for the integration and deconvolution methods	-----	-----	70
Figure 57 PWV values using the integration and the deconvolution methods	-----	-----	72
Figure 58 Mean PWV (from a single pulse) versus average pulse PWV (from a single pulse), for the integration method	-----	-----	72
Figure 59 Mean PWV (from a single pulse) versus average pulse PWV (from a single pulse), for the deconvolution method	-----	-----	73
Figure 60 Relationship between mean PWV from a single pulse for the integration and deconvolution methods	-----	-----	73
Figure 61 PWV from two pulses. Values for the integration and deconvolution methods	-----	-----	75
Figure 62 Mean PWV (from two pulses) versus average pulse PWV (from two pulses), for the integration method	-----	-----	75
Figure 63 Mean PWV (from two pulses) versus average pulse PWV (from two pulses), for the deconvolution method	-----	-----	76
Figure 64 Relationship between mean PWV from two pulses for the integration and deconvolution methods	-----	-----	76
Figure 65 Relationship between mean AIx , mean PWV from a single pulse and mean PWV from two pulses, for the integration method	-----	-----	77
Figure 66 Relationship between mean AIx , mean PWV from a single pulse and mean PWV from two pulses, for the deconvolution method	-----	-----	77
Figure 67 Relationship between the STD of HRV and respiration	-----	-----	79
Figure 68 Relationship between HRV and respiration at LF	-----	-----	79
Figure 69 Relationship between HRV and respiration at HF	-----	-----	80
Figure 70 Relationship between the HR frequency obtained with the <i>PulScope</i> software and with the happy life® device	-----	-----	82
Figure 71 Schematic of the PZ probe used in the PWV assessment project	-----	-----	92
Figure 72 Schematic of a semi-ring PZ Probe (example)	-----	-----	92

LIST OF TABLES

Table I Team members of the project <i>Hemodynamic Parameters – New Instrumentation and Methodologies</i> and its contributions	2
Table II Clinical conditions associated with increased arterial stiffness	10
Table III <i>PWV</i> values along the arterial tree	13
Table IV Selected time domain measures of <i>HRV</i>	22
Table V Impulse main characteristics	42
Table VI Experiment Settings	47
Table VII Maximum mean displacement, pulse pressure and systolic pressure obtained results	49
Table VIII <i>Aix</i> (%) values obtained by the integration method	68
Table IX <i>Aix</i> (%) values obtained by the deconvolution method	68
Table X <i>PWV</i> ($m.s^{-1}$) values - from a single pulse - obtained by the integration method	71
Table XI <i>PWV</i> ($m.s^{-1}$) values - from a single pulse - obtained by the deconvolution method	71
Table XII <i>PWV</i> ($m.s^{-1}$) values – from two pulses - obtained by the integration method	74
Table XIII <i>PWV</i> ($m.s^{-1}$) values – from two pulses - obtained by the deconvolution method	74
Table XIV <i>HRV</i> time domain analysis – standard deviation (<i>STD</i>)	78
Table XV <i>HRV</i> frequency domain analysis – high (<i>HF</i>) and low (<i>LF</i>) frequency	78
Table XVI <i>HR</i> frequency (bpm) values obtained by the <i>PuScope</i> software and happy life® device	81

CHAPTER 1

INTRODUCTION

1.1 Motivation

Cardiovascular diseases, *CVDs*, are a major cause of death globally. An estimated 17, 5 million people died from *CVDs* in 2005, which represents 30% of all global deaths, and by 2015, almost 20 million people will die from these diseases. *CVDs* are projected to remain the single leading causes of death. ^[39] Age-related changes in cardiac function, circulatory hemodynamics, blood pressure regulation, and lipid metabolism, all contribute significantly to morbidity and mortality in the elderly ^[40].

Although aging and hypertension are related with *CVDs*, in the past few years, several studies have been pointing out arterial stiffness as a major cause of these diseases. In fact, arterial stiffening increases during aging in healthy persons and is accompanied by an elevation in systolic pressure ^[40]. For this reason, the arterial stiffness has been widely investigated. The measurement of the pulse wave velocity, *PWV* – i.e. the velocity at which the pressure wave, generated throughout the cardiac contraction, propagates along the arteries – over the carotid-femoral region, is considered the standard method to assess the arterial stiffness ^[13-15].

Nowadays, although this is well accepted by the medical/scientific community, the equipments available in the market are very expensive and difficult to operate even by skilled personnel. These are the main reasons why these devices are still hard to find not just in medical offices but also in clinical/hospital unities. This context drives one of the motivations behind this work – exploring new methods for the assessment of the arterial stiffness and other hemodynamic parameters, as is the case of ankle-arm index, *AAI*, augmentation index, *AIx*, among others. This last allows the quantification of the relative change of the pressure wave in a specific region due to the *reflected wave* ^[23].

At the same time, efforts to study other hemodynamic parameters that can help to draw an overall evaluation of the general state of the cardiovascular system, as is the case of the heart rate variability, *HRV*.

As happens with *PWV*, the appliances available in the market capable of measuring *AIx*, *HRV*, and others, are also expensive and it offers little doubt that a low-priced and easy to manipulate system, capable of assessing several hemodynamic parameters, seems to have great potential in medical/clinical field.

This work also tries to shed a new light on the utilization of the piezoelectric, *PZ*, sensor. These devices have been playing a minor role in current commercial instruments where they are used just to provide timing information. This work makes a point in demonstrating that, together with the adequate software analysis tool, information carried in the shape of *PZ* sensors, with their excellent signal-to-noise ratio and large bandwidth, can reveal a great deal on a number of important hemodynamic parameters.

1.2 Purposes

The principal aim of the work described here is the study of new possible utilizations for *PZ* sensors in hemodynamic parameters assessment. The development of a software analysis tool (then named by *PulScope*) to support the ingoing study was not intended to be an objective from the beginning, but, as time went on, it became clear that it could play a fundamental role in data analysis and it turned out to become an (almost) independent objective as well.

This work also contributes to long-term goals: construction of a consistent apparatus, capable of making a general cardiovascular system evaluation; clinical experiments and validation of the developed hardware/software; and an even longer-term objective, clinical application of the hemodynamic system.

1.3 CEI Hemodynamic Research Team

This work was developed at *Grupo de Electrónica e Instrumentação* (CEI), one of the research groups of *Centro de Instrumentação* of the University of Coimbra – <http://c-instr.fis.uc.pt/>–, in the framework of a partnership with *Instituto de Investigação & Formação Cardiovascular* (IIFC) and *Intelligent Sensing Anywhere* (ISA) – www.ISA.pt. It is inserted on a project research named *Hemodynamic Parameters – New Instrumentation and Methodologies*, which aims at developing hemodynamic related instrumentation.

The persons involved in the above referred project, as well as their main areas of contribution, are summarized in the following table.

Table I. Team members of the project Hemodynamic Parameters – New Instrumentation and Methodologies and its contributions.

Team Members		Main Contribution	Institution
Prof. Carlos Correia	Scientific and Technical Supervisors	General Software Development	CEI
Prof. Requicha Ferreira		General Hardware Development	
Eng. Helena Pereira	PhD student	Assessment of Pulse Wave Velocity	CEI/ISA
Eng. Edite Figueiras	PhD student	Assessment of Blood Perfusion in Microcirculation	CEI
Elisabeth Borges	Biomedical Engineering Project Students	Assessment of Hemodynamic Parameters	Departamento de Física Universidade de Coimbra
Patrícia Coimbra	Biomedical Engineering Project Students	Assessment of Pulse Wave Velocity	Departamento de Física Universidade de Coimbra

1.4 Overview of the Dissertation

In order to guide the reading throughout the dissertation a brief summary of the contents of each chapter is presented:

- Chapter 2 – *Theoretical Background*: theoretical concepts related with the studied hemodynamic parameters and a brief discussion on *PZ* sensors operation;
- Chapter 3 – *Process Methodology* : a description of the developed hardware and of the procedures for signal acquisition and analysis;
- Chapter 4 – *Integration vs. Deconvolution*: the integration and deconvolution methods for obtaining the pressure wave are discussed and compared;
- Chapter 5 – *Piezoelectric Probe Calibration*: the experiments and theoretical arguments for calibrating a *PZ* sensor are discussed; results are shown and some conclusions are sketched;
- Chapter 6 – *Software Analysis Tool* : the prototype of a general purpose software analysis tool is depicted and the philosophy behind it is defined;
- Chapter 7 – *Results*: plots general results;
- Chapter 8 – *Discussion* : results and the general lines of the achieved work are criticised;
- Chapter 9 – *Conclusions*: summarizes the fulfilled work and draws general conclusions;
- Chapter 10 – *Future Work*: suggestions and ideas for further research work and for the improvement of some issues are exposed.

THEORETICAL BACKGROUND

As a wide variety of themes lie underneath this work, only the matters intimately connected with its goals will be focused. This criteria, adopted only for practical reasons, sets aside, for example, some Hydrodynamic issues that undoubtedly constitute the physical and mathematical basis for a good understanding of the cardiovascular system. For the same reasons, deepened descriptions of physiological issues, that might be pertinent, are also avoided.

This chapter begins with a synopsis of the cardiac cycle and an introduction to the pressure pulse, a central concept throughout this dissertation. Afterwards, a discussion on the relationships of the pressure pulse with other hemodynamic parameters is pursued. The last section clarifies operational aspects of the main physical tool used to obtain data and to derive results - the piezoelectric, *PZ*, sensor.

2.1 Cardiovascular Physiology Concepts

2.1.1 Cardiac Cycle

A basic understanding of *cardiac physiology* is essential to interpreting the physical findings of the present study.

In humans, the cardiac cycle or heartbeat lasts for about 0.8s and can be subdivided into two major phases: the systolic phase, which corresponds to contraction periods, and the diastolic phase, which corresponds to relaxation periods. In healthy persons, when the atria contracts, the ventricles relax, and when these last contract the first relaxes. At the end of these contraction/relaxation phases, both ventricles and atria rest.

The cardiac cycle begins with the atrial filling, where the right atrium fills with deoxygenated blood from the superior and inferior vena cava and, at the same time, left atrium fills with oxygenated blood from the lungs ^[1]. During this phase, the atrioventricular valves – tricuspid and mitral (Figure 1.a) – are open allowing the ventricles to fill. The flow of blood through these valves is unidirectional and has volume related pressure increases within the ventricles ^[1].

When atria contract they force the final volume (20%)^[1] into the respective ventricles. The atrioventricular valves closure follows, preventing backflow from the ventricles into the atria, and the ventricular systole proceeds. During this phase the semilunar valves – pulmonary and aortic valves (Figure 1.a) – are open, allowing blood to pass from right ventricle to pulmonary circulation and from left ventricle to systemic circulation. When ventricular pressures fall below their respective attached

pressures, the semilunar valves close ^[1]. After emptying, both ventricles collapse to undergo a period of repolarization and refilling.

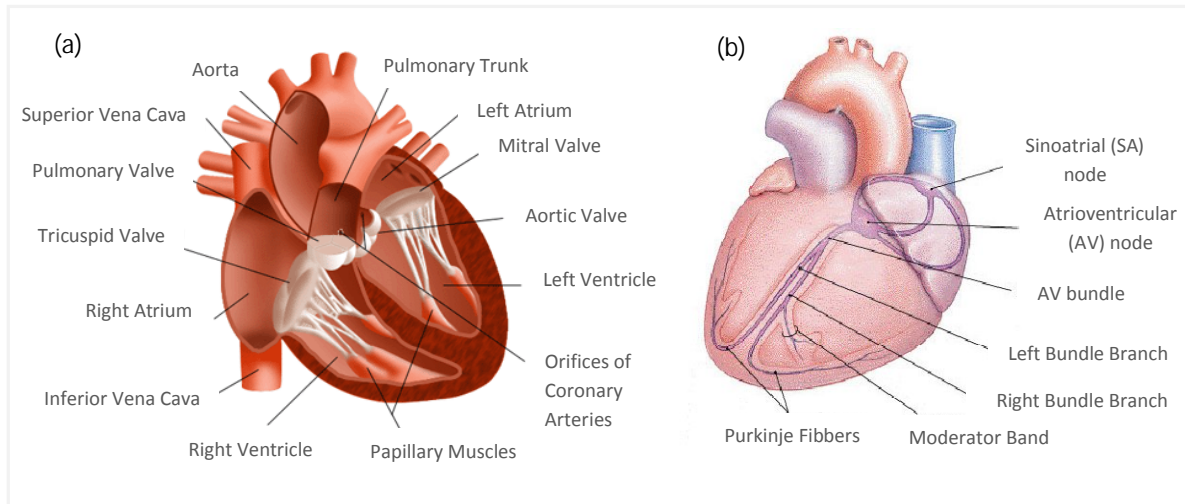


Figure 1. Heart physiology.
(a) Anatomy; (b) conduction system. Adapted from [3][4].

The sequence of heart chambers contraction and relaxation is controlled by a system of nerve fibers, which are triggered by atria and ventricles pressure thresholds, and provide the electrical stimulus to generate contraction of the heart muscles. The initial stimulus is provided by a small strip of specialized tissue called sinoatrial or SA node ^[2] (Figure 1.b). The SA node fires an electrical impulse that travels across the atria, causing them to contract, and reaches another node, the atrioventricular or AV node ^[2] (Figure 1.b). After receiving the SA impulse and once reached the pressure threshold, the AV node sends out its own electrical signal. The AV impulse propagates down a specialized set of fibers into the ventricular muscle, promoting the ventricles contraction ^[2]. In this way, the atria contraction occurs slightly before the ventricles contraction ^[2].

2.1.2 Arterial Pulse Wave

ORIGIN AND MORFOLOGY

A person's pulse corresponds to the arterial throbbing activity, as a consequence of the heart beat. The pulse can be felt at the neck (carotid artery), at the wrists (radial artery), behind the knees (popliteal artery), on the inside of the elbows (brachial artery), near the ankle joint (femoral artery) ^[5], and at other locations whose arteries have a bone support.

In fact, the pulse is a pressure wave – pulse wave – generated when the left ventricle contracts during the systole phase ^[6]. When it contracts a portion of blood is ejected in the ascending aorta, which promotes the artery distention ^[6]. This dilatation and sequent recover of the aorta produce the pulse wave, which propagates along the arterial tree with a finite, and proportional to the vase stiffness, velocity ^[5].

The oscillations caused in the arteries, when the wave pulse propagates, can be assessed and registered, at different body locations, by several methods, including non-invasive manners. By this way, it is known that the pressure wave has a characteristic shape, which varies in amplitude and shape (especially due to the *reflected waves*) depending on the measurement location. The most studied pressure wave shape is the one obtained at the ascending aorta.

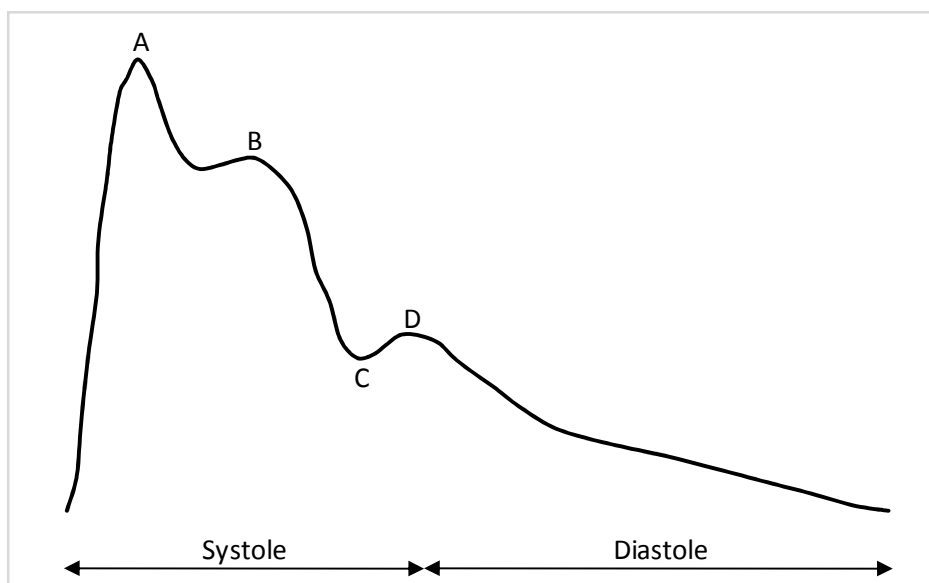


Figure 2. Aortic pressure wave shape.
 A – *Systolic peak* or *systolic wave*; B – *reflected wave*;
 C – *dicrotic incisura*; D – *dicrotic wave*.
 Drawn according to [8][9].

So, generally and in healthy individuals, the shape of the pulse wave at the ascending aorta (Figure 2) has an initial peak due to the fast and accentuated arterial distention, when blood is ejected in this artery during the ventricular systole. This peak is known by *systolic peak* or *systolic wave*. A smaller peak follows, called *reflected wave*, which is caused by the wave that is reflected at the first ramifications of the artery and returns to the location where the measurement is taken. At the end of the ventricular systole, the wave shape quickly falls, accompanying the arterial wall contraction. Nevertheless, following a characteristic depression, named *dicrotic incisura*, there is an even smaller peak that corresponds to the aortic valve (Figure 1.a) shutting up. This event promotes a smaller forced ejection of blood into the aorta which causes the artery to slightly distend for a second time. This peak is called *dicrotic wave*. From then on, the shape slowly decreases till the next systole. This portion represents the diastolic phase. ^[9]

CLINICAL SIGNIFICANCE

Despite pulse shape changes from person to person and from different body locations in the same individual, significant alterations in its morphology may bear physiological meaning. To decipher it, a good knowledge of the basic pulse shape of a healthy person is needed and, instrumentally, long enough signals (i.e. several cardiac cycles) have to be acquired to perform coherent analysis.

From the simple shape analysis is possible to identify cardiovascular pathologies if it appears different from the usual. For example, a pronounced *dicrotic incisura*, followed by a larger than normal *dicrotic wave*, can mean existing problems at the aortic valve ^[9]. Different parameters, depending only in the pulse morphology, can be calculated as well; referring: the augmentation index (non-dimensional parameter), the arterial pressure values, and others. Note that dimensional parameters, as is the case of the arterial pressure values, are only possible to achieve if there is used a calibrated sensor to acquire the pulse wave.

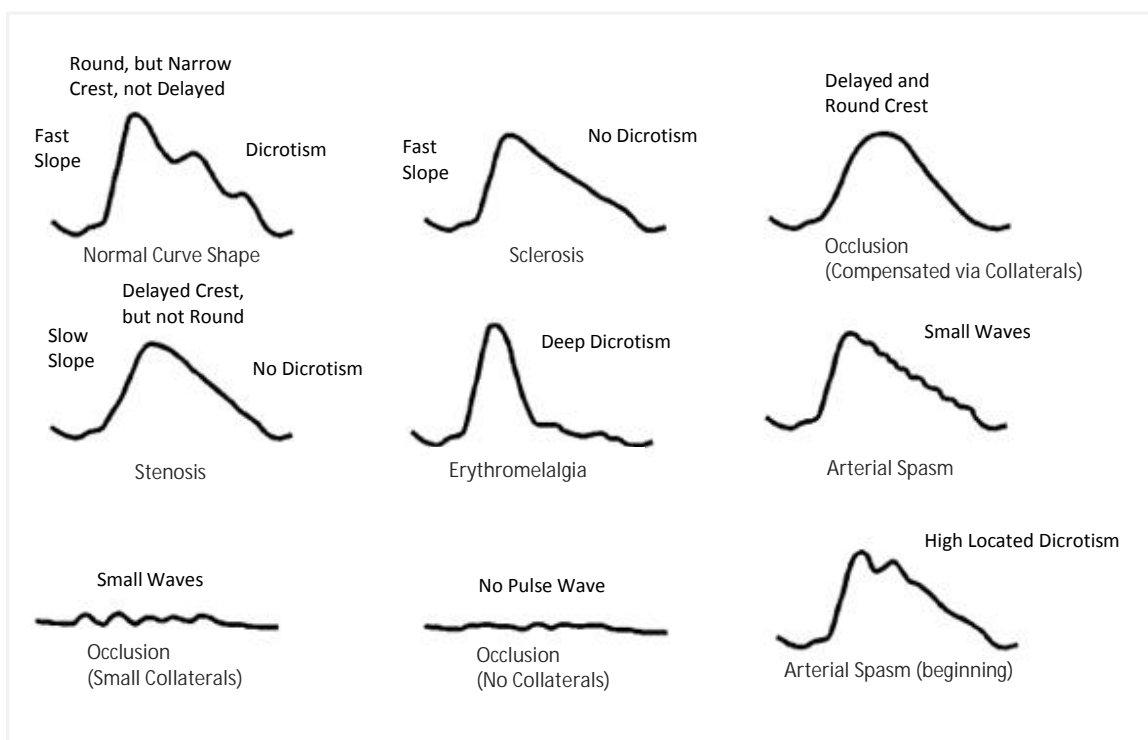


Figure 3. Changes in the pressure wave shape due to different diseases. Adapted from [10].

Pulse wave analysis can be used for ^[10]:

- Diagnosis and early recognition of arterioscleroses, chronic and/or acute arterial vascular diseases, and functional circulatory disturbances;
- Monitoring at-risk patients such as diabetics, smokers, and patients older than 50 years;
- Postoperative check-ups after vascular surgical operations;
- Determination of the impact of pharmaceuticals on the vascular system.

Besides shape analysis, it is also possible to assess the velocity of this wave. This hemodynamic parameter is widely studied and its values are easily found in the literature.

Depending on the duration of the captured signals, it is also possible to determine parameters like the heart rate variability, *HRV*, and the heart rate, *HR*, frequency.

All this parameters deviation from reported normal values permits to identify and quantify specific pathologies.

2.2 Arterial Stiffness and Its Assessment

2.2.1 Arterial Stiffness Increase and Cardiovascular Diseases

INFLUENCING FACTORS

The ageing of the arterial system is accompanied by structural alterations, including elastin fragmentation and degeneration, collagen alterations, calcium deposition, arterial wall thickness reduction, and progressive arterial dilatation^[11]. These alterations promote a gradual vascular stiffness increase and, consequently, an increase of the pulse wave velocity as it travels through the arterial vases, specially the larger ones, like is the case of the aorta. With the pulse velocity increase, a precocious superposition of the *reflected wave* takes place, even though the early systole phase is proceeding^[12]. This effect causes an increase in the systolic and central pulse pressure¹.

These are the main reasons why arterial stiffness is almost always associated with atherosclerosis and hypertension.

CLINICAL APPLICATION

Lately, there has been much interest in the relationship between arterial stiffness and cardiovascular diseases, *CVDs*. The researches indicate that arterial stiffness raises both with age and in certain diseases states that are associated with increased cardiovascular risk, referring: diabetes mellitus, hypercholesterolaemia, atherosclerosis and end-stage renal failure^[13] (table II). Arterial stiffening has been particularly implicated in the development of isolated systolic hypertension, a disease mainly affecting the elderly population (about two-thirds of people aged 65 years and older have hypertension^[14]) and associated with considerable excess morbidity and mortality^[13].

A major reason for measuring arterial stiffness in clinical practice comes from the recent demonstration that arterial stiffness has an independent predictive value for *CV* events^[15].

Table II. Clinical conditions associated with increased arterial stiffness. Adapted from [13].

AGEING	CV RISK FACTORS	CV DISEASES
PHYSIOLOGICAL CONDITIONS	Hypertension	Coronary heart disease
Low birth weight	Smoking	Congestive heart failure
Menopause status	Obesity	Fatal stroke
Lack of physical activity	Hypercholesterolaemia	PRIMARILY NON-CV DISEASES
GENETICK BACKGROUND	Impaired glucose intolerance	Moderate chronic kidney disease
Parental history of diabetes	Metabolic syndrome	Rheumatoid arthritis
Parental history myocardial infarction	Type I diabetes	Systemic vasculitis
Genetic polymorphisms	Type II diabetes	Systemic lupus
	High C-reactive protein level	Erythematosis

1. Formally the pressure pulse is the systolic pressure minus the diastolic pressure.

2.2.2 Arterial Stiffness Assessment

Arterial stiffness can be measured by a variety of techniques, although at present the majority of measurements are made for experimental and physiological studies rather than for clinical practice. Nevertheless, it is likely that over the next few years measurement of arterial stiffness will become an increasingly important part of the process of risk assessment, and may possibly also improve the monitoring of therapy in patients with conditions such as isolated systolic hypertension. ^[13]

As mentioned above, the arterial pulse wave can be modified by arterial stiffness. For this reason, and because it can be easily and non-invasively done, the pulse wave assessment is one of the preferred methods to evaluate arterial stiffness. Once the pulse wave is acquired it is possible to extract information from its shape (see section 2.1.2) or determine its propagation velocity which, as it will be shown, is intimately connected with arterial stiffness.

2.2.2.1 Pulse Wave Velocity

GENERAL CONCEPTS

The pulse wave velocity, *PWW*, measurement has been gaining distinction as it constitutes a fast, non-invasively and low-cost method to assess arterial stiffness. Presently, it is considered the standard method to assess this parameter.

The *PWW* can be expressed by the Bramwell-Hill equation:

$$PWW = \sqrt{\frac{1}{\rho_b} \times \frac{\Delta P}{\Delta A} \times A}, \quad (2.1)$$

where ρ_b is the blood density and A the cross-sectional area of the artery in the diastolic phase.

It should be noted that arterial complacency is determined by the rate of change in volume with the pressure, i.e. $C = \Delta V / \Delta P$. Alternatively, the variation in volume can be replaced by the variation of the cross-sectional area of the artery, ΔA , as is expressed in the previous equation.

Moreover, the *PWW* can be expressed by the Moens-Korteweg equation, which is related to the elasticity of the artery:

$$PWW = \sqrt{\frac{Eh}{2Rx\rho_b}}, \quad (2.2)$$

where E represents the elasticity module, h is the thickness of the artery, R the artery radius and ρ_b the blood density. ^[16]

As the arterial stiffness occurs at the beginning or even before the development of a specific CVD, the *PWV* is a good predictive index, allowing the clinician to administer specific drugs that may reduce the arterial stiffness.

MEASUREMENT

Several references can be found in the literature concerning *PWV* measurements in various artery sites. However, the carotid-femoral is the one that has gained the higher clinical relevance, since the carotid artery and its main branches are the major components of blood elasticity ^[7]. The measurement of *PWV* normally uses the *systolic foot* (see Figure 4) of at least two pulse wave shapes of an arterial segment. This method is called *foot-to-foot velocity*. There are methods that use other parts of the pulse wave, such as the *systolic peak*.

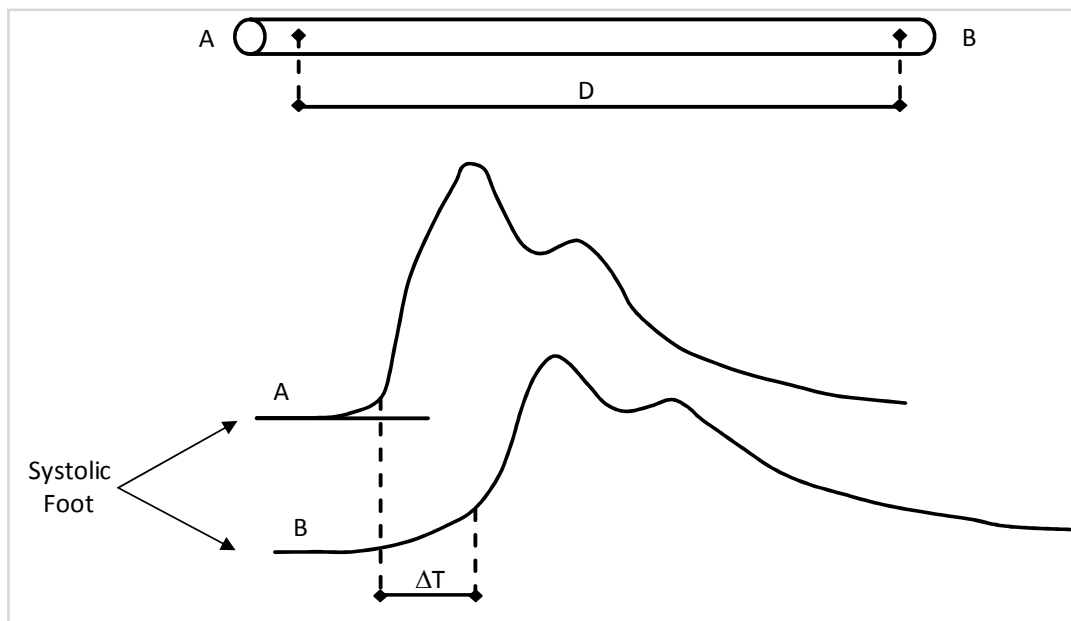


Figure 4. PWV measurement using the foot-to-foot velocity method.
Drawn according to [17].

The *PWV* can be simply calculated from the *transit time*, ΔT , that a pulse wave takes to travel a distance D through the vascular system:

$$PWV = \frac{D}{\Delta T} (m.s^{-1}) \quad (2.3)$$

The distance D should be measured precisely, since small inconsistencies can influence the absolute PWV value. Indeed, this is the greatest difficulty that impairs these techniques, since the distance between the sites where the sensors are placed is measured externally, and the curvatures of the arteries cannot be taken into account. In fact, the method will become even more precise if a smaller distance is used, reducing the absolute error in determining the *transit time*. However, a PWV measurement on major courses, such as the carotid-femoral, still constitutes a good method of evaluation, since it allows assessment of the mean arterial stiffness along it. ^{[7][18]}

NORMAL VALUES

At the aorta, the pulse wave is pronounced but moves relatively slow (3 to 6 $\text{m}\cdot\text{s}^{-1}$), although, as it spreads along the peripheral blood vases, its amplitude diminishes and its velocity raises, both progressively. In healthy persons, the mean PWV at the major arteries is about 7 to 10 $\text{m}\cdot\text{s}^{-1}$. In its turn, in peripheral arteries the mean velocity can reach about 15 $\text{m}\cdot\text{s}^{-1}$ (see Table III). ^{[5][7][19]}

Artery	PWV ($\text{m}\cdot\text{s}^{-1}$)
Ascending Aorta	5,2
	3,87
	5,45
	4,4
Thoracic Aorta	5,5 – 6,5
	4
	5,3
Abdominal Aorta	5
	5,7
Iliac	8,8
Femoral	8
Radial	7,3
Pulmonary	1,82
	1,68
Ascending aorta to femoral	7,67

Table III. PWV values along the arterial tree. Adapted from [19].

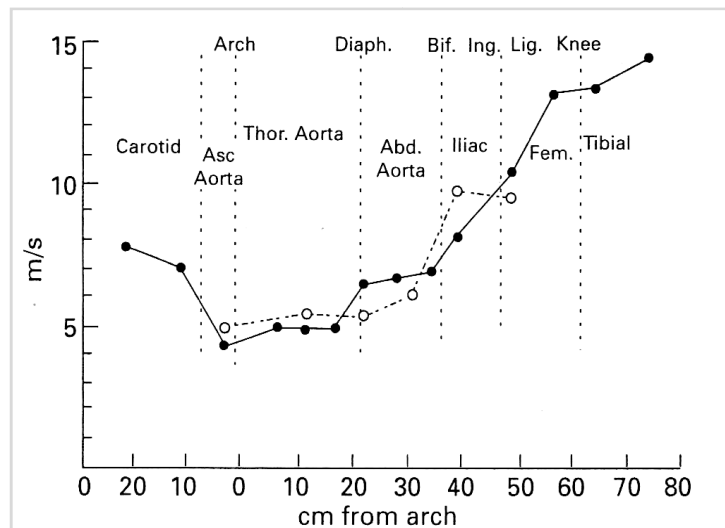


Figure 5. PWV values along the arterial tree. Adapted from [19].

STATE OF THE ART

The more widely spread systems for PWV assessment are the Complior® (Colson, France), which is the *gold standard* for the PWV assessment, and SphygmoCor® (AtCor, Australia). These systems are based on the measurement method described above, although the latter uses an electrocardiogram, ECG^2 , as a reference.

2. For better understanding see reference [44].



Figure 6. Complior® system.
 (a) Acquisition unit; (b) radial *PZ* sensor; (c) carotid *PZ* sensor. Adapted from [20].

The Complior® system allows a simultaneous acquisition over several arterial segments, including carotid-femoral, carotid-radial and carotid-distal using piezoelectric, *PZ*, sensors (see 2.4 section). The *transit time* is determined by a correlation algorithm between each simultaneously recorded wave. ^[20]

The system acquisition module connects to the computer via USB and runs a simple Windows® program, providing a friendly environment to the clinician ^[20].

In addition to *PWV* the system also records the heart rate frequency (in bpm), the *transit time* of the pulse (in msec) and estimates the central pulse pressure (in mmHg). ^[20]

Other features ^[20]:

- Number of sensors: 4 *PZ*s (for the carotid artery, radial, distal and femoral);
- Acquisition time: 10 seconds (covers the respiratory cycle);
- Acquisition mode: manual, by pedal action or by clicking the computer mouse;
- Signal quality control: visual confirmation by the operator.

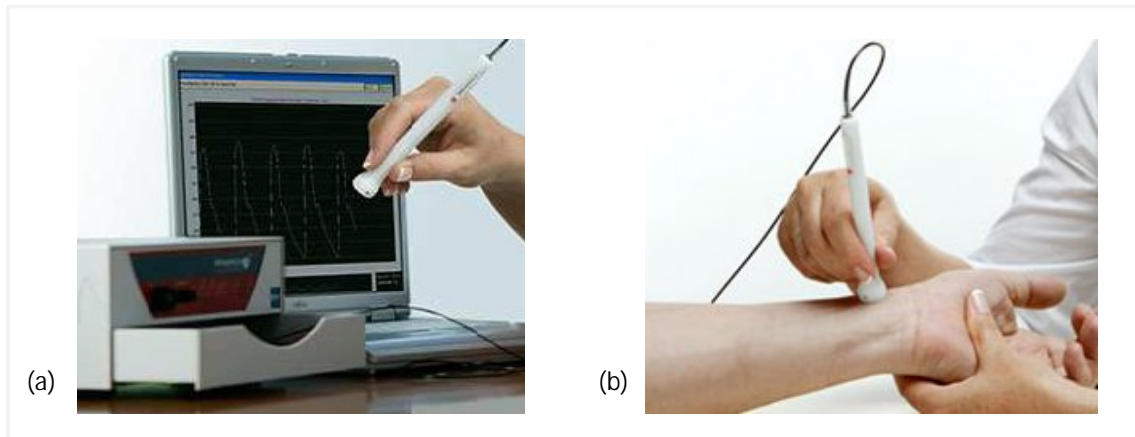


Figure 7. SphygmoCor® system.
(a) Acquisition unit; (b) radial tonometer. Adapted from [21].

The SphygmoCor® system employs applanation tonometers (Millar®)³ and *ECG* electrodes. The *transit time* is determined relatively to the *ECG* R-wave. For this purpose, the time between *ECG* and the proximal pulse is subtracted from the time between the *ECG* and the distal pulse. Besides evaluating the *PWV* along the carotid-femoral segment, it may still determine the *PWV* in the carotid-radial and carotid-distal courses.^[21]

The acquisition module also uses an USB interface, and runs a simple Windows® based program^[21].

Besides measuring the *PWV* (in $\text{m}\cdot\text{s}^{-1}$), the system also records the heart rate frequency (in bpm) and provides charts of *transit time* for each wave pulse.^[21]

Other features^[21]:

- Number of sensors: 2 manometers and 2 *ECG* electrodes;
- Acquisition time: 10, 20 or 30 seconds;
- Signal quality control: visual confirmation by the operator;

3. For better understanding see reference [45].

2.2.2.2 Augmentation Index

GENERAL CONCEPTS

As was mentioned before, pressure waves generated by the heart are reflected from peripheral sites in the arterial tree and influence the contour of the pressure waveform. The timing and amplitude of reflected waves may therefore influence cardiac function and their modification may be considered a target for therapeutic measures ^[22].

The timing of the *reflected wave* can be determined by measuring the time interval between the foot of the pressure wave and the inflection point ^[22]. This point occurs at the beginning of the secondary pressure rise, the *reflected wave* (see section 2.1.2), and represents the time of travel of the pressure wave from the heart to the periphery and back.

Once the inflection point is determined the augmentation index, *Alx*, is easily obtained. This parameter is defined as the proportion of central pulse pressure due to the *systolic peak* (see section 2.1.2), which is attributed to the *reflected wave*.

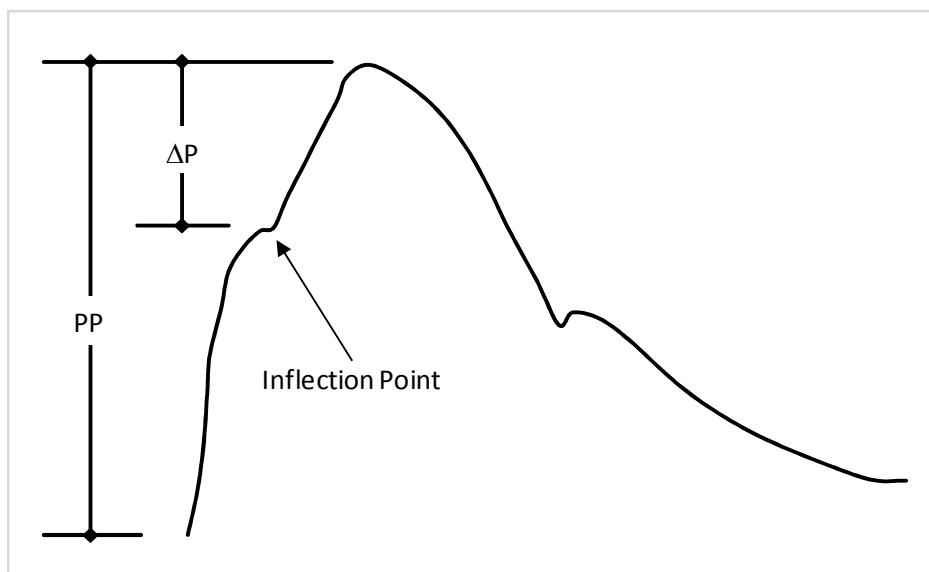


Figure 8. Graphic representation of *Alx* (%).
Drawn according to [23].

The *Alx* is a dimensionless ratio, expressed as follows:

$$Alx = \frac{\Delta P}{PP} (\%) \quad (2.4)$$

Where *PP* is the central pressure pulse and ΔP is the difference between the early and late pressure peaks, i.e. the systolic wave and the *reflected wave* (at the inflection point).

NORMAL VALUES

With aging, arterial stiffness and, hence, *PWV* are greater, causing the *reflected wave* to arrive earlier, increasing pressure amplitude and originating *AIx* higher values ^[22]. Usually, young and healthy people have small or negative *AIx* values while older persons have higher values. So, *AIx* can vary from around -30% to about 70% ^[24] (see Figure 9).

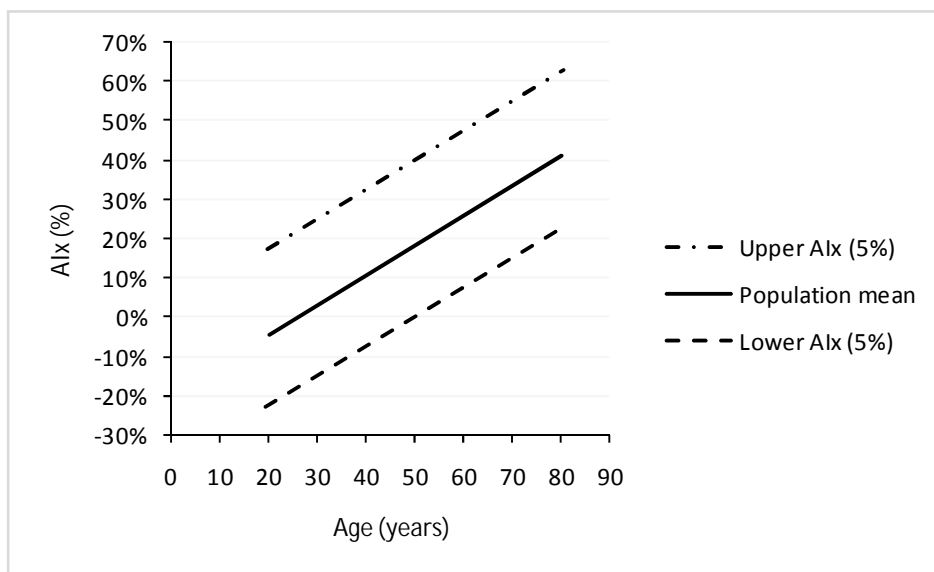


Figure 9. AIx (%) against age.
Reference values for SphygmoCor®. Adapted from [24].

Besides these values, recent studies show that *AIx* and heart rate, *HR*, frequency both are inversely and linearly correlated. It has been shown that a 10bpm increment in *HR* causes a *AIx* increase of -0,39% ^[24]. It is also known that women have lower *AIx* values comparatively with men ^{[22][24]}.

STATE OF THE ART

AIx can be determined by the same systems used to assess *PWV*, like those referred in the last section. Nevertheless, there is at least one specific apparatus, patented by the Colin Technology Corporation, for this purpose - the HEM 9000ai® (Omron Healthcare Inc., Japan), that has been designed for personal use.



Figure 10. HEM 9000ai® system.
From left to right: *A/x* pulse wave measurement unit, main unit and cuff. Adapted from [26].

This system is based in cuff-pulse-wave signals. The water contained in the skin and subcutaneous tissue of the portion being pressed by the cuff is squeezed out, so that the thickness of the skin and subcutaneous tissues decreases to a value corresponding to the pressing. The cuff is attached to a pressure sensor that detects the air pressure in the cuff and supplies a pressure signal, which permits triggering the acquisition of the pressure wave, processed by a patented multi-sensor array technology (applanation tonometers) at the wrist (radial artery) ^{[25][26]}.

An advanced version of this system, used in clinical and hospital units, has turned out to become the *gold standard* for this method. It is known as Colin-Omron VP 2000® (Omron Healthcare Inc., Japan) and it also provides multi-segment *PWV* ^[26].



Figure 11. Colin-Omron VP 2000® system.
Adapted from [26].

2.3 Heart Rate Variability

The last two decades have witnessed the recognition of a significant relationship between the autonomic nervous system and cardiovascular mortality, including sudden cardiac death ^[27]. Because there is experimental evidence of an association between propensity for lethal arrhythmias and signs, of either increased sympathetic or reduced vagal activity ^[27], efforts have been made to define hemodynamic parameters of autonomic activity. The heart rate variability, *HRV*, represents one of the most promising such parameters ^[27].

2.3.1 Definition and Physiological Meaning

HRV refers to the beat-to-beat alterations in heart rate. This rhythmic phenomenon, known as respiratory sinus arrhythmia, *RSA*, fluctuates with the phase of respiration ^[28]. The relationship between heart rate and respiration is such that heart rate increases coincidentally with inhalation and decreases coincident with exhalation in a *sinusoidal* fashion, hence the name respiratory *sinus* arrhythmia ^[29].

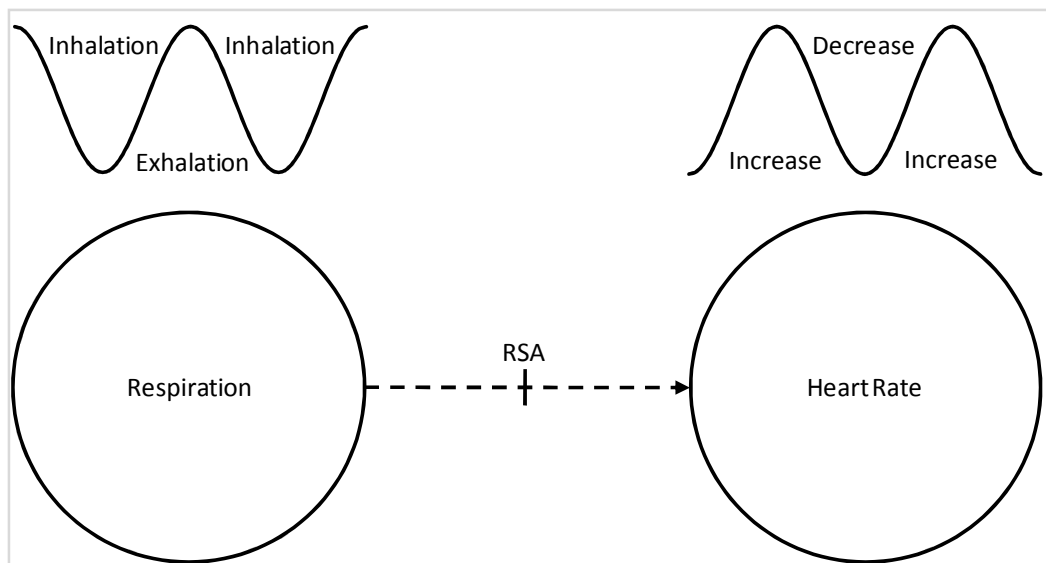


Figure 12. Heart rate variability.
Respiration and heart rate are 180 degrees out of phase.
Adapted from [29].

Although variable respiratory rhythm results in variable heart rhythm, i.e. the *HRV*, it is known that breathing rhythm is not the only factor affecting heart rhythm ^[29].

RSA and its result, *HRV*, are predominantly mediated by autonomic nervous system, *ANS*, via the baroreceptor reflex. Baroreceptors⁴ work in opposition to changes in blood pressure, i.e. if blood pressure decreases, the *ANS* facilitates an increase and vice versa [28][29]. These receptors actuate specially by controlling the *SA* node (see Figure 1.b). By this way, is logic to infer that *HRV* influences arterial pressure. Actually there is much evidence that it does, however not much is known about how [29].

As it is known, arterial pressure rises and falls with blood volume. So it is also possible to correlate blood volume with *HRV*.

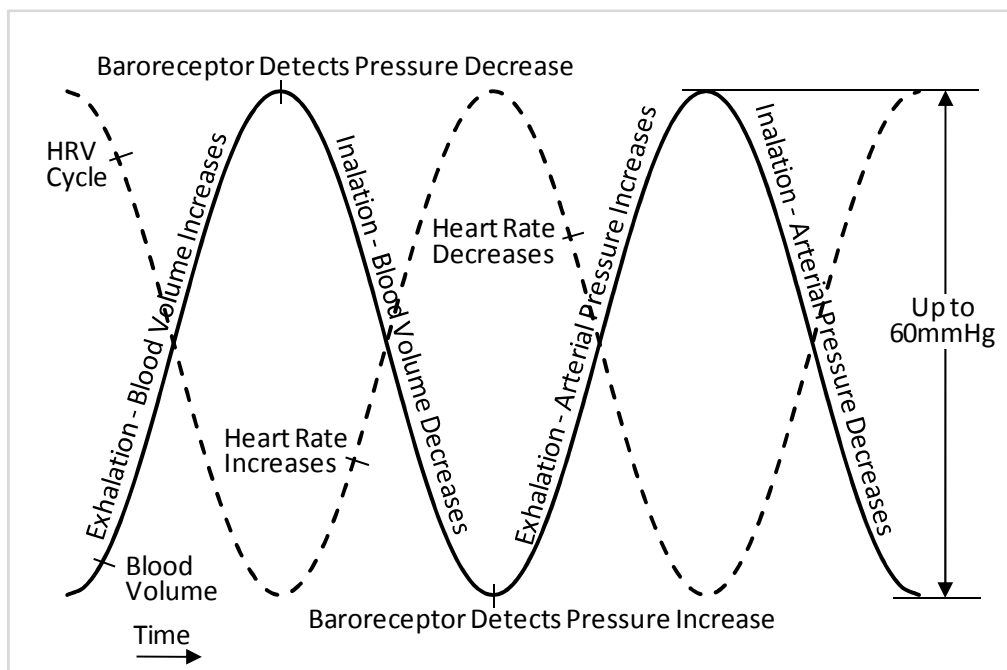


Figure 13. Heart rate and blood volume. Blood volume and heart rate are 180 degrees out of phase. Drawn according to [29].

4. Baroreceptors are specialized neurons located throughout major arteries. Their function is to monitor arterial pressure.

2.3.2 Clinical Significance

Generally, reduced *HRV* has been used as a marker of reduced *ANS* activity. Nevertheless, the major reason underneath the interest in measuring *HRV* comes from its ability to predict survival after heart attack ^[28]. Recent studies have shown that reduced *HRV* predicts sudden death in patients with myocardial infarction, independently of other prognostic indicators ^[28].

HRV also appears to be a marker of fatal ventricular arrhythmia. Moreover, a small number of studies seem to suggest that reduced *HRV* may predict risk of survival even among individuals free of heart diseases ^[28]. Alterations (mostly reductions) in *HRV* have been reported to be associated with various pathologic conditions such as hypertension, hemorrhagic shock and septic shock.

2.3.3 Measurement

HRV is usually calculated by analyzing a time series of beat-to-beat intervals from the *ECG* or beat-to-beat intervals derived from an arterial pressure tracing. Several measures of *HRV* have been proposed, which can roughly be subdivided into time domain and frequency domain measures.

TIME DOMAIN

Initially, *HRV* was assessed from calculation of the mean R-R interval and its standard deviation measured on short-term (e.g., 5 minute) *ECGs*. These are generally called by normal-to-normal, *NN*, intervals. The smaller the standard deviation in *NN* intervals, the lower is the *HRV* ^{[28][30]}. To date, over 26 different types of arithmetic manipulations of *NN* intervals have been used in the literature to represent *HRV* (table IV) ^[28]. Examples include: the standard deviations of the normal mean *NN* interval obtained from successive 5-minute periods over 24-hour recordings (*SDANN* index); the number of instances per hour in which two consecutive *NN* intervals differ by more than 50msec over 24-hours (*pNN50* index); the root-mean square of the difference of successive *NN* intervals (*rMSSD* index); and so on ^{[27][28][30]}.

Table IV. Selected time domain measures of HRV. Adapted from [28].

Variable	Units	Description
STATIC MEASURES		
SDNN	ms	Standard deviation of all <i>NN</i> intervals
SDANN	ms	Standard deviation of the averages of <i>NN</i> intervals in all 5-minute segments of the entire recording
RMSSD	ms	The square root of the mean of the sum of the squares of differences between adjacent <i>NN</i> intervals
SDNN index	ms	Mean of the standard deviations of all <i>NN</i> intervals for all 5-minute segments of the entire recording
SDDSD	ms	Standard deviation of differences between adjacent <i>NN</i> intervals
NN50 count		Number of pairs of adjacent <i>NN</i> intervals differing by more than 50ms in the entire recording; three variants are possible counting all such <i>NN</i> intervals pairs or only pairs in which the first or the second interval is longer
pNN50	%	NN50 count divided by the total number of all <i>NN</i> intervals
GEOMETRIC MEASURES		
<i>HRV</i> triangular index		Total number of all <i>NN</i> intervals divided by the height of the histogram of all <i>NN</i> intervals measured on a discrete scale with bins of 7.8125ms (1/128seconds)
TINN	ms	Baseline width of the minimum square difference triangular interpolation of the highest peak of the histogram of all <i>NN</i> intervals
Differential index	ms	Difference between the widths of the histogram of differences between adjacent <i>NN</i> intervals measured at selected heights (eg, at the levels of 1000 and 10 000 samples)
Logarithmic index		Coefficient k of the negative exponential curve $k \cdot e^{-x/T}$, which is the best approximation of the histogram of absolute differences between adjacent <i>NN</i> intervals

Experimental and simulation data appear to indicate that the various methods of expressing *HRV* are largely equivalent, and there is no evidence that any one method is superior to another, provided measurement windows are 5 minutes or longer.

FREQUENCY DOMAIN

Frequency domain measures involve spectral analysis, mainly by the use of the Fourier transform.

The *HRV* spectrum contains two major components: the high frequency, *HF*, component (0,18 to 0,4 Hz), which is synchronous with respiration and is identical to *RSA*, and the low frequency, *LF*, component (0,04 to 0,15 Hz) that appears to be mediated by both the vagus and cardiac sympathetic nerves, from the *ANS* ^{[27][28][30]}. The power of spectral components is the area below the relevant frequencies presented in absolute units (square milliseconds) ^[28]. The total power of a signal, integrated over all frequencies, is equal to the variance of the entire signal ^[28].

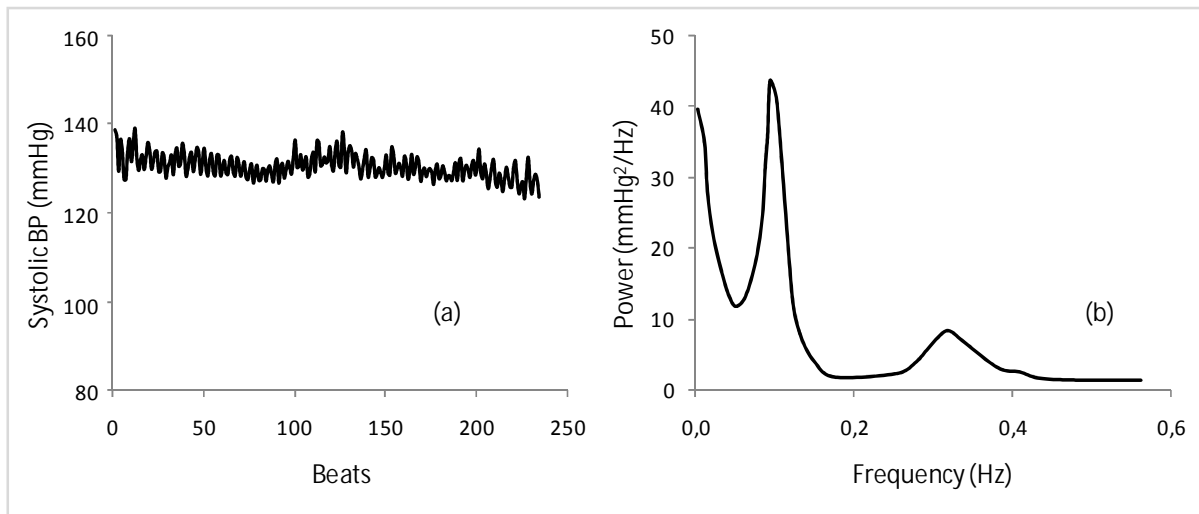


Figure 14. HRV frequency domain measurement. Adapted from [31]. *NN* interval data are represented on a tachogram (a), in which the y-axis plots the *NN* intervals, and the x-axis the total number of beats. Spectral analysis of the tachogram (b) transforms the signal from time to frequency on the x-axis, by representing the signal as a combination of sine and cosine waves, with different amplitudes and frequencies.

2.3.4 State of the Art

Normally, systems used for *ECG* or pulse wave record can also provide *HRV* data. For example, the widely used 24-hours *ECG* record Holter[®], can also produce *HRV* values. However, specific equipments exist, especially software tools, to assess and/or calculate *HRV*. The most relevant is the HRVlive[®] software (Biocom Technologies, USA), which can be purchased along with the acquisition systems.

This software measures *NN* intervals using an *ECG* or a pulse wave record, depending on the acquisition system used. It repetitively computes and updates *HRV* parameters every half of a second and displays measured data in various graphical forms, besides giving *HRV* values.^[32]



Figure 15. HRVlive® software. Adapted from [32].

The supported hardware includes: Biocom HRM-02 pulse wave sensor, Biocom 3000 *ECG* recorder and Active*ECG* recorder®. The first is a pulse wave sensor which is placed on earlobe or, alternatively, on a finger. It connects to computer via USB port. The Biocom 3000 unit uses two *ECG* electrode pads placed on wrists of both hands, and also connects computer via USB port. The last device is a single-channel *ECG* recorder from Active Corporation®, which are standard off-the-shelf pre-gelled *ECG* electrodes. These electrodes can be placed on either both wrists or chest [32].



Figure 16. HRVlive® hardware. Adapted from [32].
(a) Biocom HRM-02 pulse wave sensor; (b) Biocom 3000 *ECG* recorder;
(c) Active*ECG* recorder®.

2.4 Piezoelectric Sensors

2.4.1 General Concepts

Piezoelectric, *PZ*, sensors rely on the piezoelectric effect, which was a discovery by the Curie brothers. The *PZ* effect is a process by which energy is converted from mechanical into electrical forms. Specially, when pressure (*piezo* means *pressure*, in Greek) is applied to a polarized crystal, it causes a mechanical deformation and a displacement of charges, which promotes an electrical bias. Those charges are highly proportional to the applied pressure^{[33][34]}.

Two main groups of materials are used for *PZ* sensors: piezoelectric ceramics and single crystal materials. As the *PZ* crystals behave like electrets, which have permanent polarization, each constituting cell has an electric dipole, and all the cells are oriented such that the electric dipoles are aligned. This results in excess surface charge which attracts free charges from the surrounding atmosphere making the crystal electrically neutral. If a force is applied to the *PZ* crystal, a deformation will take place. This can disrupts the orientation of the electrical dipoles in a way that the charge is not completely canceled. Thus, it results a temporary excess of surface charge, which subsequently is manifested as a voltage developed across the crystal.^[34]

The developed voltage can be expressed as:

$$V = \frac{Q_f}{C}, \quad (2.5)$$

Where Q_f is the charge resulting from the applied force f , and C is the capacitance of the material.

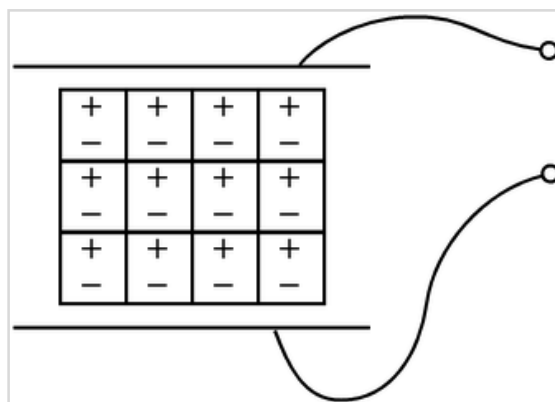


Figure 17. Sensor based on the *PZ* sensor. Common method of using a *PZ* crystal to make a force sensor. Two metal plates are used to sandwich the crystal making a capacitor. Adapted from [34].

In the manner described above, *PZ* crystals act as transducers. Alternatively, if one was to apply a voltage to the plates of the system described in the figure above, the resultant electric field would cause the internal electric dipoles to re-align which would cause a deformation of the material. An example of this behavior is the fact that *PZ* transducers find use both as speakers (voltage to mechanical) and microphones (mechanical to electrical) ^[34].

2.4.2 Physical Quantities Measured with PZs

Based on piezoelectric technology it is possible to measure several physical quantities; the most common ones are pressure and acceleration. Pressure sensors employ a thin membrane and a massive base, which ensures that an applied pressure specifically loads the elements in one direction. In accelerometers, a seismic mass is attached to the crystal elements. When the accelerometer experiences a motion, the invariant seismic mass loads the elements according to Newton's second law of motion: $F = ma$ ^{[34][36]}.



Figure 18. Metal disks with PZ material.
Adapted from [36].

The main difference in the working principle between these two sensor types is the way forces are applied to the sensing elements. In a pressure sensor a thin membrane is used to transfer the force to the elements, while in accelerometers the forces are applied by an attached seismic mass ^{[34][36]}.

Sensors often tend to be sensitive to more than one physical quantity. For example, pressure sensors show false signal when exposed to vibrations ^[36].

2.4.3 Electrical Properties

A *PZ* transducer actuates as a differentiator since its equivalent circuit is basically an RC (Figure 19). It has very high DC output impedance and can be modeled as a proportional voltage source and filter network. The voltage V at the source is directly proportional to the applied force, pressure or strain. The output is then related to this mechanical force as if it had passed through the equivalent circuit ^[35].

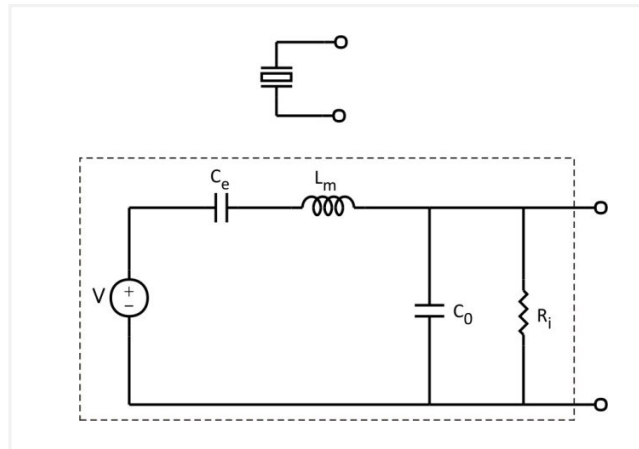


Figure 19. Schematic symbol and electronic model of a PZ sensor. Drawn according to [35].

A detailed model, as the one in the figure above, includes the effect of the sensor's mechanical construction and other non-idealities. The inductance L_m is due to the seismic mass and inertia of the sensor itself. C_e is inversely proportional to the mechanical elasticity of the sensor and C_0 represents the static capacitance of the transducer, resulting from an inertial mass of infinite size. R_i is the insulation leakage resistance of the transducer element. If the sensor is connected to a load resistance, this also acts in parallel with the insulation resistance, both increasing the high-pass cutoff frequency. In low frequency applications, the resistance R_i is very high and can be ignored^[35].

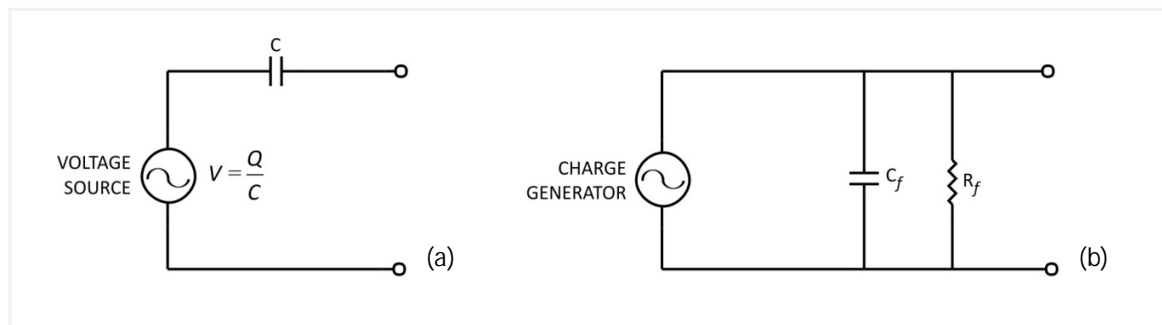


Figure 20. Basic equivalent circuits of a PZ sensor (flat region). Drawn according to [35].

A simplified circuit model can be used to represent the flat region. It can be modeled as a voltage source in series with the sensor's capacitance (Figure 20.a). Here, C represents the capacitance of the sensor surface itself, determined by the standard formula for capacitance of parallel plates. It can also be modeled as a charge source in parallel with the source capacitance, with the charge directly proportional to the applied force (Figure 20.b)^[35].

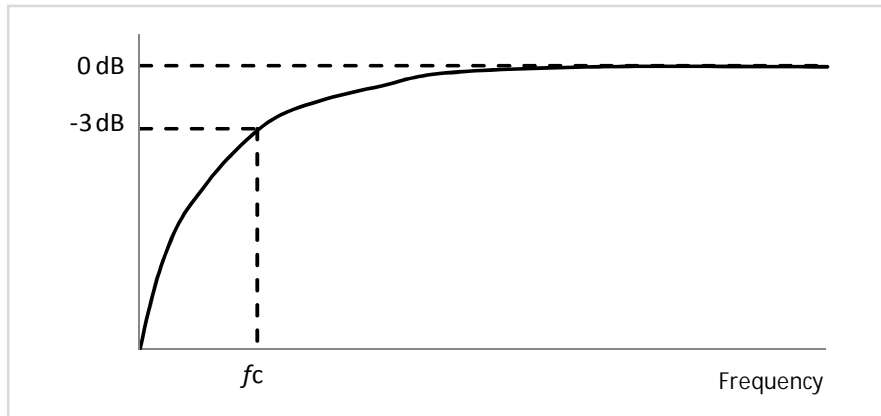


Figure 21. High pass filter characteristic of a PZ sensor.
Drawn according to [35].

The circuit exhibits an RC high-pass filter characteristic as shown in Figure 21. In this figure, the vertical axis implies the ratio of observable output signal to the developed signal (open circuit voltage of the *PZ* sensor). Zero dB implies no loss of signal. The cutoff frequency, f_c (3 dB down) is inversely proportional to the time constant. When a *PZ* sensor is operated below this cut-off frequency, the output signal is significantly reduced. For a low frequency measurement, an input resistance needs to be high enough so that the cut-off frequency is well below the desired operating frequency^[35].

PROCESS METHODOLOGY

This chapter begins with an insertion of the present work in the one previously developed by the hemodynamic team of GEI.

The hardware developed for this work is described, followed by a brief discussion of the methods adopted.

3.1 Context

The utilization of piezoelectric, *PZ*, sensors on pulse wave assessment started more than one year ago in our group. These have been used as a support tool for studies carried out with other sensors. Hence, different geometries for *PZ* probes were designed and built for the multi-sensor acquisition modules under development.

By that time the potential for pulse wave assessment with *PZ* probes, at several body locations, was recognized. Results were quite reproducible and signal-to-noise ratios were very good, when compared with data from other sensors. This, added to the low price and variety of shapes of *PZ* sensors, made a new objective naturally arise: using a single *PZ* probe to assess the pulse wave signal at the left common carotid artery, the human body location closer to the aorta, with enough fidelity to extract information from its waveform.

Although *PZ* sensors have been used for years in various commercial instruments to assess pulse wave, generally for *PWV* determination along an arterial segment, they normally employ two probes in two body locations.

Using a single *PZ* sensor to determine, not only *PWV* but other hemodynamic parameters as well, seemed an interesting work topic and, if successful, a significant step forward in the state of the art.

3.2 Acquisition System

To fulfill the above mentioned objectives, two *PZ* probes and one multi-sensor acquisition unit, quite similar to already existing acquisition units, were built. Although its design and construction were not a main concern in the present work, its architecture will be briefly described.

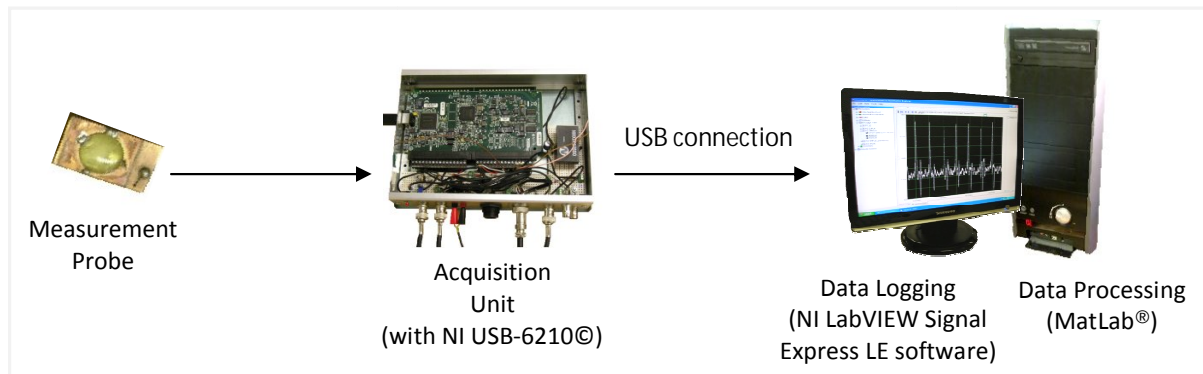


Figure 22. General measurement system architecture.

3.2.1 Piezoelectric Single Probes

Regarding the *PZ* probes, a small batch of units was built to prove the accuracy and repeatability of the results, and also to improve small geometrical aspects that influence the user-operator interface.

The probe uses a typical circularly shaped sensor (MuRata®), based on a double layer printed circuit board, *PCB*, as shown in Figure 23. The perforation allows the *PZ* oscillations and guarantees the electrical connection between the *PZ* disc and the *PCB*. A spherically shaped silicone interface is placed on the metal disk, in order to obtain a more efficient contact between the moving tissues covering the artery and the transducer.



Figure 23. Initial PZ probe.
 (a) Photo; (b) cross scheme; A and B – signal and ground connectors;
 C – PCB; D – metal disk; E – PZ material; F – silicone interface.

In order to verify the consistency of the results and to improve the signal-to-noise ratio, a new version of the previous probe was built later; they were built two similar *PZ* probes. The main difference from first one was the use of a coaxial cable and of a sandwich geometry with three plates instead of one, as shown in Figure 24. The introduction of these plates permits, on one hand, more space for *PZ* oscillations, and on the other, a holding support at the acquisition moment, avoiding the *PZ* disk to be pushed.

It is worth noticing that the difference between these two probes was only the shape of the probe.



Figure 24. Final *PZ* probe.
 (a) Photo; (b) cross scheme; A – coaxial Cable; B – *PZ* signal conductor; C – ground conductor; D – perforated plate; E – perforated plate (small perforation); F – plate with no perforation; G – *PZ* material; H – metal disk; I – silicone rubber.

All the *PZ* probes produced similar results when used in the same circumstances. However, the latter probes show a better signal-to-noise ratio, specially the last one (Figure 24), which was used to collect the signals in this study.

3.2.2 Acquisition Unit

The built acquisition unit supports not only the single *PZ* probe but also other sensors and additional inputs used in other works/experiences. This unit can be subdivided in two main parts: the data acquisition, *DAQ*, module and a prototype *veroboard* area which contains conditioning circuits. Power is supplied by the USB port of the *DAQ* module and a DC/DC converter is used (NMXD0505S0) to provide isolation and the biasing voltages (+5V/-5V) of the conditioning circuitry.

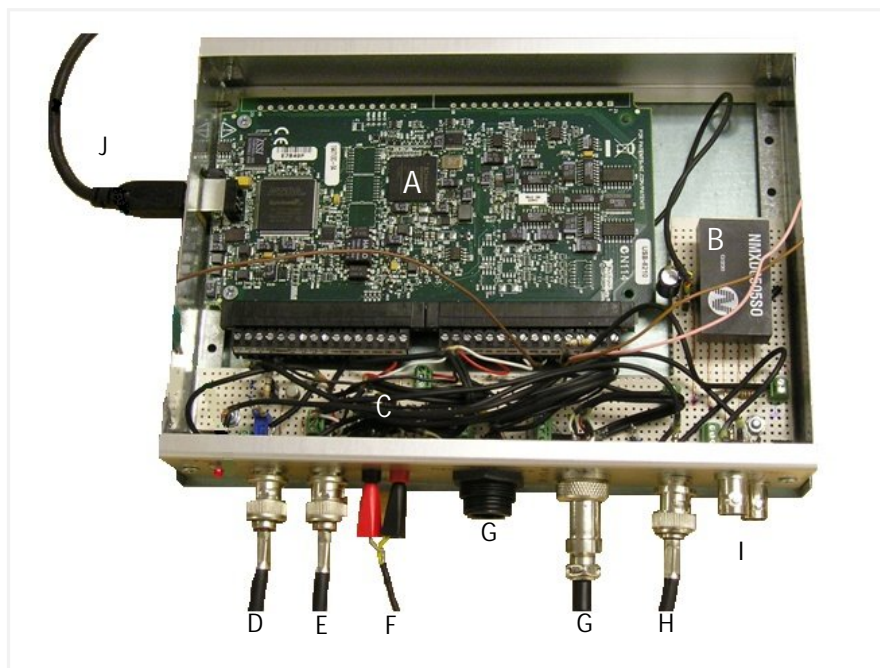


Figure 25. Acquisition unit.
 A – *DAQ* module; B – DC/DC converter; C – *veroboard*; D – pulse generator input; E – switcher output; F – single *PZ* probe input; G – other sensors input; H – synchronizer input; I – oscilloscope outputs; J – USB cable.

DAQ MODULE

The *DAQ* module used in the acquisition unit is the NI USB-6210© (Figure 26). It has 16 analog inputs and can sample up to 250KSpss. This device comes with a driver software, the NI-DAQmx©, running on Windows Operative System®, for interactive configuration and programming interfaces (ex. *DAQ* Assistant). Besides, a copy of NI LabVIEW SignalExpress LE data-logging software, a configuration software package, is also provided and used for data logging. The logged data can be saved in a .txt format for further processing.^[37]

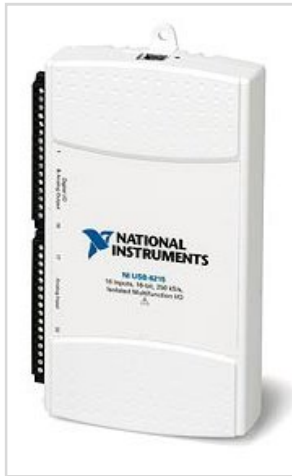


Figure 26. NI USB-6210©.
Adapted from [37].

NI USB-6210© Specifications [37]:

- 16 analog inputs (16-bit, 250 kSps);
- 4 digital inputs; 4 digital outputs; two 32-bit counters;
- 4 programmable input ranges (± 0.2 to ± 10 V) per channel, digital triggering and 2 counters/timers;
- Bus-powered USB;
- Compatible with LabVIEW, LabWindows™/CVI, and Measurement Studio for Visual Studio .NET
- NI-DAQmx© driver software and NI LabVIEW SignalExpress LE interactive data-logging software.

VEROBOARD PROTOTYPE

Signal conditioning of the *PZ* probe is a basic charge amplifier for the *PZ* signal input, and a buffer circuit, for driving the actuator that will be explained in the following chapter. The charge amplification has been duplicated in order to accommodate experiments with a dual probe discussed elsewhere. The circuit employs a TL082 amplifier in a standard configuration as depicted in Figure 27.

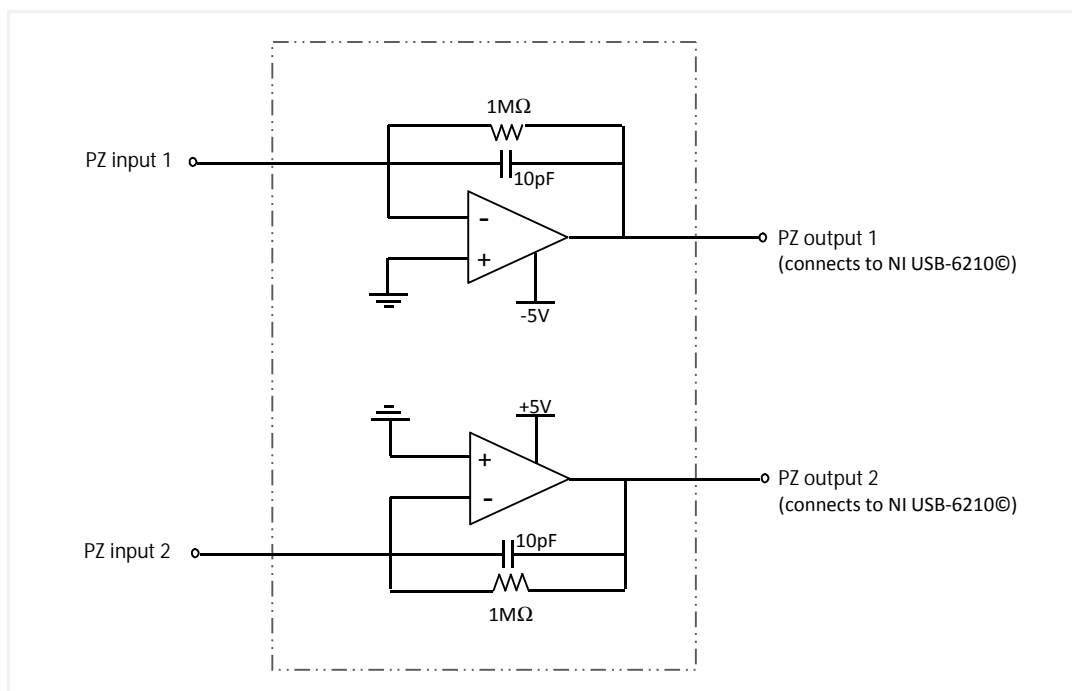


Figure 27. Veroboard circuitry – Charge amplification circuit.

3.2.3 Respiratory Signal

At the final stages of this work, when heart rate variability was studied, a respiratory signal had to be acquired simultaneously with the carotid hemodynamic signals.

Initially a *respiratory band*, which employs a *PZ* sensor to measure the chest oscillations of breathing, was used. Nevertheless, the respiratory signal recorded by this method exhibited very poor signal-to-noise ratio and didn't yield consistent results.

A different approach to assess the respiratory signal was required and the thermal element method was used. A *NTC* (*Negative Temperature Coefficient*) resistor was placed in the path of expired air path to detect the corresponding temperature variation and results were very satisfactory. Figure 28 shows the electronic circuit that uses $68\text{K}\Omega$ *NTCs* in a standard *Wheatstone* bridge configuration combined with an *INA126* instrumentation amplifier. One of the *NTCs* is placed close to a nostril and other is placed in the conditioning circuit, to compensate for room temperature variations.

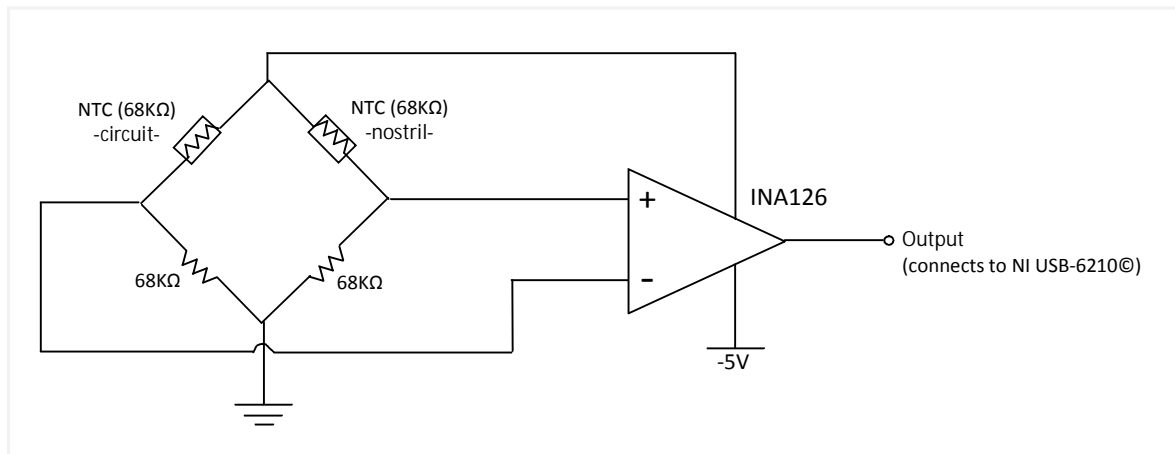


Figure 28. NTC respiration detection circuit.

3.3 Experimental Trials

3.3.1 Data Acquisition

Data was acquired under the following protocol:

1. The subject rests on a gurney a few minutes;
2. The operator places the *PZ* probe on the carotid site and, by visualizing the data in the NI screen, optimizes signal detection;

3. When the signal appears clear, data logging is initiated and, 1 minute later, it is stopped (data is recorded at a 20KSpss sample rate);
4. The operator repeats steps 2 and 3 at another carotid location (about 2cm away from the first one) and records a second signal;
5. Finally, the operator places the *NTC* close to one of the nostrils and the *PZ* probe at the first location (the carotid and the respiratory signals are recorded simultaneously for 5 minutes at a 1KSpss sample rate);
6. Data recorded is exported in .txt files and analyzed in the developed MatLab® software tool, the *PulScope*.

It were analyzed 10 individuals, and for each one they were recorded 3 signals (A,B and C) at 20KSpss and also another 3 signals (A,B and C) at 1KSpss.

3.3.2 Data Processing

At the early stages of this work, data was collected just to test the equipments and the analysis routines.

Also, to increase confidence on the equipment, data acquired with several months of distance in time and with slightly different versions of the equipment was compared.

Figure 29 shows two sets of data acquired with around 9 months of interval in the same subject.

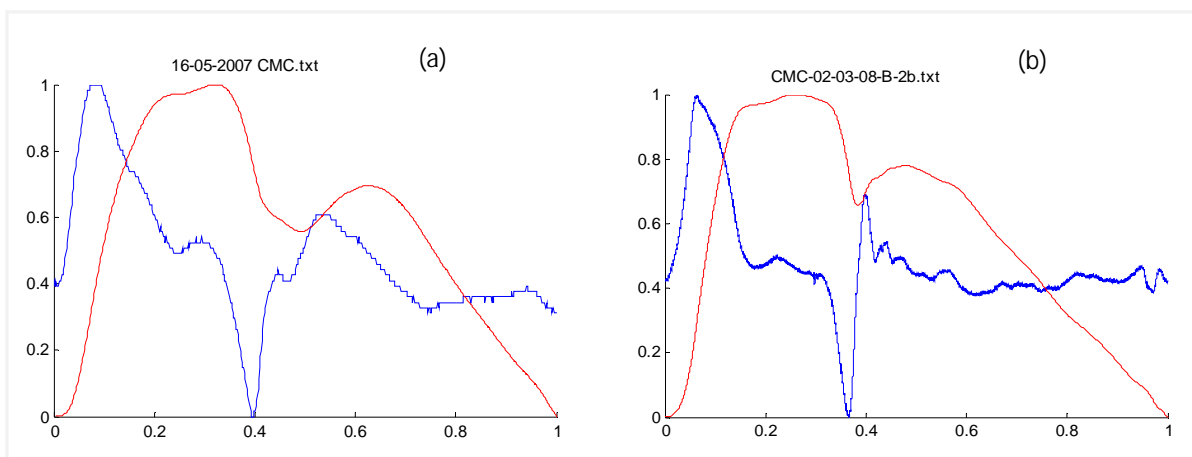


Figure 29. Results consistency.
Carotid signal recorded by the *PZ* sensor (blue) and its time integral (red).
These signals were acquired from the same person (a) in May 2007 and (b) March 2008. Although the sample rates are different - 1KSpss for (a) and 20KSpss for (b) - the shapes are very similar.

For that, they were constructed basic MatLab® routines, which permit to transform the hemodynamic signals collected in data with physical meaning appearance. Once the *PZ* probes actuates as a differentiator, the signal recorded by them is also differentiated. So, basically, the initial routines integrated the collected data to obtain signals that were very close related, in shape, with the known (from literature) pulse pressure acquired at the aorta (see section 2.1.2).

Once it was shown the repeatability and accuracy of the *PZ* probe, it started the software tool construction.

The constructed software tool (*PulScope*) is popup menu-based. It has several signal analysis levels and the routines it undergoes permit to determine some hemodynamic parameters. The exported .txt files, from the NI software, are here processed and analyzed, even by non-skilled personnel. It is only necessary to give few utilization directions of it. More detailed explanations about the construction and functioning of the built software tool will be given in an individual chapter (chapter 6), once this software constitutes one of the main parts of the fulfilled work.

3.4 To Retain

Once the environment of the work is sketched, it is important to retain some considerations before going into details explanations as will be done in the following chapters.

Firstly, the acquisition system and software proved to be an adequate and versatile tool, appropriate for research in this area. Among others, the following advantages can be pointed out: the acquisition method is easy to process; only one operator is needed to acquire data; several parameters can be assessed with the same software and hardware.

On the other hand, two main questions arose throughout many sessions of its use; specifically:

- The integration could not be the ideal and accurate method to obtain pressure pulses from the *PZ* signal, since the electrical equivalent of a *PZ* sensor can be a bit more complex than a simple RC circuit. Could deconvolution be used to obtain a better pressure waveform?
This issue will be addressed in chapter 4.
- All parameters that could be expressed in absolute units suffer from the non-calibrated nature of the *PZ* sensor. So, the question has to be - is there any possible technique capable of calibrating the *PZ* sensor probe output in such a way that parameters such as arterial pressure could be expressed in pressure units?

In chapter 5, some possible answers to this question will be tried out.

INTEGRATION vs. DECONVOLUTION

This chapter deals with the experimental determination of the *impulse response* of the *PZ* probe and with the use of this function in a deconvolution algorithm that computes the pressure pulse.

A brief discussion about whether, the pulse obtained by integration or the one obtained by deconvolution, is the best estimate of the real pressure pulse, is also made.

4.1 Motivation for the Experiment

As was referred in the section 2.4.3, for the majority of its applications, a *PZ* sensor can be modelled as a simple RC circuit. It is therefore reasonable to infer that a *PZ* sensor behaves like a simple differentiator and the information it delivers has the physical meaning of a velocity. To obtain the originating signal, a time integration is mandatory and its result represents the displacement of the sensor surface imposed by the surrounding tissues. This displacement has been demonstrated to be linearly related with the pressure pulse^[38].

However, we must realize that the simple RC model may be far from reality, and even more so when the sensor is mechanically attached to a structure, as is the case in our probes.

So, an alternative method, based on the deconvolution concept, was devised in order to obtain a more precise pressure pulse.

As the method requires the knowledge of the *impulse response* of the sensor-in-the-probe, a special purpose experimental set-up had to be developed to obtain this information.

4.2 Deconvolution Method

4.2.1 General Concepts

In general, the object of deconvolution is to reverse the effect that a specific system exerts on its input signal^[39]. Normally, the output data of the system $y(t)$ is known, and is related to its input $x(t)$, by means of a convolution product:

$$y(t) = x(t) * h(t) \quad (4.1)$$

where $h(t)$ is the *impulse response*, *IR*, of the system.

As deconvolving in time domain is rather complex, the frequency domain is used instead to solve the expression above. The convolution theorem applied to the previous expression yields

$$Y(j\omega) = X(j\omega) \times H(j\omega) \quad \text{or} \quad (4.2)$$

$$X(j\omega) = Y(j\omega) / H(j\omega) . \quad (4.3)$$

where $H(j\omega)$ is the system's transfer function, the Fourier transform of IR .

Once $H(j\omega)$ and $Y(j\omega)$, the *FFT (Fast Fourier Transform)* of the recorded signal, are known it is possible to find $X(j\omega)$ and, hence, $x(t)$ is readily obtained.

In our particular case, the input $x(t)$ to be assessed is the arterial pressure pulse while $y(t)$ is the measured *PZ* sensor output. To obtain $h(t)$ we have to follow the theoretical principles by exciting our system with a Dirac like mechanical impulse, $\delta(t)$. In Figure 30, that depicts the relationship between the signals, $y(t) = h(t)$ when $x(t) = \delta(t)$.

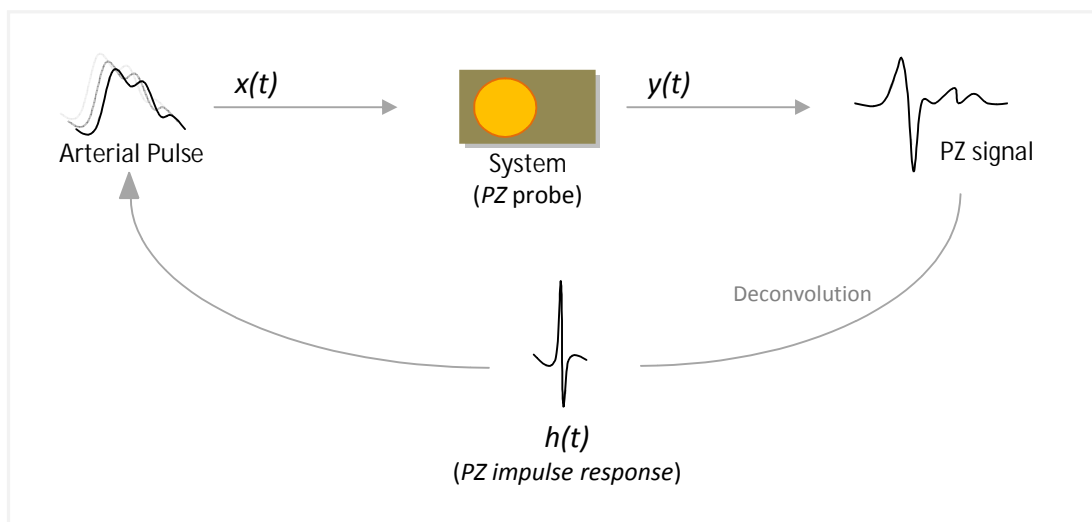


Figure 30. Schematic of the deconvolution process.

4.2.2 Experimental Settings

To obtain IR experimentally, some equipment capable of exciting the system with a Dirac like impulse had to be purchased: a piezoelectric actuator⁵ (Pst-HD200/10/45 VS15, Piezomechanik GmbH) with a maximum stroke of 70 μm and the corresponding high voltage generator (HVP switcher, Piezomechanik GmbH).

5. Basically the functioning of a *PZ* actuator is the inverse of a *PZ* sensor, converting electric inputs into displacement.

A programmable pulse generator (Agilent©) was also used to trigger the HVP switcher action as shown in Figure 31.

To acquire IR data, the piston of the PZ actuator was held against the centre of the PZ sensor, both standing on a table, and the experimental assembly schematized Figure 31 was set up. The PZ actuator signal is conditioned by a buffer circuit (Figure 32) which stands inside the acquisition box.

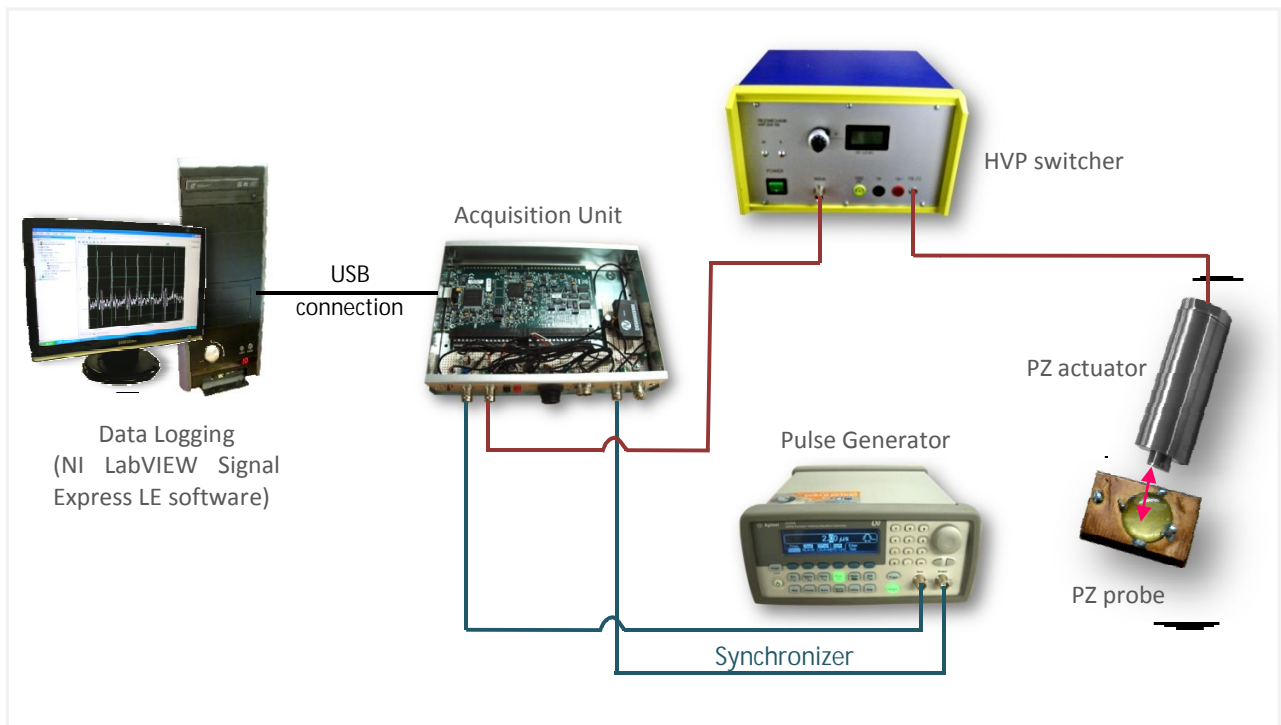


Figure 31. Scheme of the experimental assembly for the IR acquisition.

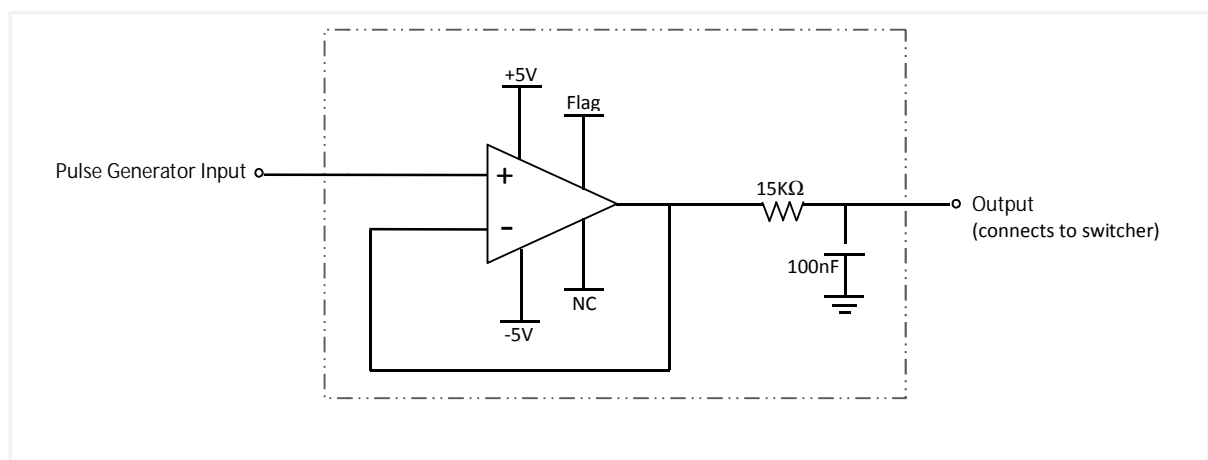


Figure 32. Veroboard circuitry - Buffer circuit.

The PZ probe signal follows the normal procedures: it is logged with the software tool provided by the NI USB-6210© and processed using MatLab® routines.

Note that a synchronism between the pulse generator and the acquisition unit is forced in order to log only the interesting portions of the signal. For that, the pulse generator output is directly connected to an input of the NI USB 6210©. This input is programmed, by means of the NI software, in order to achieve the referred synchronism.

4.3 Integration Method

Although integration is a well established concept, different results can be obtained when using real signals, depending on the upper and lower limits selected to perform the operation (see Figure 33).

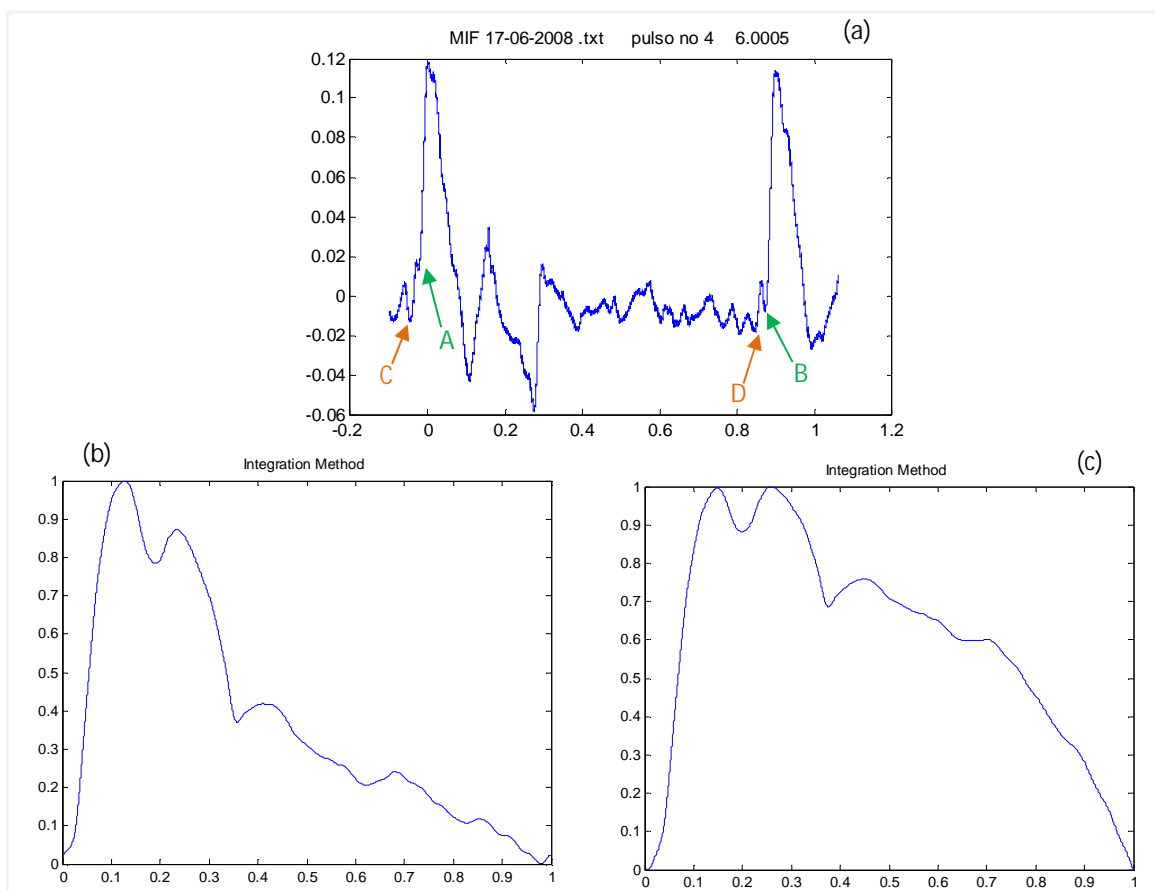


Figure 33. Influence of the integration points.
(a) PZ Carotid pulse; (b) arterial pulse obtained by integration method using the points A and B from (a); (c) arterial pulse obtained with integration method using the points C and D from (a).

Two routines have been developed to process the *PZ* pulse integration. The first one, of a more automatic nature, the program selects two consecutive maximums from the recorded signal and integrates between these points. The other routine needs the operator to select the beginning and the end of the segment to be integrated. As might be expected results strongly depend on the two selected points the integration results will be different as can be seen in Figure 33.

4.4 Results

4.4.1 PZ Probe Impulse Response

Figure 34 and Table V shows a typical *PZ IR* obtained with the experimental set-up just described in 4.2.2.

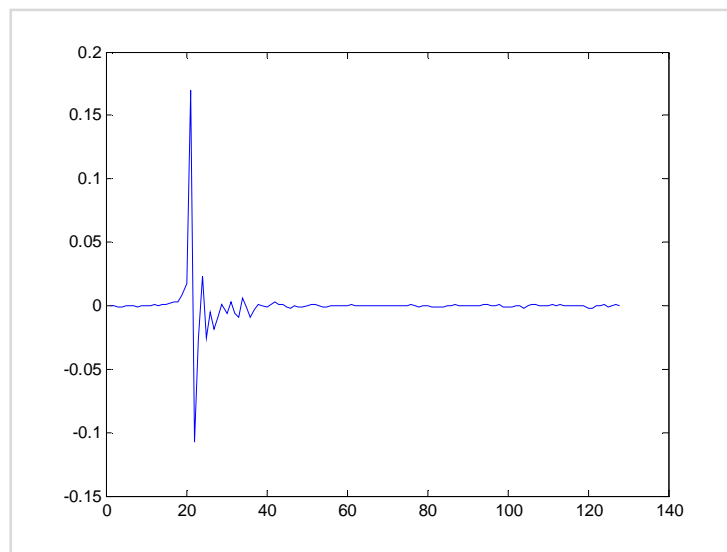


Figure 34. PZ probe IR.
The y-axis represents the amplitude. Each point of the x-axis represents $1/(\text{Sample Rate})$ or $50 \mu\text{s}$.

Table V. Impulse main characteristics

Characteristic	Equipment	Value
Width	Agilent©	2 μ s
Edge Time	Agilent©	12,5ns
Frequency	Agilent©	0,2Hz
Sample Rate	NI USB-6210©	20KSpss
Digital Filter	MatLab®	50Hz (band cut-filter)

The obtained *IR* was processed by a simple routine where the 50Hz interference was eliminated. Despite ringing, it has a shape very close to the one of a RC circuit *IR*.

4.4.2 Arterial Pulse

The *PuScope* developed software uses the *IR* in its deconvolution algorithms in a manner that is transparent to the user. The *IR* is stored in the working directory under a fixed name and is loaded whenever necessary.

It is worth noting that the average value of *IR* has to be zeroed for better results.

Following, in Figure 35, a somewhat noisy *PZ* pulse acquired at the carotid side is shown (a) alongside with the two pressure pulses obtained by integration and by deconvolution (b) and (c), respectively.

Again as expected, their shapes are very similar.

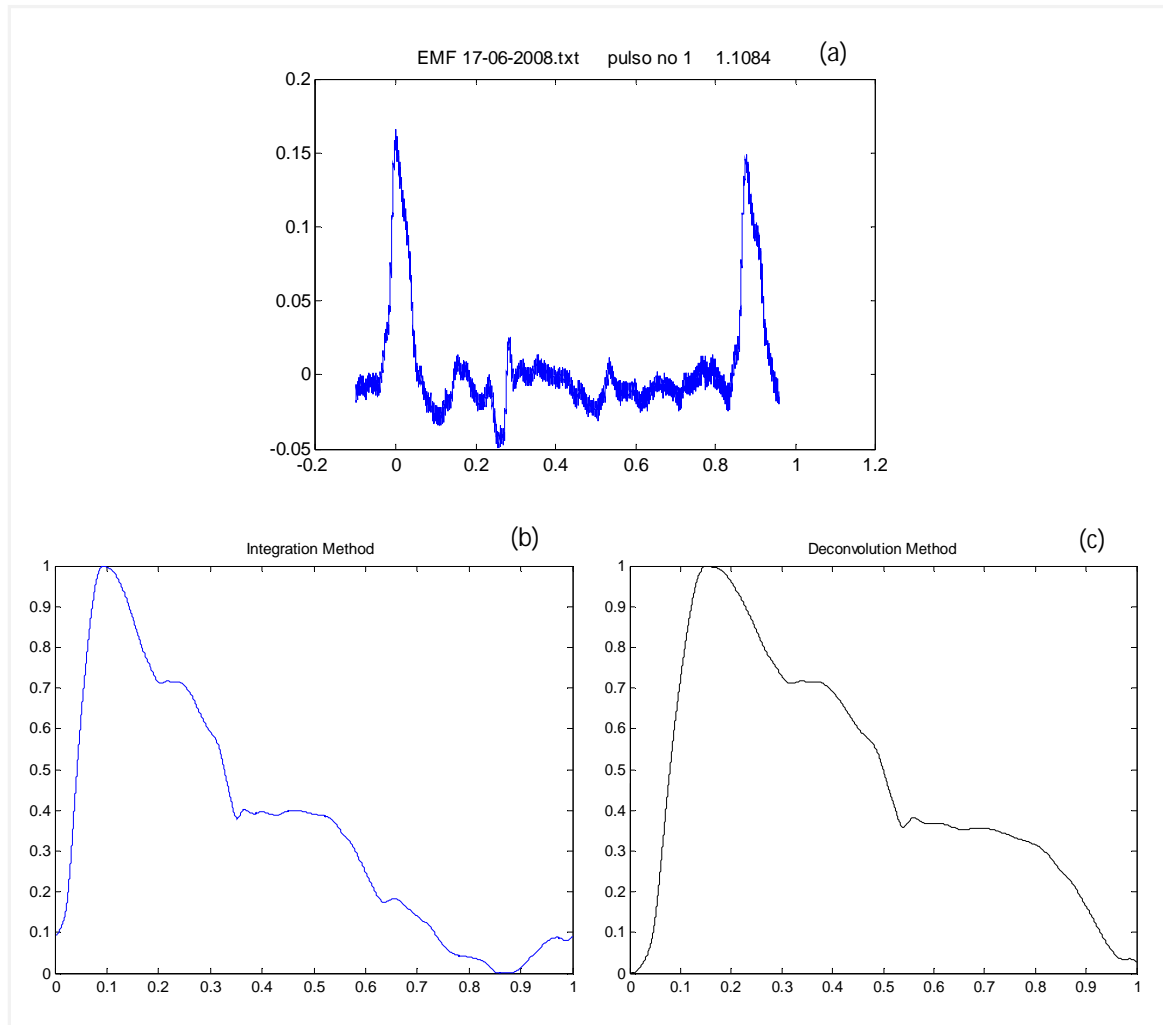


Figure 35. Integration and deconvolution results. (a) PZ carotid pulse; (b) Pressure pulse obtained by integration and (c) with the deconvolution method.

4.5 Discussion

From the vast set of signals that have been analysed, it is possible to conclude that both integration and deconvolution methods give similar results with a slight advantage to deconvolution that yield the “cleaner” results as can be observed in Figure 35.

However, the main difference comes from the fact that while integration strongly depends on the upper and lower limits selected (either automatically or by the operator) as shown in section 4.3, deconvolution does not.

Deconvolution circumvents this problem because it is processed with a *PZ* pulse longer than the real one. Another interesting advantage, that is apparent by observation, is that when the arterial pulse is built from deconvolution, it is easier to observe where it begins and ends.

In chapters 7 and 8, the same problem will be analysed under the perspective of hemodynamic parameters determination.

PIEZOELECTRIC PROBE CALIBRATION

This chapter describes an experimental approach to the calibration of the *PZ* probe. In a first step, it is shown that the sensor surface displacement is linearly related with its integrated or deconvolved output. Then, a comparison between arterial pressure as given by a commercial sphygmomanometer and by the *PZ*, is made.

Results are shown and a discussion is made about the feasibility of *PZ* calibration.

5.1 Motivation for the Experiment

When this work started it was clear that *PZ* sensors had a strong calibration limitation mainly due to the very complex relationship between the electrical output and the forces that activate the sensor surface. This makes it very difficult, if not impossible, to assess, for example, systolic pressure in absolute pressure units.

Alternatively a calibration technique, based on displacement rather than pressure, can be tried out since it is well established that a linear relationship exists between pressure and displacement^[38]. This approach lends itself to experimental trial with the instrumental means available for this work and, in the end, it can yield useful results from the hemodynamics point of view.

5.2 Calibration Method

5.2.1 Concept

In order to perform calibration a standard mechanical excitation of the sensor must be organized. For this purpose it is assumed that if the sensor surface is displaced by a certain amount, a voltage appears at the *PZ* output. If this displacement is known and if it is applied in a constant well determined way, the corresponding *PZ* output can be measured and the input-output behavior of the sensor can be plotted as a displacement vs. voltage relationship. To this end, the equipment described in the deconvolution experiments (chapter 4) can be used.

In fact, the HVP switcher and *PZ* actuator (see section 4.2.2) can be configured so as to strike the *PZ* probe with a well determined displacement.

Assuming that the displacement provided by the actuator can be coupled to the *PZ* sensor with no errors, it will be possible to sweep a range of values of displacement in order to obtain the *PZ* sensor displacement vs. voltage curve up to the 70 μm maximum, for the actuator model in use.

It is convenient to bear in mind that the previous assumptions need further verification. For example, the values for displacement are taken from the assumption of a 70 μm displacement at maximum DC bias at the switcher, but no actual displacement measurement has been done.

5.2.2 Procedures

The experimental assembly was the same as used for the deconvolution experiment (see Figure 31, from section 4.2.2). However, while in the deconvolution experiment an arbitrary DC value was used (since the amplitude of the *impulse response* was not important for the deconvolution method) in this case, on the contrary, special attention was paid to the HVP switcher DC level settings.

It is also assumed, and seems reasonable, that the displacement of the actuator is linearly proportional to the DC level of the switcher. This linearity can fail for DC values close to zero but is expected to verify for the rest of the 0 to 200V range.

Figure 36 shows the voltage amplitudes for a few DC levels of the switcher, each point of the plot representing an average of 6 measurements.

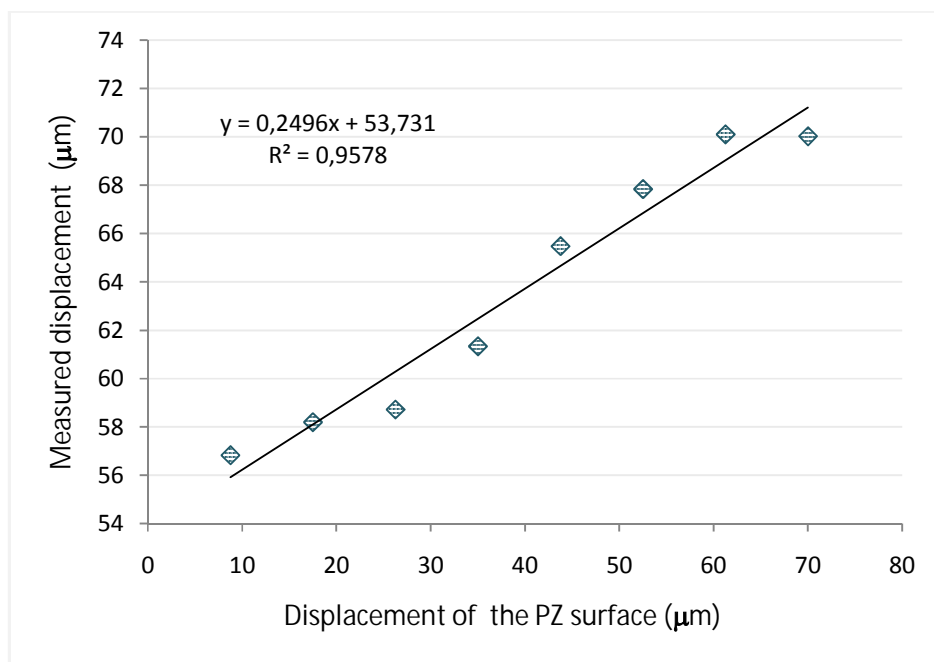


Figure 36. Input-output relationship of the PZ sensor. The input (sensor surface displacement) is taken from the DC level. The output values are measured by the probe and processed by the software. Below 25V DC the curve is strongly non-linear and is not shown.

While the displacement values are represented by the DC levels, the *PZ* displacement is derived as the peak value of the time integral of the *PZ* sensor output. This operation has been performed using the capabilities of the developed *PulScope* software.

The main settings of the experiment are summarized in the following table:

Table VI. Experiment Settings

Characteristic	Equipment	Value
Pulse width	Agilent©	1ms
Edge Time	Agilent©	12,5ns
Frequency	Agilent©	1Hz
Sample Rate	NI USB-6210©	100KSpss
Digital Filter	MatLab®	50Hz (band cut-filter)
DC level	HVP switcher	200 V

The following figures, Figure 37 and Figure 38, show the *impulse response* obtained with the presented experimental settings (table VI) and the integrated *impulse response*, respectively.

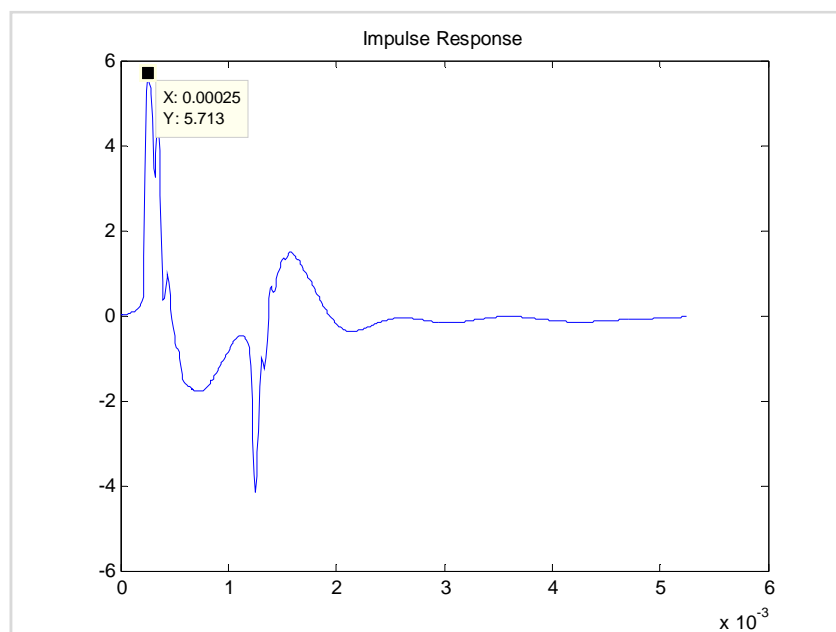


Figure 37. Impulse response (200V DC).
The absolute maximum value is signaled in the graphic.

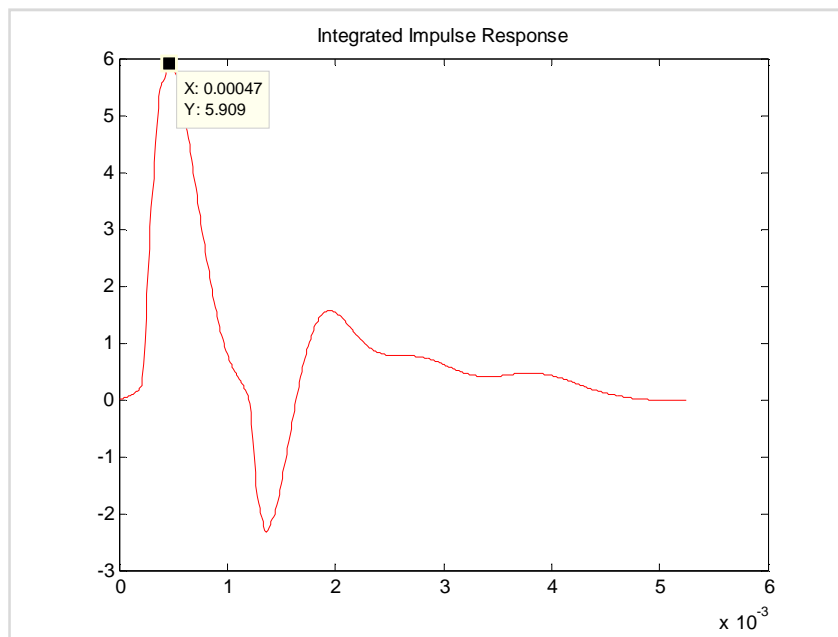


Figure 38. Integrated impulse response.
The absolute maximum value is signaled in the graphic.

5.3 Carotid Signals

The presented method was also applied to the already recorded carotid signals. The following figure (Figure 39) shows the *PZ* pulse and integrated pulse with no calibration and with a calibration in terms of displacement, respectively.

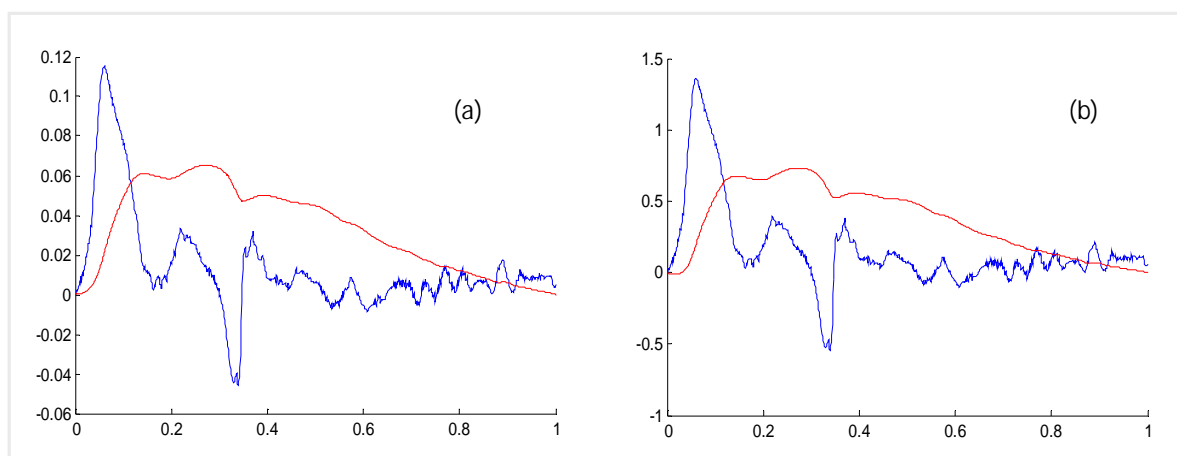


Figure 39. Y-axis calibration in terms of displacement.
(a) *PZ* signal (blue) and arterial pulse (red) without any y-axis calibration; (b) the same *PZ* signal (blue) and the same arterial pulse (red) with y-axis calibration in terms of displacement.

Carotid signals were also acquired for comparison with arterial pressure values measured with a commercial unit (happy life[®], Germany), a B-class pressure device, that complies with EU guidelines.

Table VII. Maximum mean displacement, pulse pressure and systolic pressure obtained results. The mean maximum displacement, for each recorded signal (1KSpss), was obtained calculating the mean of 10 integrated pulses maximum displacement.

Carotid Signal	Maximum Mean Displacement (μm) (<i>PulScope</i> - 10 pulses)	Pulse Pressure (mmHg) happy life [®] device	Systolic Pressure (mmHg) happy life [®] device
1 - A	0,66	31	104
1 - B	1,425	52	121
1 - C	1,072	45	108
2 - A	0,908	34	103
2 - B	0,565	43	114
2 - C	0,484	28	107
3 - A	1,502	46	121
3 - B	1,38	43	110
3 - C	1,088	27	103
4 - A	2,962	40	115
4 - B	1,502	34	118
5 - A	1,486	49	120
5 - B	0,456	39	106
5 - C	0,569	41	115
6 - A	1,779	52	129
6 - B	1,343	45	118
6 - C	1,09	43	113
7 - A	0,663	56	124
7 - B	0,62	27	104
8 - A	0,789	37	97
8 - B	0,205	37	99
9 - A	2,338	56	154
9 - B	2,731	63	157
9 - C	2,611	48	147
10 - A	0,145	28	95
10 - B	1,544	53	123
10 - C	1,639	57	119

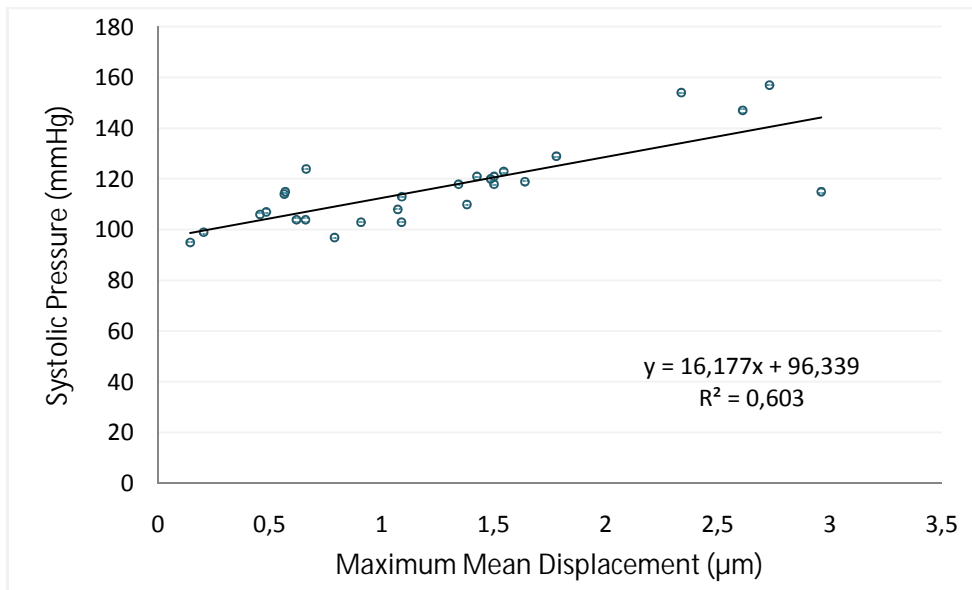


Figure 40. Relationship between the maximum displaces and the systolic pressure. Scattering (blue); calibration curve (black) and its equation and correlation coefficient.

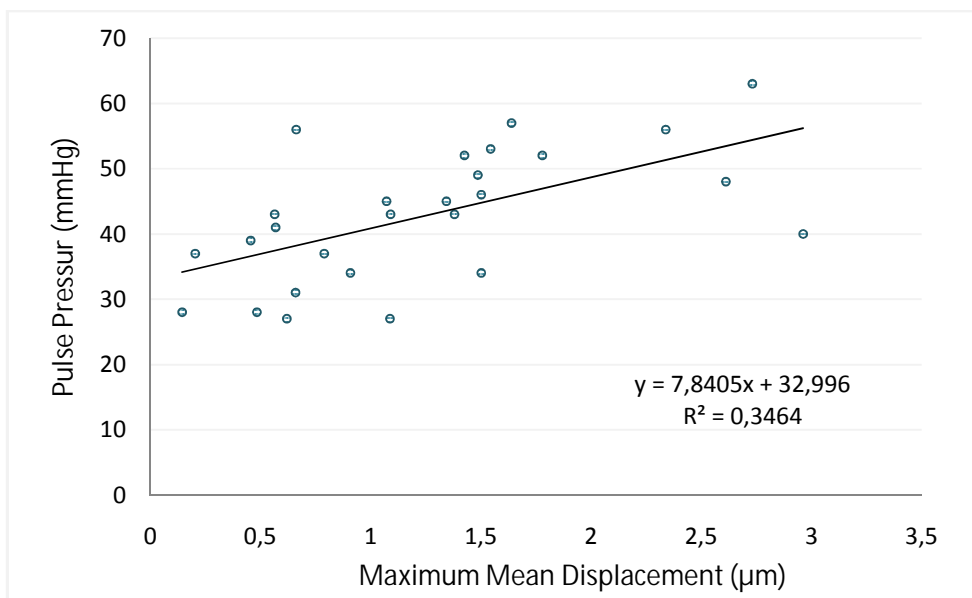


Figure 41. Relationship between the maximum displaces and the pulse pressure. Scattering (blue); calibration curve (black) and its equation and correlation coefficient.

5.4 Discussion

First of all it should be stressed that all the elapsed experience needs many more tests, confirmation and validation. The main purpose of its conception was to show that a *PZ* probe calibration may not be as impossible as it seems, since even for this quite simple experiment, the results show a possible window of opportunity to solve the ongoing problem.

The idea was to calibrate the y-axis of an integrated or deconvolved arterial pulse in terms of displacement. It should then be possible to assess parameters such as arterial pressure, since displacement and pressure have a direct relationship.

To begin with, the linear direct relationship between the DC output level of the HVP switcher of the switcher and the *PZ* voltage output was verified. As it can be shown in graphic of Figure 36, the relation is indeed approximately linear above 25V DC. In addition, it was assumed that the maximum stroke should occur at the maximum DC level.

Driving the *PZ* sensor with a short impulse (1ms) with maximum amplitude (200V DC) should correspond to a maximum displacement of 70 μ m. Under these conditions the *PZ* voltage is about 5,9V obtained from the absolute maximum voltage value of the integrated *PZ* signal. So, a scale factor of 70/5,9 μ m.V⁻¹, calibrates the y-axis of the pulses in terms of displacement.

As is known from the literature, the arterial pressure values are assessed from an arterial pressure pulse. The systolic pressure corresponds to the absolute maximum of the arterial shape, and the diastolic pressure corresponds to the second relative maximum. It was thought it would be not possible to assess the displacement values, corresponding to the systolic and diastolic pressure, with the drawn experiment. In fact, the implemented software routines plot the beginning of the arterial pulse, which correspond to the absolute minimum, i.e. to the diastolic value, in a constant value reference: zero. Hence, even multiplying by a calibration factor, the pulse shape will always initiate at zero. Nevertheless, assessing the absolute maximum displacement, and once the minimum of the shape is zero, corresponds to the pulse pressure (systolic pressure minus diastolic pressure). So, it was thought it should exist a direct relation between the absolute maximum displacement of a calibrated curve and the pulse pressure, measured by the happy life[®] device. However, the results revealed something apparently different.

As can be observed in table VII and in the scatterings of Figures 40 and 41, contrarily to what was thought initially, a stronger correlation exists between the maximum displacement and the systolic values than between the first and the pulse pressure. Taking into account the experiment conditions, the obtained correlation coefficients were satisfactory. Nevertheless, until the experiment can be repeated with the appropriate settings, these results deserve little credit.

It is relevant to refer that an effort was made to apply a constant load when the carotid signals were acquired. For that reason the operator was the same for each recording. However, as can be imagined, this methodology introduces a lot of incoherencies and errors. Unless a technique is found that guarantees a constant load, with no mediation from the operator, it will not be possible to perform an accurate calibration. It is also advisable that the device used to measure arterial pressure should be an A-class instrument for better accuracy.

A second experiment to validate these preliminary results should also include more subjects, and a larger number of signals for each subject. The arterial pressure should also be measured several times along the recording, since 5 minutes acquisition is a long enough period to verify meaningful arterial pressure variations.

Further approaches may calibrate the y-axis in such a way that it could be possible to achieve independently the systolic and diastolic pressure values. For this purpose, two independent calibration equations would be required; one for the minimum displacement values (diastolic pressure) and other, which can be derived from the same experiment, for the maximum displacement values (systolic values).

SOFTWARE ANALYSIS TOOL

This chapter presents general aspects of the software tool, the *PulScope*, which has been specially developed along this work. Its main functions will be explained and some of the theoretical aspects behind its construction will be discussed. The last section refers some functional errors detected in tests and draws a few suggestions for improvements that can be implemented in the short term.

6.1 General Performance

The developed MatLab® software is oriented in a pop-up menu philosophy that starts after a *Master Routine* has initialized the system, as described in 6.2.1. The first pop-up menu directs the user to one of three possible analysis types called, respectively:

- *Single Pulse Analysis* – dedicated to a pulse-to-pulse based analysis (see 6.2.2);
- *Local List Analysis* – in which a set of pre-selected pulses is analyzed (6.2.3); and
- *Global Analysis* – for the analysis of all pulses of a given data set (6.2.4).

Each of these options takes the user to other menu sublevels where several functions have been implemented to determine different hemodynamic parameters.

This software tool was developed to be used by a skilled user, meaning that it was not intended to be a typical commercial pack. In fact its main purpose is to support the analysis of hemodynamic data collected with the sensors that are under study.

Nevertheless, all the software structure was designed so as to make it easy to implement new functions, even by different programmers, and it can be the base of a future commercial pack that accompanies the hardware.

6.2 Software Structure

6.2.1 Master Routine

To start the software tool, a preliminary master routine must run.

Firstly, it permits the operator to select the data file to analyze and, only in the very first run, a function dedicated to the determination of the instants in time when the peak of each pulse occurs is

executed. When the all peaks are identified, an auxiliary file – called *MaxFile* – with the series of peak instants is created for further reference by other routines.

When a *MaxFile* already exists this step is skipped and the program continues showing a window that plots the entire recorded (carotid) signal and another that corresponds to the first level popup menu (see Figure 42). At the first window some additional information is shown: the total number of pulses, the total recording time and the heart rate, *HR*, frequency. The pop-up menu permits the operator to select (by clicking a button) one of the three analysis levels to undergo or, alternatively, exiting. This menu also features a box to introduce the sample rate of the signal.

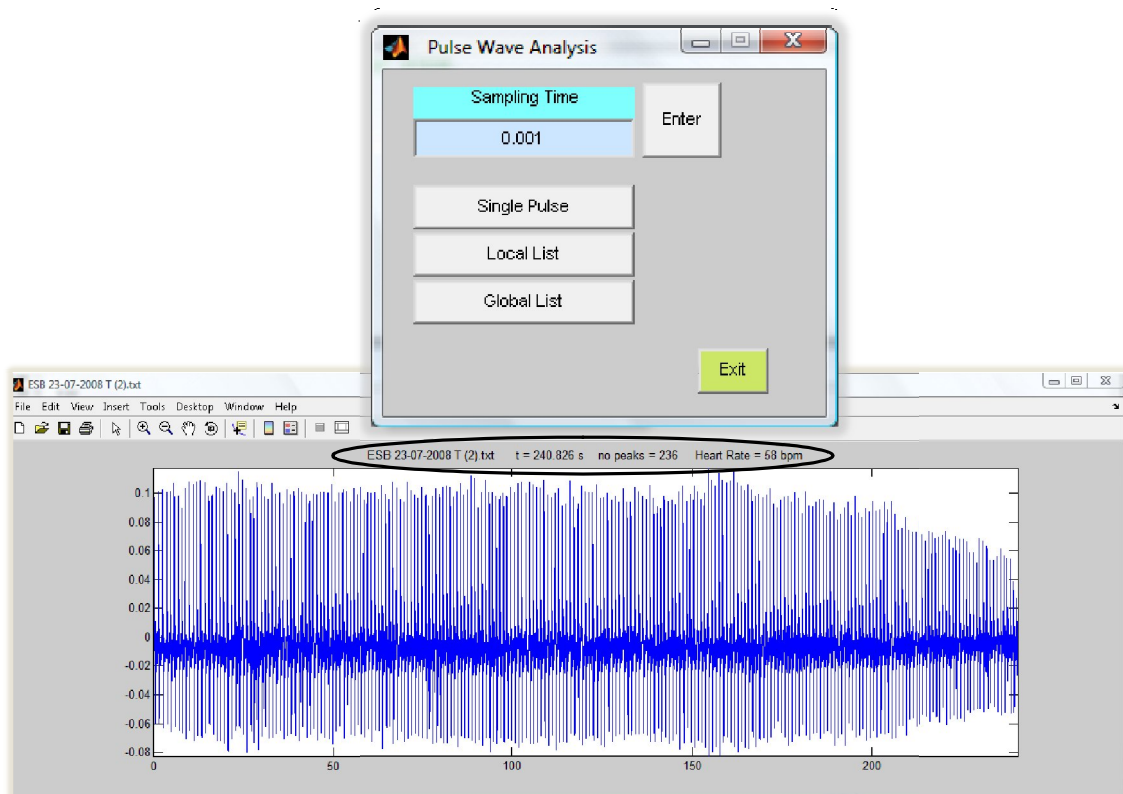


Figure 42. First pop-up menu with a real carotid signal acquired for about 250s. The parameters inside the black curve are: the file name, the total time, the number of pulses and the *HR*. Clicking one of the buttons *Single Pulse*, *Local List* and *Global List* sends the user to the corresponding 2nd level menu.

6.2.2 Single Pulse Analysis

This 2nd level menu (Figure 43) sends the operator to a pulse-by-pulse analysis. It contains several functions; some of them have to follow a specific execution order.

The basic function of this menu is the visualization of single pulses, by clicking *Next*, *Previous* or *Select* buttons. Saving the current visualized pulse in a .txt file is also possible. The other operations are: integration, deconvolution and *AIx* or *PWV* determination. It is convenient to note that these operations are executed over a single pulse. Alternatively the operator may click the *Back* button, and the software returns to the previous pop-up menu.

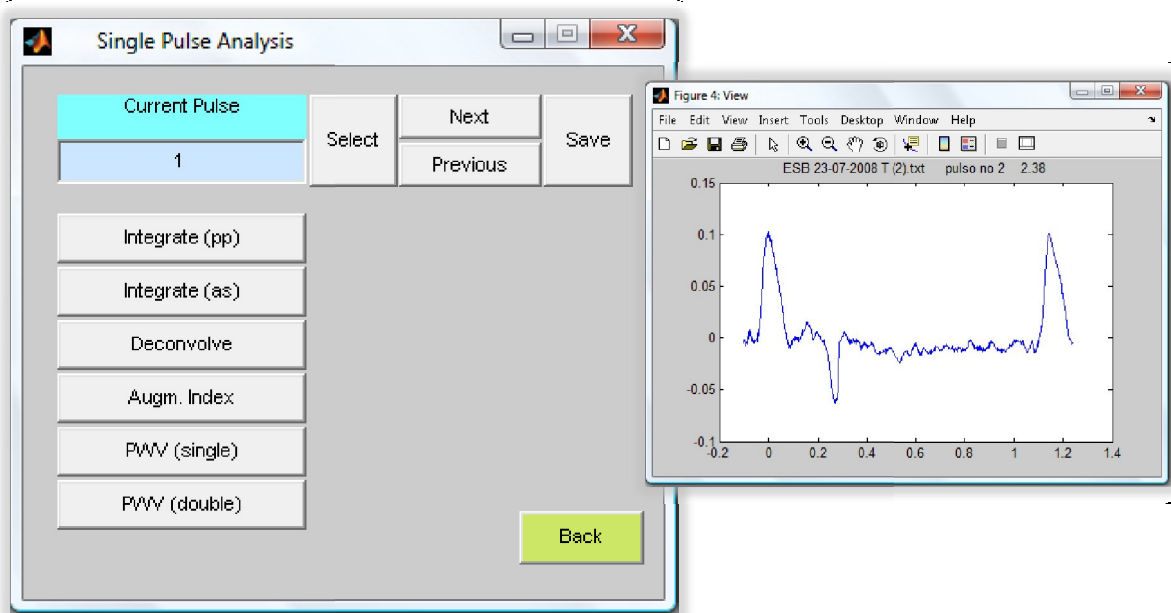


Figure 43. Single pulse analysis pop-up menu and current pulse view.

By writing the number of a specific pulse in the blue box of the popup menu and clicking the *Select* button it is possible to view any pulse in the window on the right. The default pulse, in the blue box, is the first pulse of the recorded signal. Alternatively, the *Next* and *Previous* buttons can be clicked to see the following and previous pulses, respectively.

Two types of integration have been implemented: one, that could be named automatic integration, – *Integrate(pp)* button – integrates a pulse between two consecutive absolute maximums. The other needs the operator intermediation – *Integrate(as)* button. The operator must select the initial and final instants of a pulse, by placing the cursor on the appropriate coordinates and clicking the ‘A’ and ‘S’ key respectively.

Deconvolution is a straightforward procedure that gives a similar result (see chapter 4). At this stage, the *impulse response* is also shown in the window (see Figure 44).

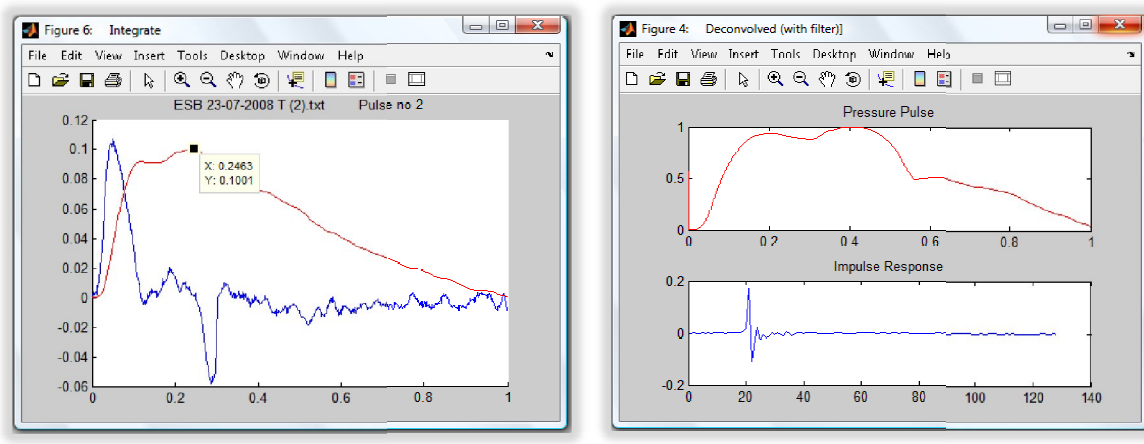


Figure 44. Integration and deconvolution windows. The left-hand window shows the initial pulse (blue) and the result of an integration (red). This window appears when the *Integration(as)* button is clicked. The right-hand window shows the result of a deconvolution (red pulse) and the impulse response (blue) used in the operation. This window appears when the *Deconvolve* button is clicked.

The three buttons *Augm. Index*, *PWV (single)* and *PWV (double)* start routines that assess the corresponding hemodynamic parameters. They all require that the pressure pulse has been previously computed either by integration or deconvolution. If this does not verify, an error message is generated.

In addition, *PWV* determination requires *Aix* to be determined first, since it uses variables from the latter. Again, an error message warns the operator if this fails to verify.

Aix determination requires the operator to select, using the cursor, the instant when the *reflected wave* occurs. The *reflected wave* is then signaled in the corresponding window and the *Aix* value, in percentage, in a second window. The two types of *PWV* determination do not require any operator intermediation. By clicking the respective buttons the *PWV* values are plotted in a window.

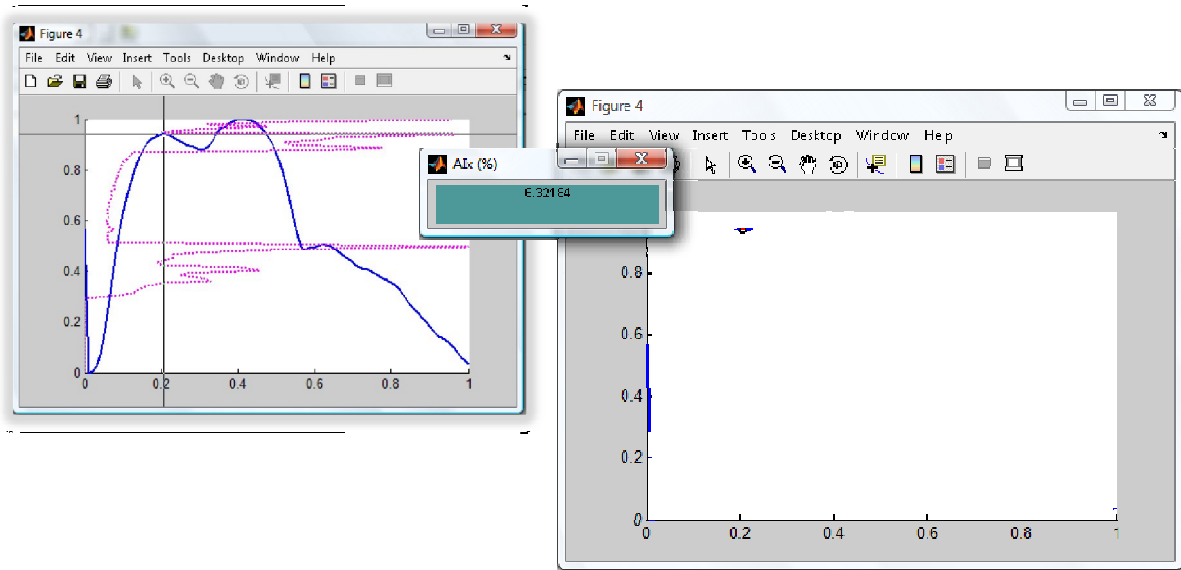


Figure 45. Alx determination windows. The left-hand window shows an arterial pulse (blue), the probability density function, pdf , of the pulse (magenta). The cursor for selecting the *reflected wave* is also shown. The pdf helps the operator to select the right arrival instant of the *reflected wave*. The right-hand window shows the arterial pulse with the *reflected wave* signaled by a red dot and the Alx value in a separated smaller window.

The theoretical concepts behind these hemodynamic routines construction will be later explained in section 6.3.

6.2.3 Local List Analysis

The *Local List* button on the first pop-up menu (Figure 42) starts a different menu pops up. It permits the operator to visualize pulses one by one, and to include the pulses he wants in a local list (*Add to list* button), (Figure 46). Removal from the local list is also possible (*Remove last entry* button). The *Back* button exits, and the program returns to the first pop-up menu.

Once the local list is built an average pulse can be computed. The operator has an option between two different types of average pulses: a normal average pulse, which adjusts pulses by their absolute maximums, or a time adjusted average pulse, which adjusts the pulses in time by means of an interpolation algorithm. The radio buttons *Normal* and *Time Adjust*, are meant to distinguish between the two cases.

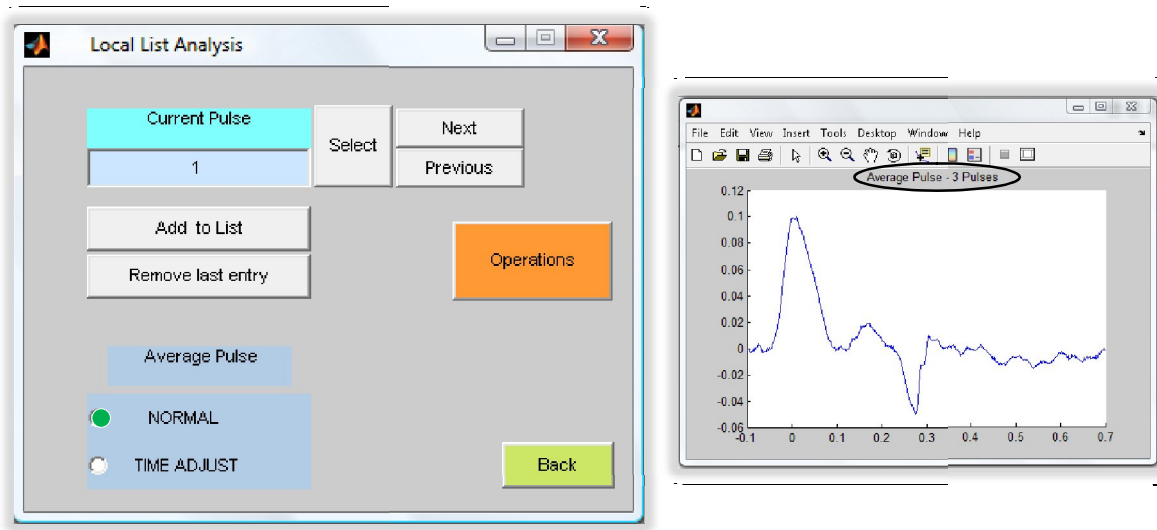


Figure 46. Local list analysis pop-up menu and normal average pulse. The left-hand window shows the local list analysis pop-up menu with the radio button selected for a normal average pulse execution. The right-hand window shows the result of a normal average pulse over 3 pulses. The number of pulses involved in the average calculation is shown on the graphic's top (inside the black curve).

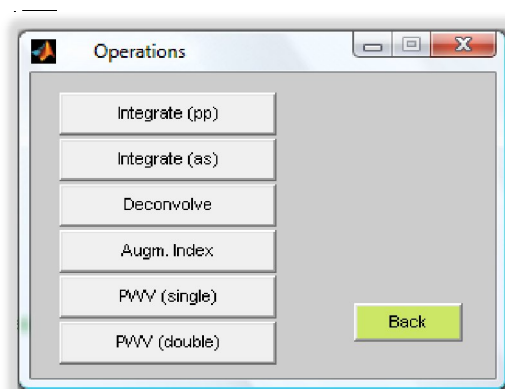


Figure 47. Operation pop-up menu for the local list analysis.

Once one average pulse is built, the operator can start analysis with the *Operations* button that pops up the *Operations* menu (Figure 47) with the same functions as the single pulse analysis. The *Back* button returns to the local list analysis menu for building a different local list, selecting another type of averaging or going back to the initial menu.

6.2.4 Global Analysis

The *Global List* button starts the global analysis menu (Figure 49). The philosophy behind this menu is starting with all pulses and, then, using *Remove from list* button to delete unwanted pulses from the list. The edited list can be saved (*Save list* button) for future reference. A *Reset* button sends the list back to the initial state where all pulses are considered.

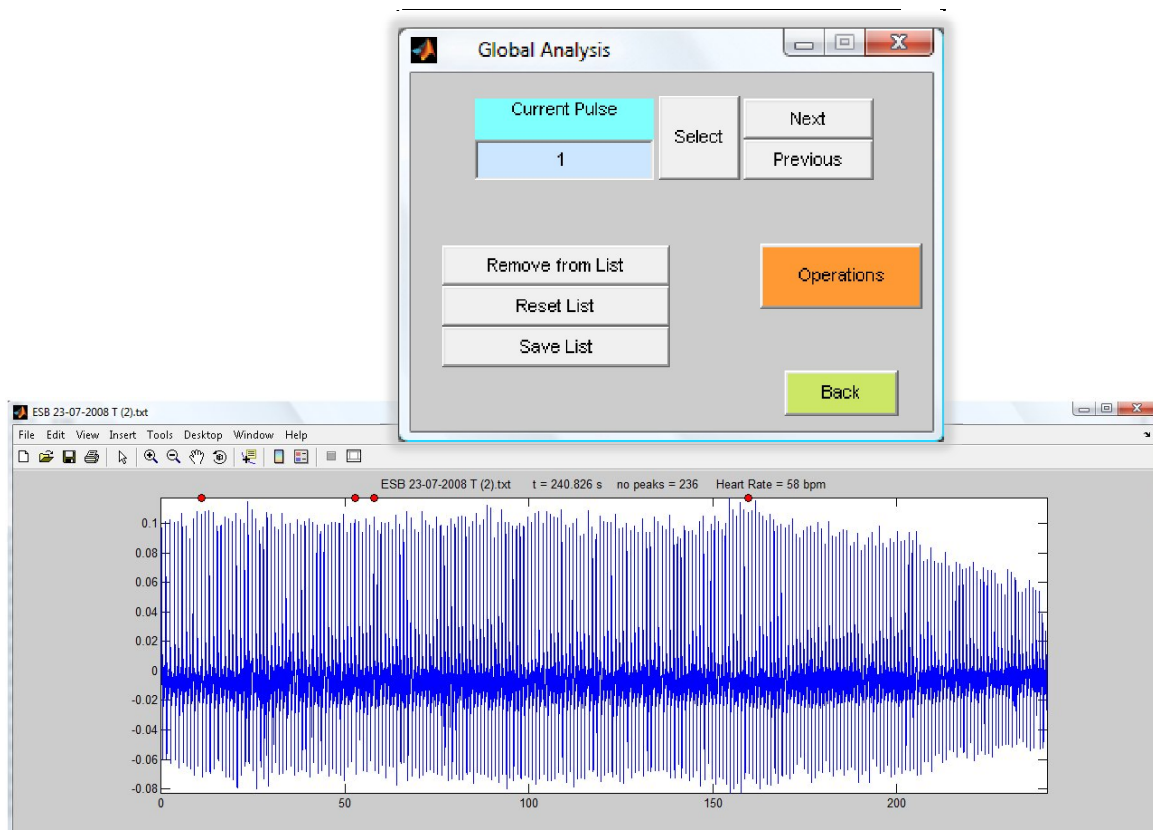


Figure 48. Global analysis pop-up menu and analysing carotid signal. The *Remove from list* button, on the popup menu (top window), plots a red dot above the eliminated pulse.

The edited list or the list without any alterations can be analyzed in the *Operations* menu (Figure 49). At this stage, only two operations are available: 1) the *Heart Rate Variability* that plots the *HRV* and the respiration signals and gives the *HRV* value in the time domain (Figure 50). A second window is also shown with the *HRV* and respiration signals in the frequency domain (Figure 51). The *Spectrogram* button is planned but requires some more test work to be in a useful status.

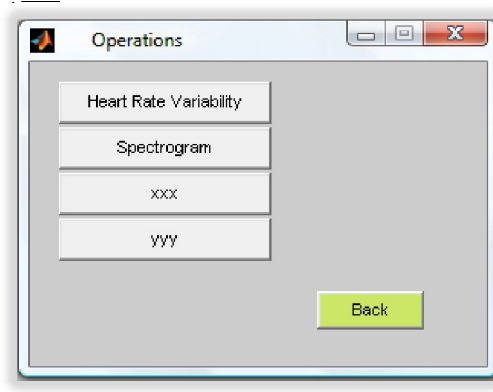


Figure 49. Operation pop-up menu for global analysis.

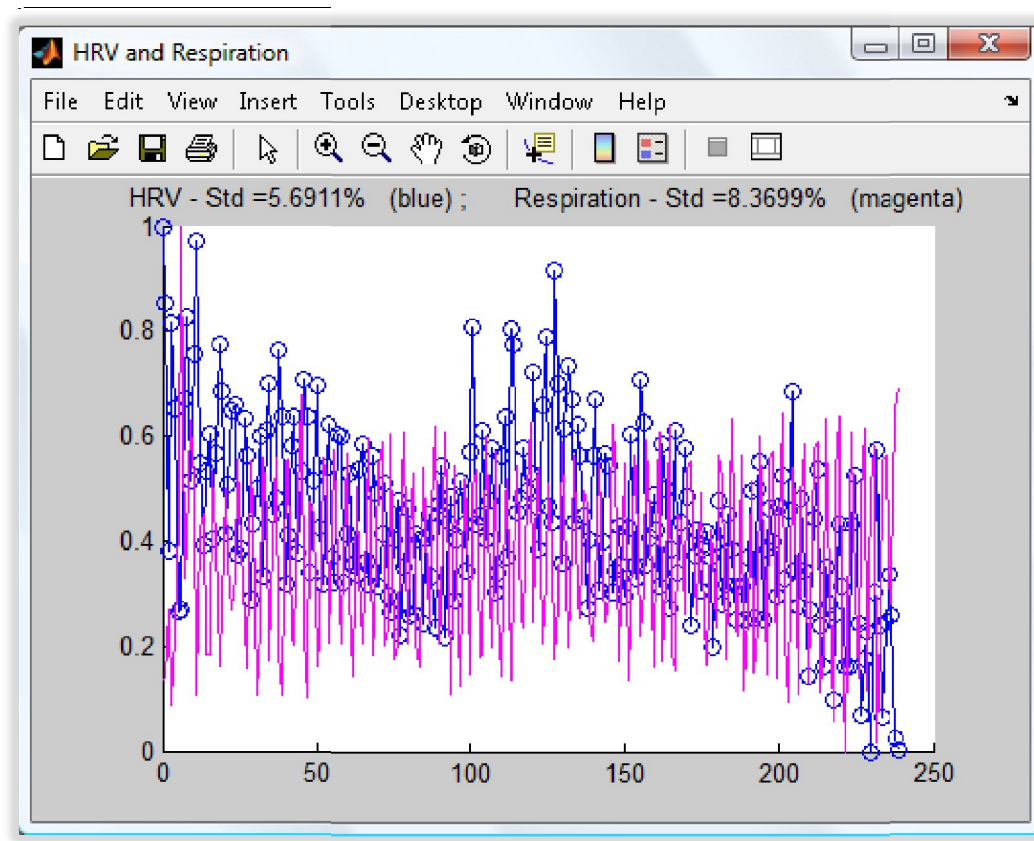


Figure 50. HRV and respiration signals (time domain).
The HRV value (standard deviation) and the respiration standard deviation are shown at the graphic top.

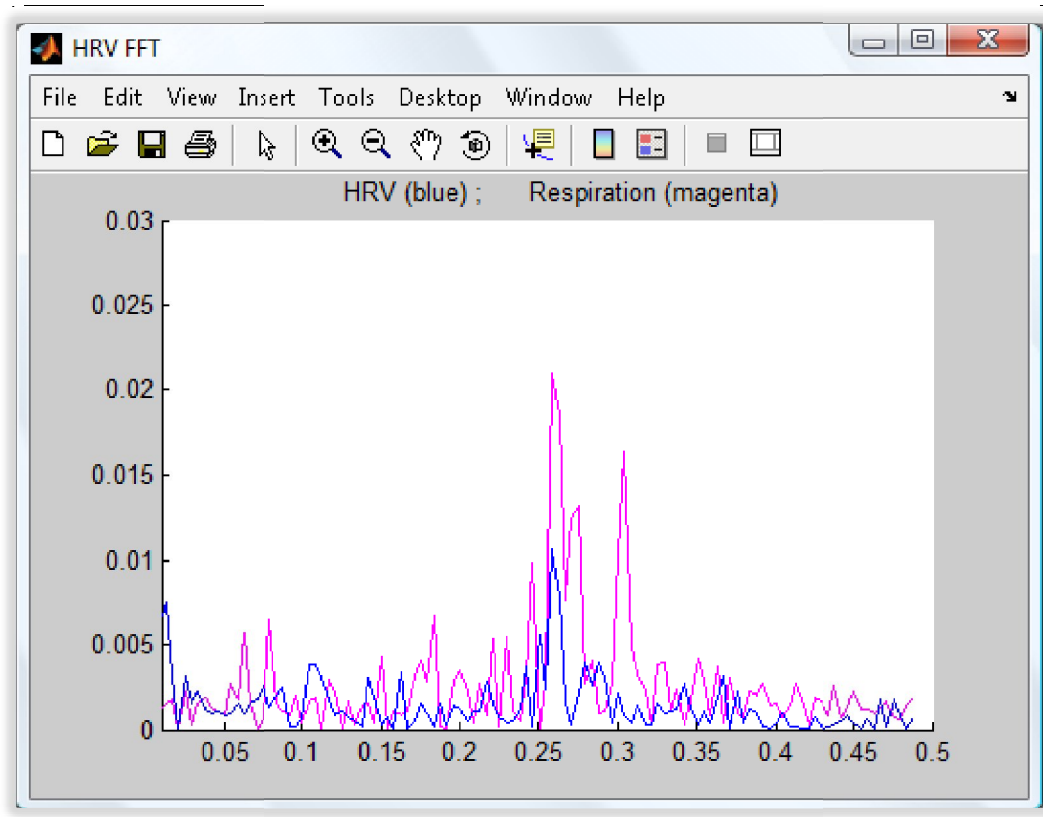


Figure 51. HRV and respiration signals (frequency domain).

6.3 Theoretical Background for some Software Routines

The routines written for the hemodynamic parameters determination were based on theoretical concepts, most of them exposed in chapter 2. However, since the way these parameters are accomplished is an integral part of this work, a brief explanation about their elaboration will be given.

6.3.1 HR

The heart rate, *HR*, as the name implies, is the frequency at which the heart beats. As each pulse of the carotid signal corresponds to an individual cardiac cycle (or heartbeat), it is rather simple to determine how many pulses occur per minute. The *HR* routine computes the *FFT* of the entire signal and finds out the abscissa of the amplitude spectra maximum in the range between 0.5 and 3 Hz. Some

subjects, namely the ones with high heart rate variability, *HRV*, may pose particular problems since their amplitude spectra does not show a clear maximum in the *HR* location but, rather, a cluster of scattered maxima. Some might even show the maxima in a high order harmonic, which justifies the use of band limitation to the interval 0.5 to 3 Hz.

6.3.2 *AIx*

AIx determination follows the steps referred to in section 2.2.2.2. In this version of the software, the time of arrival of the *reflected wave* is not automatically computed and the operator must intervene to indicate it. The exact instant at which the *reflected wave* arrives corresponds to an inflection point ^[41] in the pressure pulse. To help the operator find it, the routine plots the probability density function, *pdf*, of the arterial pressure pulse (integrated or deconvolved). The inflection point localization should coincide with the *pdf* maximum closer to the *reflected wave* ^[41]. When the operator selects the inflection point localization (see Figure 45), the routine saves its ordinate (amplitude) value for further use by the program.

One of the two following expressions may determine *AIx*:

- If the inflection point occurs before the absolute maximum then,

$$AIx = 1 - y(\%), \quad (6.1)$$

where *y* is the amplitude of the *reflected wave* (inflection point ordinate).

- If the inflection point occurs after the absolute maximum then,

$$AIx = y - 1(\%), \quad (6.2)$$

where *y* is the amplitude of the reflection wave (inflection point ordinate).

Note, that these equations are basically the same as the one referred before ($AIx = \Delta P / PP$). However, division by the difference between the absolute maximum and the *reflected wave* (ΔP) by the pressure pulse (*PP*) is not required because the routine uses pulses normalized at one.

6.3.3 *PWV* from a Single Pulse

PWV determination uses a different method from the one explained in section 2.2.2.1. Instead of using the *transit time* between two consecutive arterial pulses the travelling time of the *reflected wave* is used ^[42]. Actually, when one visualizes the *reflected wave* in a certain arterial pulse, that wave has already travelled along an arterial tree and back again to the measurement location. If the referred

wave occurs earlier or later in the arterial pulse than it took less or more time, respectively, in its travel. So, the instant at which the *reflected wave* occurs in the arterial pulse, relatively to its beginning (considered the zero instant), may give a good estimate of *PWV*. Note that the velocity of the *reflected wave* alone is the same as the arterial pulse velocity.

Once the time that the *reflected wave* takes to its travel is determined, it is necessary to know the distance the wave travelled, to calculate a pulse velocity. On this matter, some doubts exist because the main reflection point in the arterial tree isn't precisely known. After some discussion it was considered that the arterial point responsible for the wave reflections, seen at the carotid artery, is the abdominal artery bifurcation. In this point the abdominal artery divides in two: the left and right common iliac which goes through the left and right leg respectively (see Figure 52). However, this assertion needs further validation.

Assuming this, the *reflected wave* travels about 1m long between the heart and abdominal artery bifurcation and between this point and the common left carotid (measurement location) ^[19]. Consequently, the routine processes the following calculation:

$$PWV = \frac{x}{2} (m.s^{-1}), \quad (6.3)$$

where x is the time instant at which the *reflected wave* occurs, more precisely the inflection point abscissa obtained by the *Alx* routine. This variable is passed to the *PWV from a single pulse* routine and that's the reason why the *Alx* should be determinate afterwards.

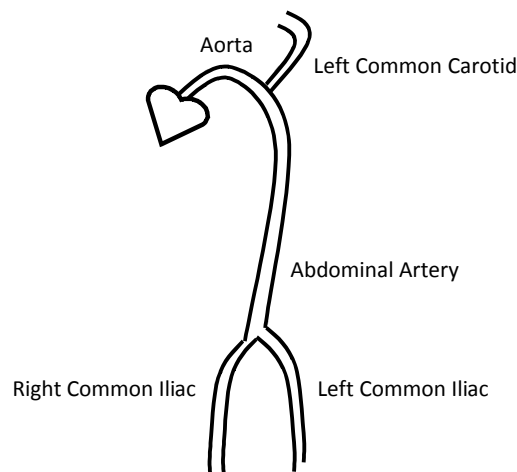


Figure 52. Main branches of the arterial tree. Drawn according to [19].

6.3.4 PWV from Two Pulses

This method for *PWV* determination follows the same principles as explained above. However, two different signals are simultaneously used, both on the left common carotid, but in two different localizations, placed 2-3cm apart. So, this time, the vessel distances both pulses travel are known and correspond to the distance between the two measurement locations.

The pulse travelling time is obtained again by the instant at which the inflection point occurs for a certain arterial pulse. However, this routine uses a *transit time* rather than an absolute instant. The *transit time* is obtained by subtracting the inflection point instant of an arterial pulse of a signal recorded at a determinate location along the carotid and the inflection point instant of an arterial pulse of the signal recorded about 2 cm away from the first. Note that the instants at which the inflection time occurs in both signals are slightly displaced making it possible to work out the reflected pulse wave *transit time* between the two locations.

6.3.5 HRV and Respiration Signal

As explained in section 2.3.3, the Heart Rate Variability, *HRV*, corresponds to the normal-to-normal intervals. It is obtained by assessing the arterial pulse peak-to-peak intervals, along the entire signal. *HRV* is expressed in terms of the standard deviation, *STD*, of the intervals. The *HRV* routine also computes the *FFT* to the *HRV* signal in order to visualize it in the frequency domain.

The respiration signal is submitted to a similar analysis, i.e. its *STD* and *FFT* are determined. Dispersed results between *HRV* and respiration could have a physiologic meaning (for example, respiratory problems).

6.4 Software Short-Term Improvements

Looking at the general structure of the software, at least one suggestion of restructuration arises: the obligation of a specific sequence of execution of operations in some functions. In fact, in a self-explanatory software this specific order shouldn't exist. As an example, the operator can only compute *Alx*, after having integrated or deconvolved.

The deconvolution routine also needs improvement, since the current one is only available for signals acquired at a 20KSpss sample rate. This happens because the *impulse response* used in the routine was acquired at that sample rate. A set of *impulse responses*, acquired at different sample rates should be made available, and the software must be smart enough to select the right *impulse response* to deconvolve from a certain arterial pulse.

The routine for the computation of *PWV* between two points is the one that needs more improvement effort. In the current version the inflection point of a carotid signal must be saved, then

the operator must exit the program and call a second carotid signal to calculate a second inflection point. To solve this problem, a future version of the software must allow the opening of two or more carotid signals simultaneously.

The routine that determines absolute maximums locations of the arterial pulse, executed in the master routine, also needs rethinking. In fact, it has been verified that the routine misses some pulses, when the signal shows drastic amplitude changes (due to different *PZ* sensor applied loads). This interferes strongly with *HRV* determination.

Several failures and errors can occur from the software incorrect utilization. For example, if the operator closes some windows, the program breaks up. Another example: if some operations are executed several consecutive times, the program breaks up too. Actually, the software must prevent incorrect utilization and avoid the program break-ups as well as sending error messages.

A help tool should also exist to facilitate utilization and maybe to explain briefly how the parameters are assessed.

CHAPTER 7

RESULTS

This chapter presents sets of results for each analyzed parameter. It also summarizes how data was processed in order to obtain these results.

All results were obtained using the software pack developed along this thesis.

In the later phase of the work, this software has been baptized, and is sometimes referred to, by the name *PulScope*.

7.1 A/x

A/x was computed from signals recorded at 20KSpss in the first location along the carotid artery (see section 3.3.1). For each subject 3 signals are collected. However, some signals still showed very poor signal-to-noise ratio and were rejected.

A/x analysis was carried out using both: the integration and deconvolution methods. For each of them, the average A/x of 10 individual pulses was determined, using the functions available in the single pulse analysis menu (see chapter 6), and also the A/x of an average pulse (normal and with scale adjust) using the local list analysis. Each average pulse was also built from 10 different pulses. Tables VIII and XIX show A/x values while figures 53 to 56 plot graphics that help to analyze the information.

Table VIII. Alx (%) values obtained by the integration method.

Carotid Signal	Mean (10 Pulses)	Average Pulse (10 Pulses)	Average Pulse (Scale Adjusted) (10 Pulses)
1 - A	-28,2	-22,8	-29,7
1 - B	-8,6	-8,6	-8,6
1 - C	-15,4	-12,1	-13,6
2 - A	21,6	15,1	13,6
2 - B	-17,4	-15,9	-16,3
2 - C	2,9	-7,5	-5,5
3 - A	5,1	-1,0	Uncertain
3 - B	-3,1	-2,9	-6,7
3 - C	0,8	-7,9	Uncertain
4 - A	1,4	2,1	2,5
5 - A	-22,0	-29,7	Uncertain
5 - B	-15,5	-16,3	-0,2
5 - C	-0,9	-6,7	Uncertain
6 - A	15,9	12,8	Uncertain
6 - B	19,7	17,0	Uncertain
6 - C	14,4	13,6	4,8
7 - A	-6,6	-11,3	-13,6
7 - B	-31,7	-41,2	Uncertain
8 - A	-9,3	2,9	-2,9
8 - B	6,6	-0,6	Uncertain
9 - A	28,5	28,2	27,4
9 - B	28,7	27,0	27,4
9 - C	16,3	10,2	Uncertain
10 - A	10,8	12,5	Uncertain
10 - B	17,0	16,3	Uncertain
10 - C	7,8	6,4	Uncertain

Table XIX. Alx (%) values obtained by the deconvolution method.

Carotid Signal	Mean (10 Pulses)	Average Pulse (10 Pulses)	Average Pulse (Scale Adjusted) (10 Pulses)
1 - A	-22,5	-16,7	-19,0
1 - B	-16,9	-15,1	-15,7
1 - C	-16,2	-9,8	-14,0
2 - A	6,8	6,3	0,6
2 - B	-13,2	-10,5	-11,2
2 - C	-7,8	-11,3	-10,9
3 - A	-5,8	-5,9	Uncertain
3 - B	-1,3	0,6	-9,0
3 - C	-17,1	-17,0	Uncertain
4 - A	-1,6	1,3	3,7
5 - A	-25,7	-27,8	Uncertain
5 - B	-14,7	-14,4	-13,6
5 - C	-8,0	-9,0	Uncertain
6 - A	5,8	5,9	Uncertain
6 - B	14,1	14,8	Uncertain
6 - C	3,6	3,3	-13,2
7 - A	-19,1	-18,2	-23,9
7 - B	-37,5	-37,4	Uncertain
8 - A	-11,0	-9,8	-19,7
8 - B	-11,3	-14,0	Uncertain
9 - A	29,5	27,4	18,2
9 - B	25,0	26,2	22,8
9 - C	3,9	1,7	Uncertain
10 - A	3,0	2,1	Uncertain
10 - B	11,3	12,1	Uncertain
10 - C	-5,6	-6,3	Uncertain

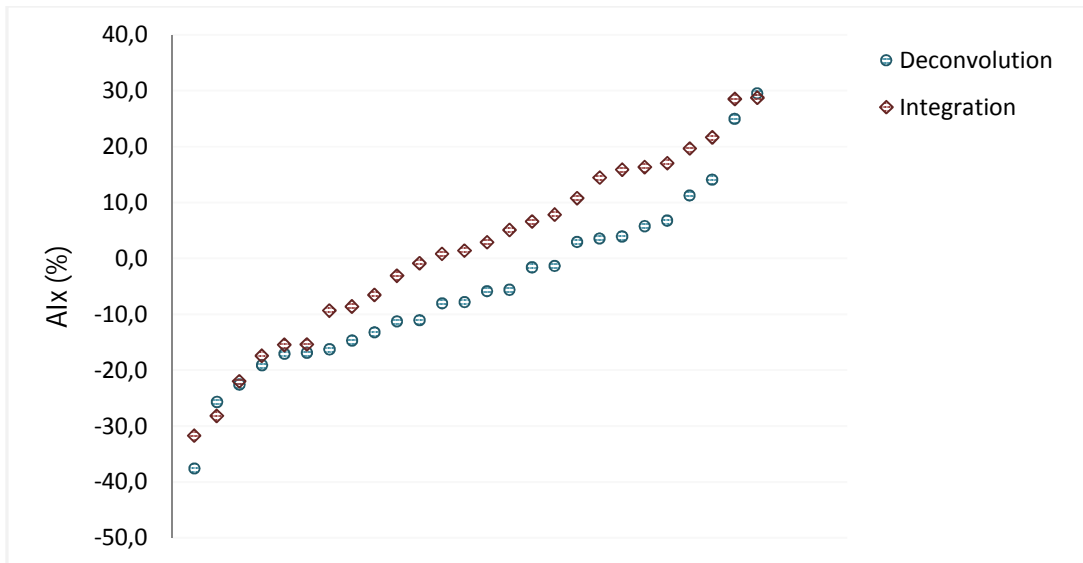


Figure 53. Comparison of A1x values obtained using the integration and the deconvolution methods (mean column of tables VIII and XIX).

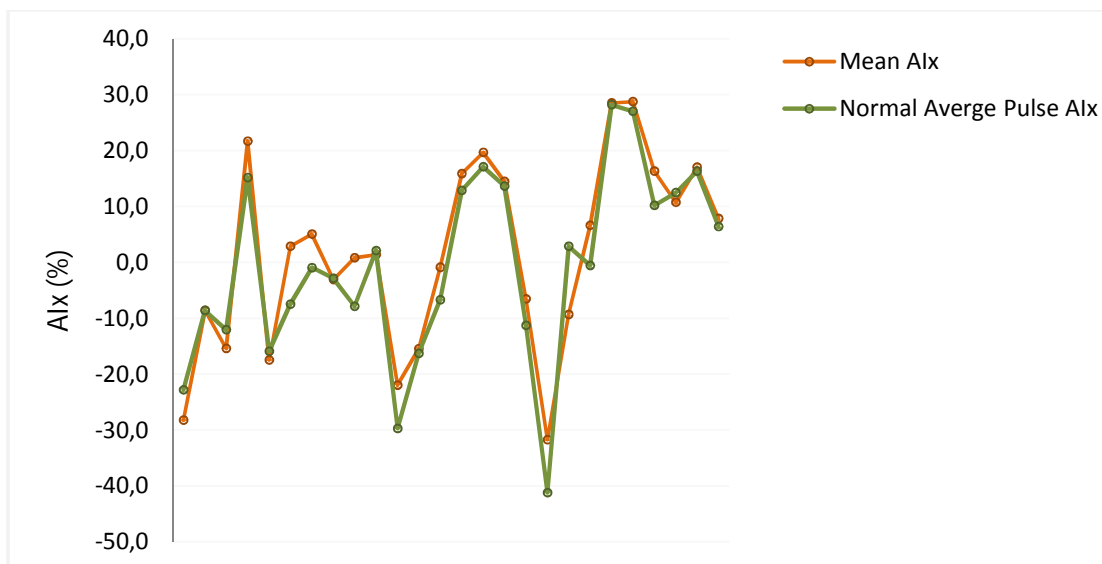


Figure 54. Mean A1x versus average pulse A1x (for the integration method).

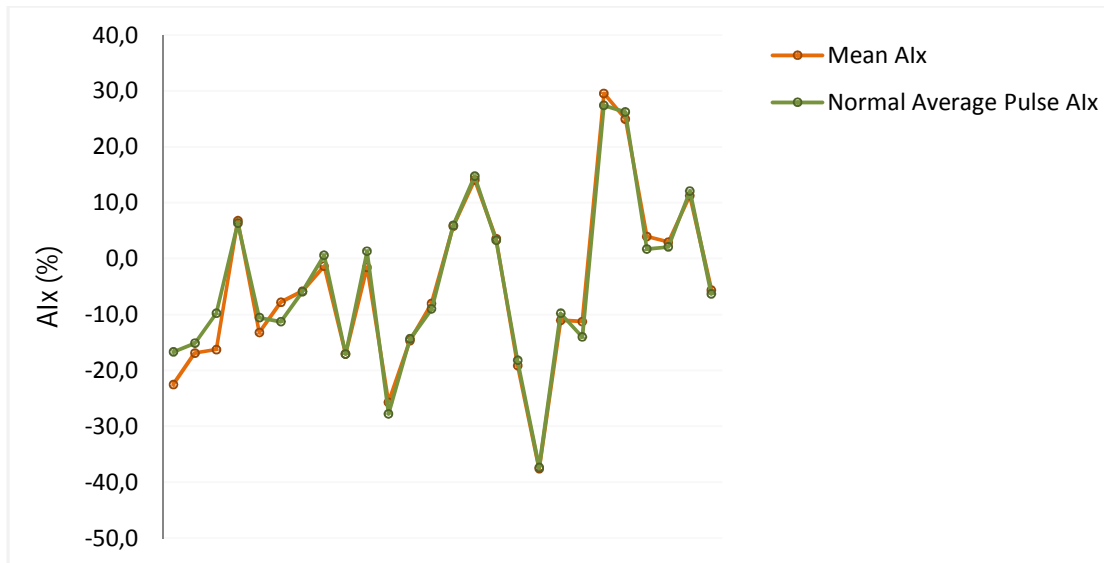


Figure 55. Mean AIx versus average pulse AIx (for the deconvolution method).

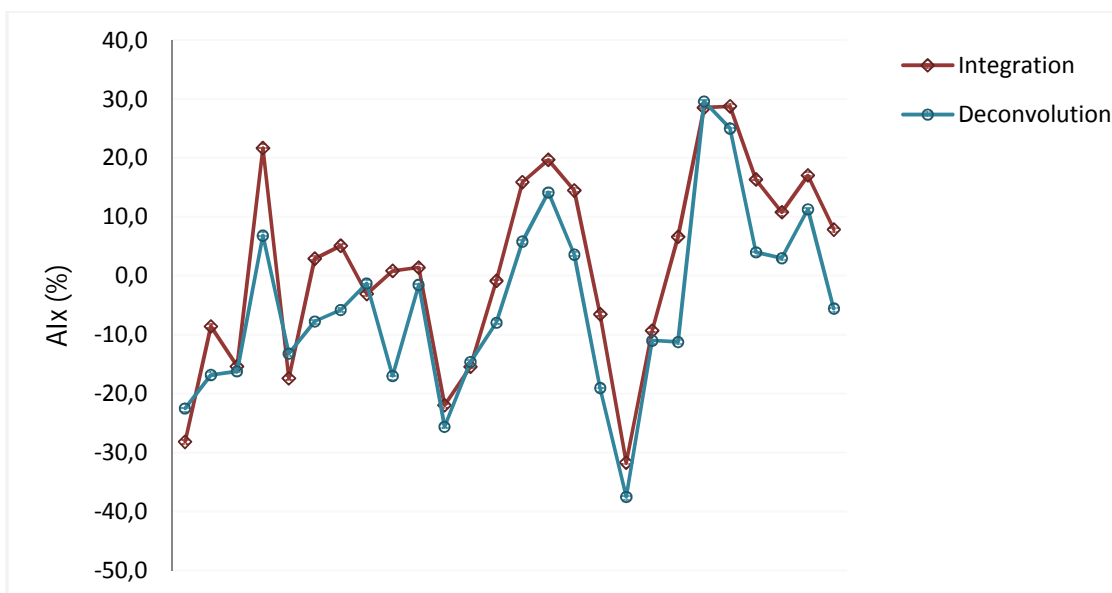


Figure 56. Relationship between mean AIx for the integration and deconvolution methods.

7.2 PWV from a Single Pulse

For *PWV* determination, procedures as the ones previously described, were adopted. However, average pulse with time adjust was not worked out successfully, since the results obtained with this function were erratic (as it was realized for the *A/x* determination), then this was not considered.

Tables X and XI and Figures 57 to 60 show *PWV* values that help to analyze information.

Table X. *PWV* ($\text{m}\cdot\text{s}^{-1}$) values - from a single pulse - obtained by the integration method.

Carotid Signal	Mean (10 Pulses)	Average Pulse (10 Pulses)
1 - A	2,6	2,9
1 - B	2,8	2,3
1 - C	4,7	2,6
2 - A	9,3	6,5
2 - B	5,8	2,8
2 - C	5,7	2,8
3 - A	7,0	4,9
3 - B	9,2	6,0
3 - C	8,0	3,0
4 - A	5,5	5,5
5 - A	4,1	2,7
5 - B	6,2	3,1
5 - C	6,6	5,2
6 - A	9,1	7,4
6 - B	6,9	4,9
6 - C	7,2	5,0
7 - A	6,3	5,4
7 - B	3,4	2,6
8 - A	8,1	6,2
8 - B	7,8	3,2
9 - A	9,5	5,7
9 - B	11,3	7,3
9 - C	10,3	7,8
10 - A	8,1	7,8
10 - B	8,0	6,4
10 - C	7,6	6,4

Table XI. *PWV* ($\text{m}\cdot\text{s}^{-1}$) values - from a single pulse - obtained by the deconvolution method.

Carotid Signal	Mean (10 Pulses)	Average Pulse (10 Pulses)
1 - A	3,2	3,2
1 - B	2,5	2,5
1 - C	3,7	2,7
2 - A	6,0	6,5
2 - B	2,7	2,7
2 - C	2,6	2,7
3 - A	2,8	2,8
3 - B	4,5	5,3
3 - C	2,7	2,8
4 - A	5,5	5,5
5 - A	3,0	2,8
5 - B	2,7	2,8
5 - C	2,8	2,9
6 - A	5,9	6,4
6 - B	5,0	4,2
6 - C	4,2	4,9
7 - A	2,5	2,3
7 - B	2,5	2,7
8 - A	2,8	2,8
8 - B	3,0	2,7
9 - A	7,5	7,4
9 - B	6,8	6,7
9 - C	8,1	8,0
10 - A	5,9	7,1
10 - B	6,8	6,5
10 - C	3,3	2,9

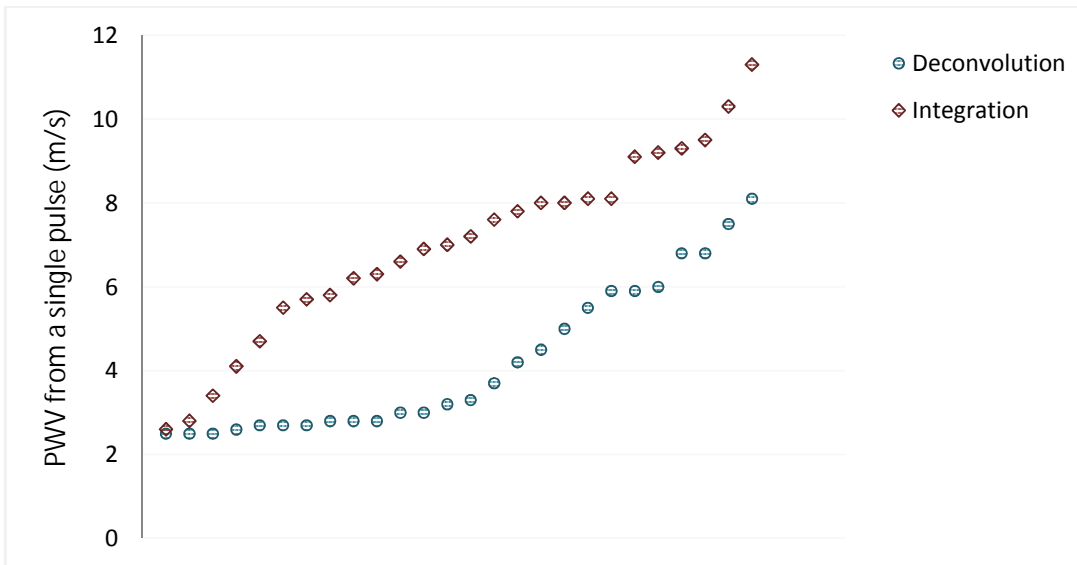


Figure 57. PWV values using the integration and the deconvolution methods.

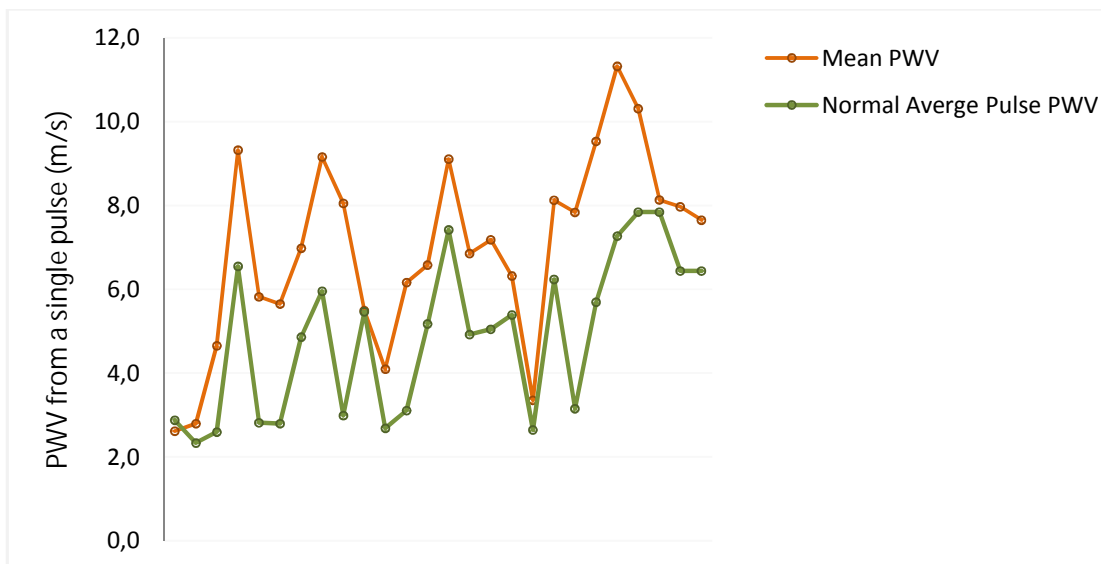


Figure 58. Mean PWV (from a single pulse) and average pulse PWV (from a single pulse), for the integration method.

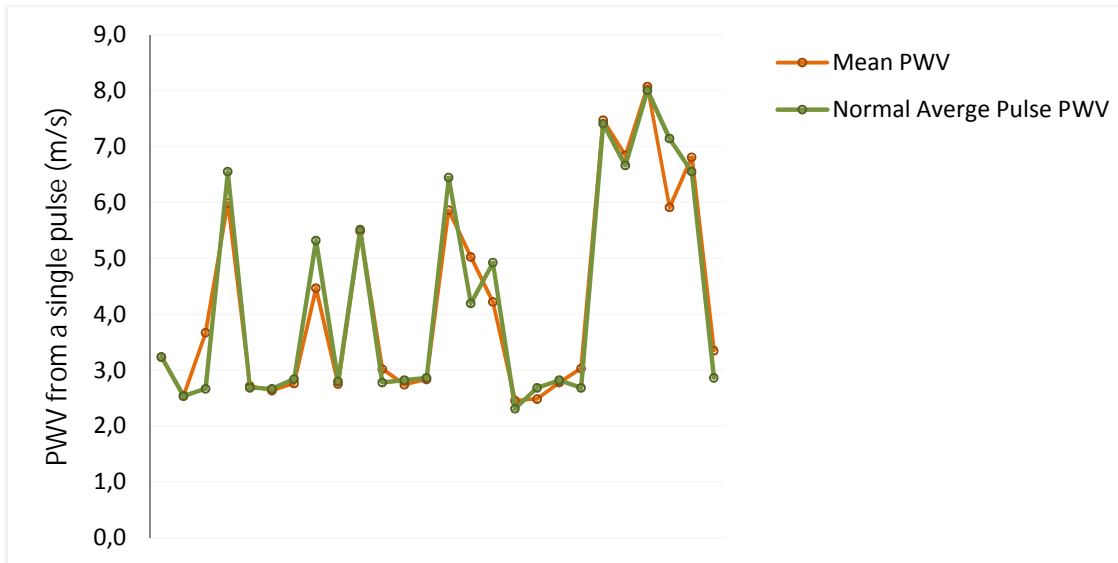


Figure 59. Mean PWV (from a single pulse) versus average pulse PWV (from a single pulse), for the deconvolution method.

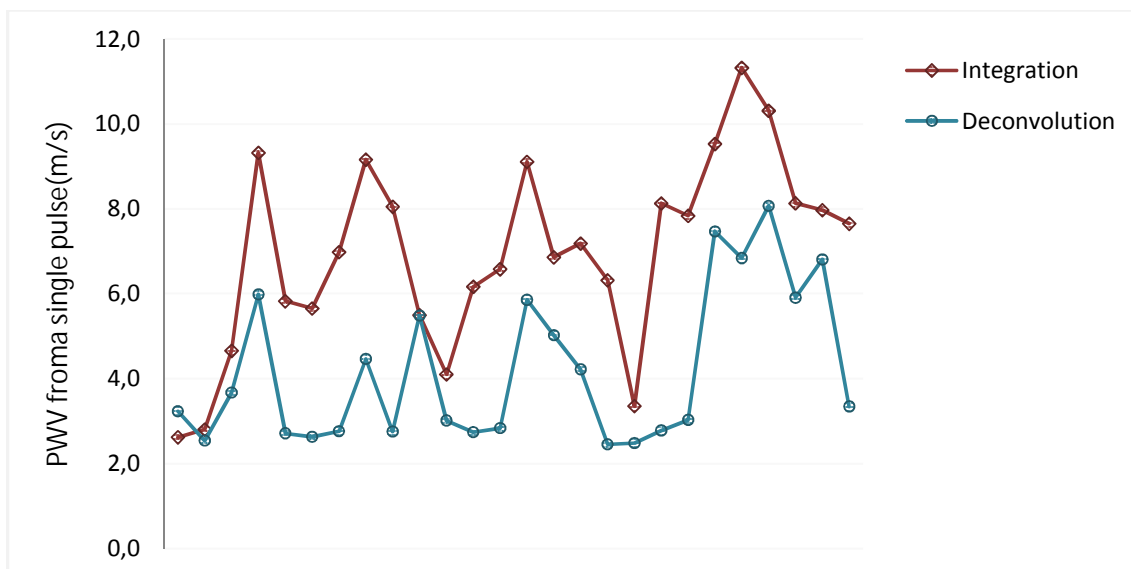


Figure 60. Relationship between mean PWV from a single pulse for the integration and deconvolution methods.

7.3 PWV from Two Pulses

PWV from two pulses required the same carotid signals used for the assessment of the *AIx* and the *PWV* from a single pulse. Carotid signals acquired at the secondary location along the carotid artery were used also (see section 3.3.1). *PWV* determination followed the same procedures taken for the hemodynamic signals presented above. Nevertheless, it was necessary to reject few more carotid signals due to the low signal-to-noise ratio of the signals acquired at the secondary location.

Tables XII and XIII below show *PWV* values and graphics of figures 61 to 64 help envisage the information.

Table XII. *PWV* ($\text{m}\cdot\text{s}^{-1}$) values – from two pulses - obtained by the integration method.

Carotid Signal	Mean (10 Pulses)	Average Pulse (10 Pulses)
1 - A	0,435	0,176
1 - B	0,522	0,137
1 - C	0,104	0,109
2 - A	1,724	0,255
2 - B	0,188	0,847
2 - C	0,543	0,528
3 - A	0,535	0,262
3 - C	0,417	0,344
4 - A	0,455	3,636
5 - A	1,976	7,692
5 - B	0,219	1,325
5 - C	0,285	0,172
6 - A	0,785	1,101
6 - B	0,388	0,495
6 - C	2,083	2,632
7 - A	1,516	0,155
7 - B	1,321	0,565
9 - A	0,158	0,990
9 - C	0,959	0,593
10 - B	1,522	0,794

Table XIII. *PWV* ($\text{m}\cdot\text{s}^{-1}$) values – from two pulses - obtained by the deconvolution method.

Carotid Signal	Mean (10 Pulses)	Average Pulse (10 Pulses)
1 - A	0,211	0,231
1 - B	0,232	0,417
1 - C	0,139	0,529
2 - A	4,132	2,632
2 - B	2,287	0,350
2 - C	0,922	0,000
3 - A	0,609	0,332
3 - C	0,325	0,441
4 - A	0,305	0,156
5 - A	0,682	1,130
5 - B	5,682	2,597
5 - C	0,990	1,587
6 - A	5,507	1,412
6 - B	0,842	0,172
6 - C	0,477	0,104
7 - A	20,000	0,440
7 - B	0,408	0,273
9 - A	0,872	1,325
9 - C	0,110	0,063
10 - B	1,984	8,000

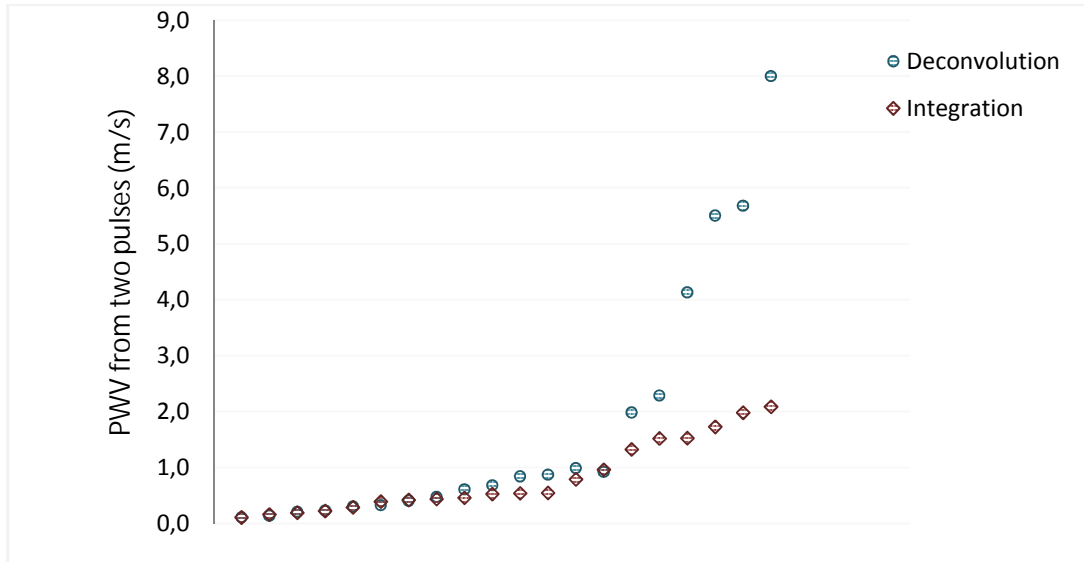


Figure 61. PWV from two pulses. Values for the integration and deconvolution methods.

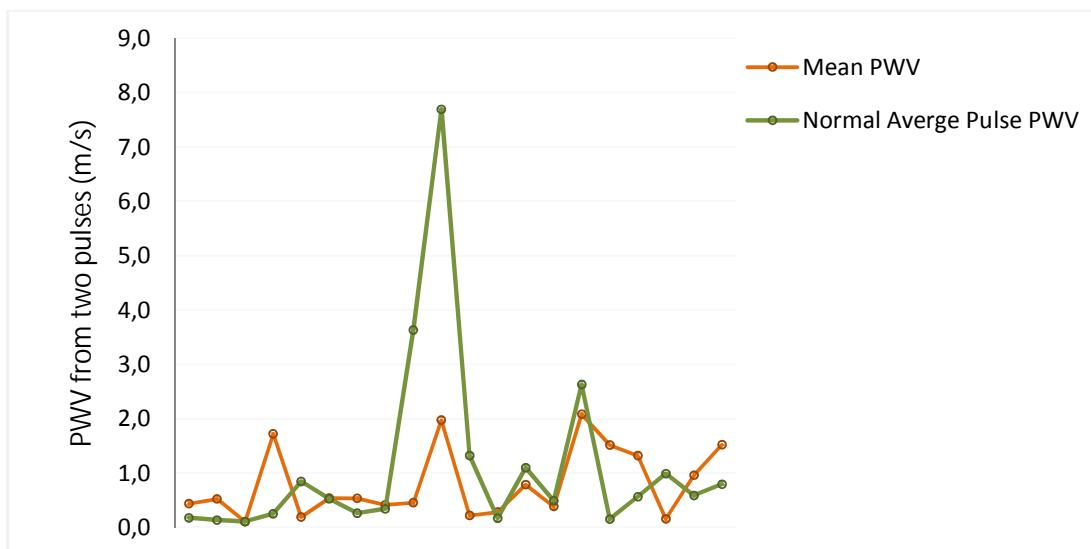


Figure 62. Mean PWV (from two pulses) versus average pulse PWV (from two pulses), for the integration method.

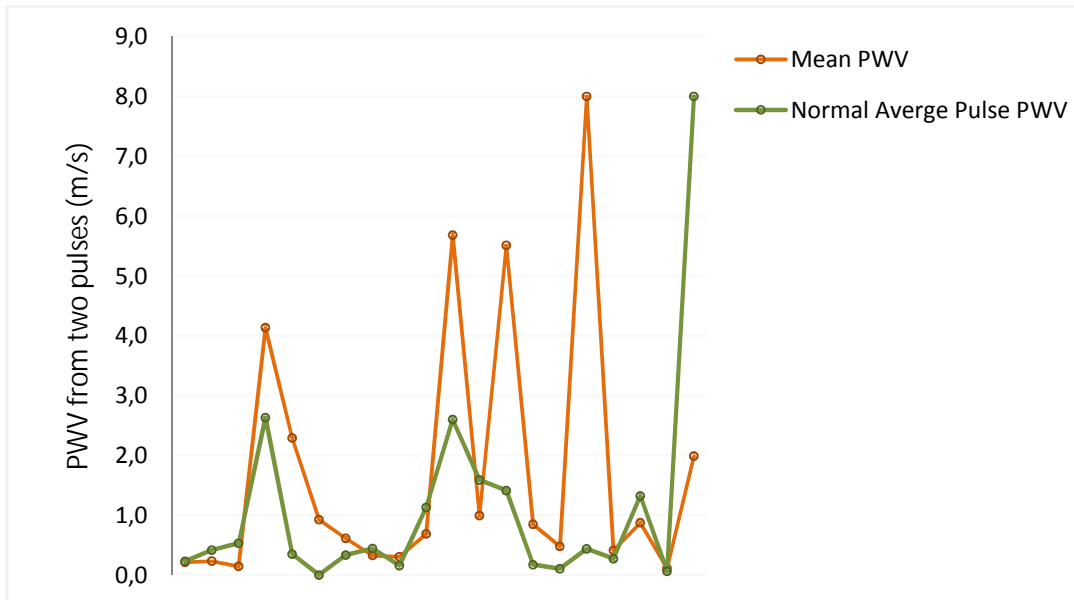


Figure 63. Mean PWV (from two pulses) versus average pulse PWV (from two pulses), for the deconvolution method.

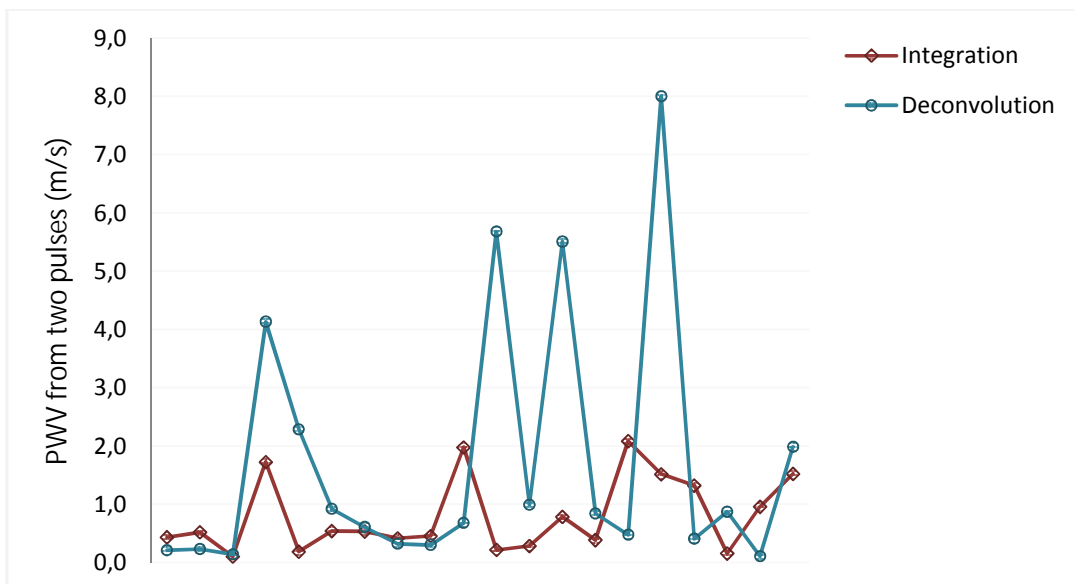


Figure 64. Relationship between mean PWV from two pulses for the integration and deconvolution methods.

7.4 Comparison Results

It may be interesting to observe the relationship between the three hemodynamic signals that have been studied. Graphic of Figure 65 shows the relation between the values obtained for AIx , PWV from a single pulse and PWV from two pulses. In these graphics, some values of the PWV between two points are zeroed whenever the corresponding signal-to-noise ratio was so poor that PWV could not be determined.

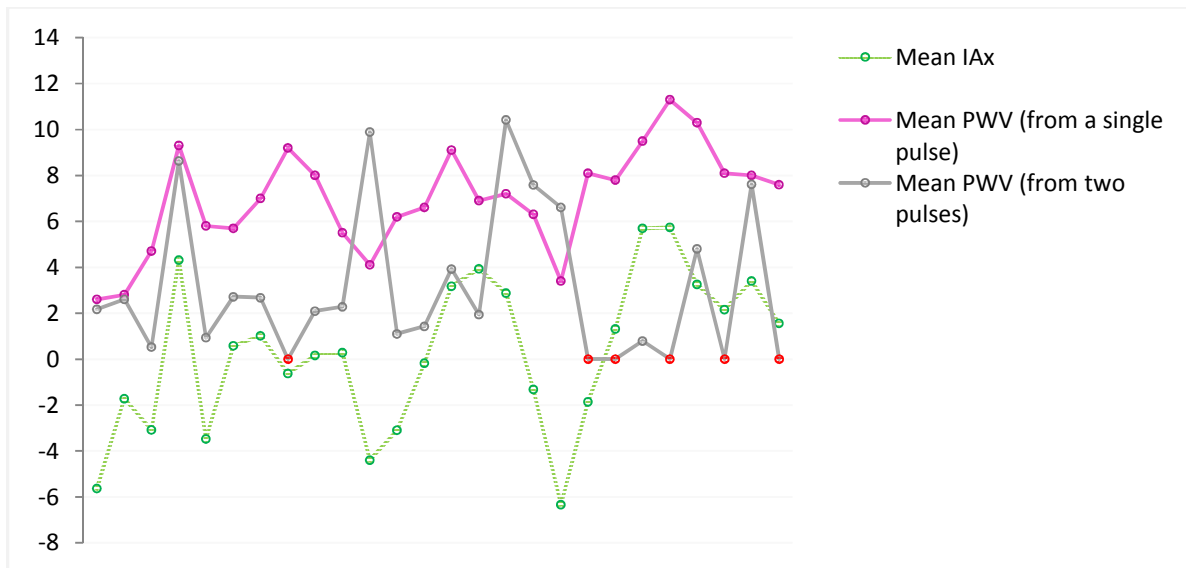


Figure 65. Relationship between mean AIx , mean PWV from a single pulse and mean PWV from two pulses, for the integration method. The red dots at zero, for the PWV from two pulses, correspond to inexistent values.

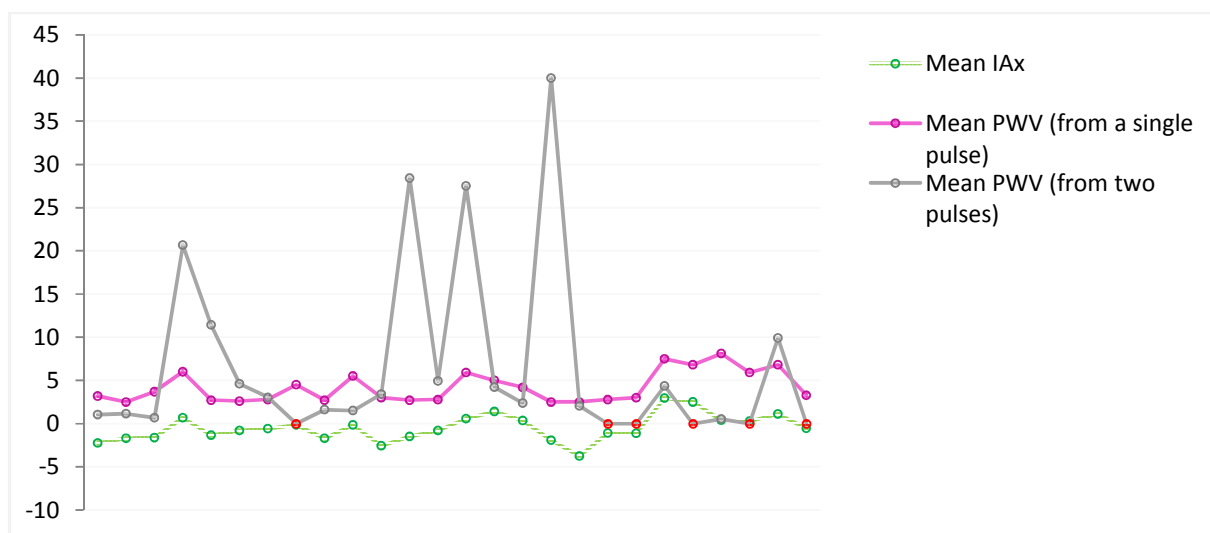


Figure 66. Relationship between mean AIx , mean PWV from a single pulse and mean PWV from two pulses, for the deconvolution method. The red dots at zero, for the PWV from two pulses, correspond to inexistent values.

7.5 HRV

To analyze *HRV*, signals recorded at 1KSpss were used (see section 3.3.1) and 3 or 2 data sets were collected for each subject.

Both, time and frequency domain analysis was performed. For that it was determined the standard deviation, *STD*, (time domain) and the high frequency, *HF*, and low frequency, *LF*, (frequency domain) of the *HRV* signal. The same measures were made for the respiration signal.

The following tables show the obtained values for both *HRV* and respiration signal. The graphics help to analyze the relationship between them.

Table XIV. HRV time domain analysis – standard deviation (STD).

Carotid Signal	HRV Signal (STD (%))	Respiration Signal (STD (%))
1 - A	5,10	1,97
1 - B	35,25	20,90
1 - C	6,76	6,12
2 - A	5,52	5,87
2 - B	4,72	7,90
2 - C	5,05	11,16
3 - A	7,81	5,75
3 - B	9,08	8,78
3 - C	7,06	6,95
4 - A	7,89	11,13
4 - B	6,69	14,92
4 - C	5,19	27,16
5 - A	5,15	8,04
5 - B	36,31	4,18
5 - C	7,38	5,40
6 - A	5,20	25,30
6 - B	6,66	21,88
6 - C	5,60	9,98
7 - A	13,71	9,99
7 - B	17,94	6,45
8 - A	7,43	4,80
8 - B	33,07	4,98
8 - C	11,00	5,42
9 - A	6,45	2,07
9 - B	11,46	7,22
9 - C	5,49	13,66
10 - A	21,39	15,40
10 - B	8,20	5,32
10 - C	4,12	3,46

Table XV. HRV frequency domain analysis – high (HF) and low (LF) frequency.

Carotid Signal	HRV Signal		Respiration Signal	
	LF	HF	LF	HF
1 - A	0,01	0,24	0,09	0,26
1 - B	0,10	0,31	0,11	0,23
1 - C	0,01	0,19	0,06	0,22
2 - A	0,01	0,25	0,06	0,21
2 - B	0,05	0,24	0,06	0,24
2 - C	0,10	0,32	0,09	0,30
3 - A	0,07	0,24	0,07	0,24
3 - B	0,13	0,34	0,06	0,31
3 - C	0,02	0,31	0,06	0,32
4 - A	0,03	0,13	0,06	0,13
4 - B	0,05	0,12	0,05	0,14
4 - C	0,03	0,17	0,07	0,15
5 - A	0,13	0,26	0,07	0,26
5 - B	0,04	0,22	0,05	0,27
5 - C	0,12	0,28	0,09	0,28
6 - A	0,04	0,25	0,08	0,26
6 - B	0,08	0,24	0,07	0,24
6 - C	0,90	0,26	0,08	0,26
7 - A	0,08	0,32	0,08	0,33
7 - B	0,06	0,26	0,07	0,25
8 - A	0,10	0,26	0,11	0,30
8 - B	0,05	0,35	0,07	0,36
8 - C	0,10	0,31	0,06	0,34
9 - A	0,07	0,25	0,06	0,29
9 - B	0,03	0,32	0,05	0,29
9 - C	0,11	0,28	0,07	0,31
10 - A	0,07	0,26	0,08	0,40
10 - B	0,10	0,28	0,07	0,29
10 - C	0,05	0,31	0,06	0,32

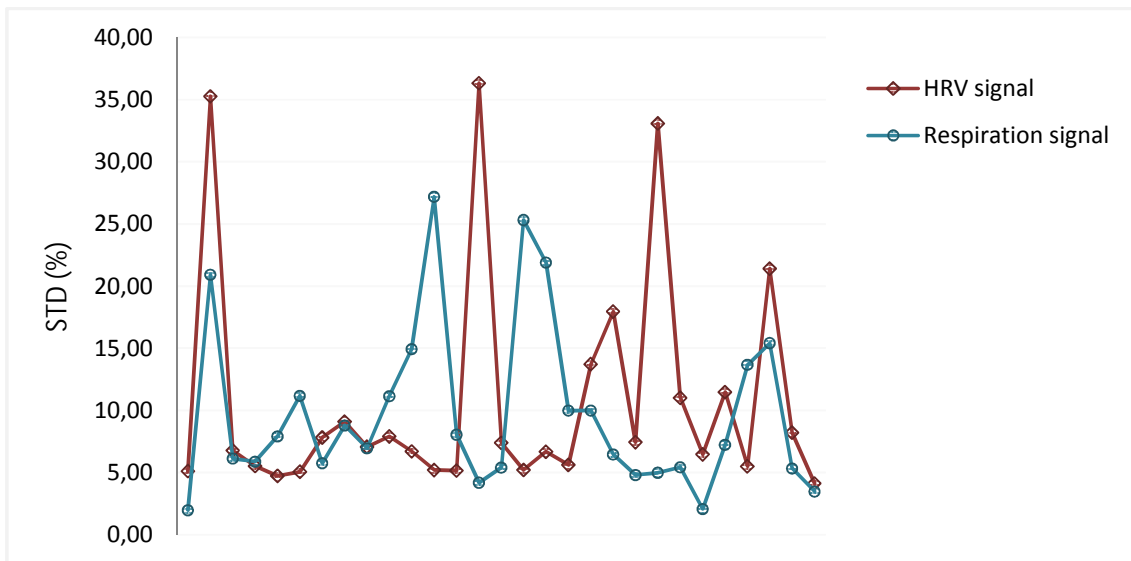


Figure 67. Relationship between the STD of HRV and respiration.

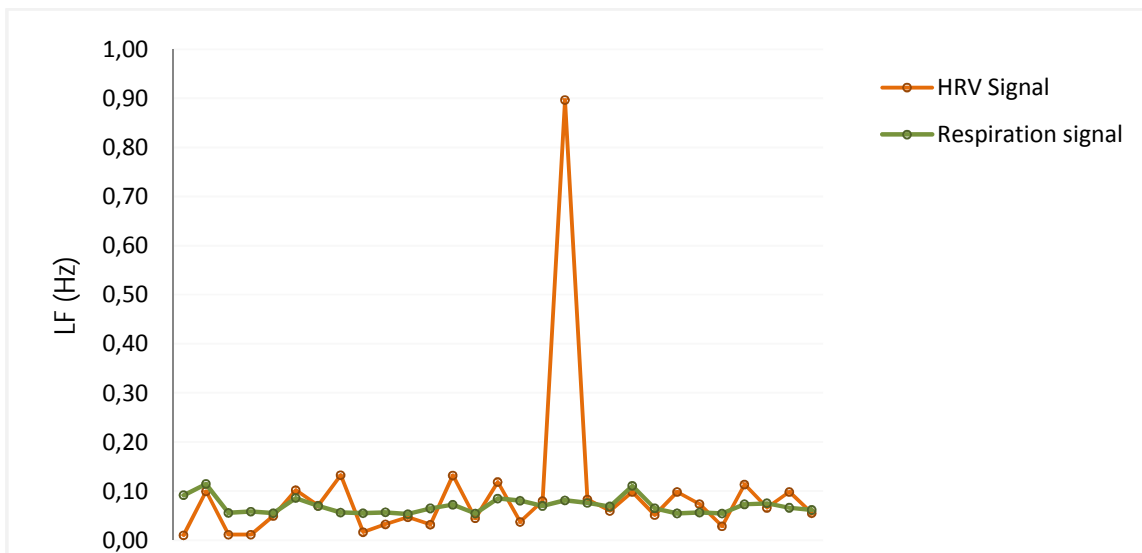


Figure 68. Relationship between HRV and respiration at LF.

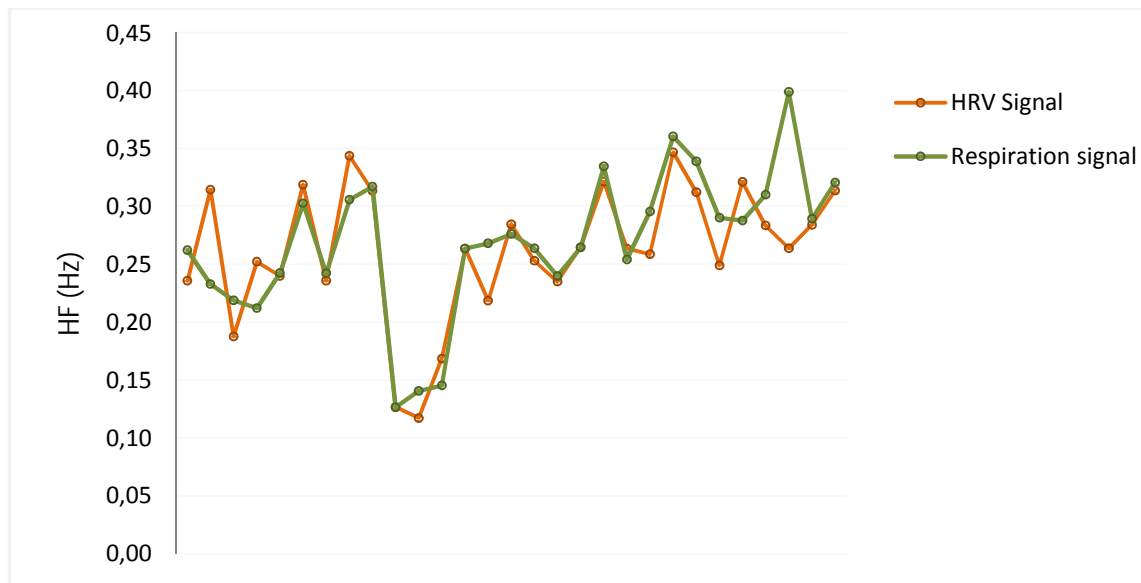


Figure 69. Relationship between HRV and respiration at HF.

7.6 HR

As happened in the *HRV* study, *HR* frequency analysis also required long recording duration signals, making it mandatory to lower the sample rate to 1KSpss. The obtained values were compared with the *HR* values from a commercial device (happy life®, German - introduced in chapter 5).

Table XVI and graphic of Figure 70 show the relationship between the *HR* frequency obtained with *PulScope* and the *HR* frequency obtained with the commercial device.

Table XVI. HR frequency (bpm) values obtained by the *PulScope* software and happy life® device.

Carotid Signal	<i>PulScope</i> software (<i>HR</i> (bpm))	happy life® device (<i>HR</i> (bpm))
1 - A	93	77
1 - B	89	77
1 - C	86	89
2 - A	66	73
2 - B	67	71
2 - C	69	74
3 - A	68	73
3 - B	58	63
3 - C	54	67
4 - A	85	97
4 - B	73	81
4 - C	74	80
5 - A	68	66
5 - B	64	64
5 - C	59	65
6 - A	67	64
6 - B	60	63
6 - C	60	57
7 - A	68	81
7 - B	70	76
8 - A	71	71
8 - B	90	92
8 - C	74	76
9 - A	63	68
9 - B	68	66
9 - C	70	86
10 - A	103	81
10 - B	76	77
10 - C	75	77

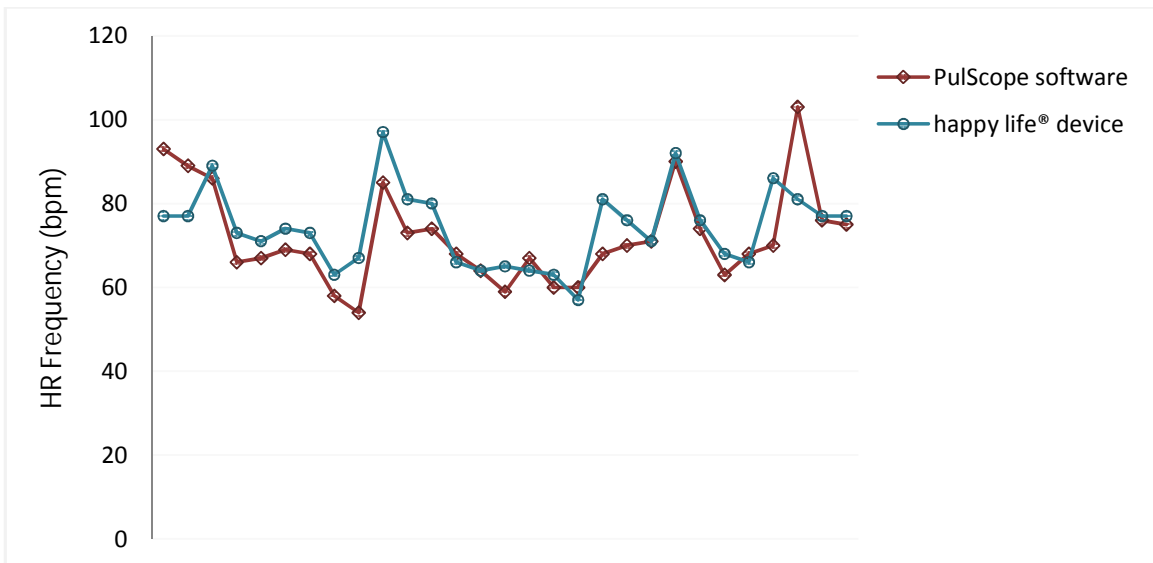


Figure 70. Relationship between HR obtained with the PulScope software and with the happy life® device.

CHAPTER 8

DISCUSSION

Results presented in the previous chapter are now discussed and the fundamental issues underneath the determination of each hemodynamic parameter discussed. The order is as follows: *Aix*, *PWV* from a single pulse and *PWV* from two pulses and finally *HRV* and *HR*. The first three parameters will be grouped in the same discussion, since they all are related with the same basic parameter - arterial stiffness.

8.1 Arterial Stiffness Related Parameters

The study of *Aix*, *PWV* from a single pulse and *PWV* from two pulses follows a similar procedure. The analysis was made in three different ways. Firstly, the consistency of the results was studied and their agreement with values found in the literature verified. Next, the suggestion introduced in chapter 4 is deepened in order to clarify which one, the deconvolution or the integration method, is preferable. Finally, the use of an average pulse as an alternative to assessing a mean of several hemodynamic parameters is evaluated.

Basically, for this study, the single pulse analysis and the local list analysis of the *PulScope* software (see chapter 6) were used. The carotid signals studied are about 1 minute long since long duration signals are not required for these parameters. On the other hand, a high sampling rate is (20KSpss) used since some extra time resolution is need to gather the necessary information from the arterial pulses.

RANGE VALUES

The values obtained for *Aix* and *PWV* from a single pulse (Figure 53 and Figure 57, of chapter 7) were coincident with the values found in the literature: between -30% and 70% for the *Aix*, and rounding $7\text{m}\cdot\text{s}^{-1}$ for the *PWV*. Besides, it was verified that the same individuals have similar values for different acquired carotid signals, showing the consistency of the results.

PWV from two pulses did not reveal the same consistency. The values found (Figure 61, of chapter 7) should agree with the values found for the *PWV* from a single pulse and with the values in the literature; however, *PWV* values were generally lower than expected. In addition, lower consistency in the results was observed. Occasionally, the same subject presented rather different *PWV* values from different carotid signals. These results suggest that, possibly, the use of the *reflected wave* arrival instant for the *PWV* determination is not the best choice in this case. In fact, the analysis of the arterial pulse shape from two different carotid locations, from the same individual, revealed

significant variations. It is possible that these alterations have been provoked mainly by the *reflected wave* arrival. In this way, there should exist a time displacement of the *reflected wave* arrival between both carotid locations, and then the *PWV* should be determined. However, it is possible that the verified alterations can result from causes different from the *reflected wave*. Besides that, for assessment of *PWV* from two pulses, it is required to use an arterial pulse point which doesn't depend on the shape, as is the case of the systolic foot (see section 2.2.2.1). In this way, the *reflected wave* does not match since this arterial pulse point varies a lot depending on the measurement location.

On the other hand, the use of the *reflected wave* arrival instant for the *PWV* from a single pulse, seemed to produce valid results. Since a single arterial pulse is used in this determination, the arterial shape alterations did not interfere. Besides, the considered distance of the arterial tree at which the wave reflects (abdominal artery bifurcation – see section 6.3.3) seemed to be correct, since the range of values of the results are in good agreement with the literature. However, this assumption needs to be confirmed by cardiologists or other skilled persons of this area.

AIx determination did not rise many problems, since it corresponds to a quotient between the *systolic peak* and the *reflected wave* (see section 2.2.2.2). So, the analysis requires only that the operator correctly finds the *reflected wave* peak of the arterial pulse. Once this point is well determined, the *AIx* values show good consistency.

INTEGRATION AND DECONVOLUTION METHODS

It was already referred in chapter 4 that the deconvolution method seems to show a better accuracy when compared to the integration method. This assumption is supported by the analysis of a wide range of signals in several subjects.

Obtaining of a good arterial pulse shape (i.e. free from noise and from artifacts) is essential for determining the *reflected wave* arrival instant. Since this point is used for all the three parameters, it is vital that the operator correctly indicates it, meaning that no doubts can exist in identifying which peak of the arterial pulse represents the *reflected wave*. Generally, this point is easily found with the aid of the *pdf* that shows a higher amplitude for the *reflected wave* location. However, it was verified that sometimes the arterial pulses obtained by means of integration gave strange results. In fact, in some cases it was really impossible to realize where the *reflected wave* was located even using the *pdf*. This difficulty in finding the *reflected wave* is due to the irregularities of the arterial pulse shape given by the integration method. This method requires that operator to indicate where the pulse begins and where it ends, however, sometimes, it is hard to do it correctly. An inaccurate indication of these points occasionally produces strange arterial pulses, making it very hard to know which peak corresponds to the *reflected wave*.

Besides that, when the carotid signal presents a low signal-to-noise ratio, the arterial pulses obtained by the integration method didn't show consistency along the same signal. As a result, the values of parameters presented a rather variation along the same signal, once it became more difficult to indicate the correct *reflected wave* location.

On the other hand, the deconvolution method seemed to behave like a filter in such a way that the noise did not interfere in these cases. Actually, the resulting arterial pulses were very similar along

the same signal and also between different signals of the same subject. The results show consistency for the deconvolution method, at least for AIx and for PWV from a single pulse.

PWV from two pulses showed inconsistencies either with the integration or the deconvolution methods. This suggests that the way the arterial pulse is achieved is not the main reason for these unsatisfactory results; as was already explained, the cause should be the way the PWV is assessed, i.e. the method itself.

Despite the problems found when using the integration method, the hemodynamic parameters determined with both, deconvolution and integration, exhibited a certain degree of correlation (Figures 56, 60 and 64, of chapter 7), especially for AIx .

It is also interesting to realize that, generally, the integration method yields higher values for PWV from a single pulse and AIx than the ones obtained by the deconvolution method. As was explained along the work, higher values for both PWV and AIx suggest higher arterial stiffness. Since the subjects analyzed in this study were all healthy people, low AIx and PWV values were expected. In fact, this is verified for parameters determined by the deconvolution method, but was not confirmed with the integration method. For the same subject, the integration method shows higher values than the deconvolution method. Referring to Figure 57 of chapter 7, for example, it is possible to see that PWV from a single pulse has higher values for integration than for deconvolution. The same was not verified for PWV from two pulses. However, and once again, this can be attributed to the PWV assessment method itself.

AVERAGE PULSE

AIx , PWV from a single pulse and PWV from two pulses were assessed using the single pulse analysis and a local list analysis. In the first, each parameter was assessed from a mean of 10 individual pulses. In the second an average pulse was constructed, with the same pulses used in the single pulse analysis, and the hemodynamic parameters were obtained from it.

Two different types of average pulse were analyzed: a normal average pulse and a time adjusted average pulse (see section 6.2.3). The results obtained with the time adjusted average pulse were inconsistent and most of the times it was impossible to obtain a satisfactory average pulse. Possibly the function which determines this average pulse needs to be improved, however the few results suggest that this type of average pulse may misrepresent the real arterial pulse shape and consequently lead to false hemodynamic parameter values. Since the results obtained with this function were unsatisfactory, this analysis was only made for one hemodynamic parameter, the AIx (see tables VIII and XIX, of chapter 7).

On the other hand, the normal average pulse show consistency, especially if it was used the deconvolution method (see, for example, Figure 55 of chapter 7). This suggests that an average pulse can be used instead of determining the mean value from the hemodynamic parameters of several pulses, without introducing significant errors. However, it is possible that the average pulse should only be used for the deconvolution method and not for the integration method, once, for this last, the correlation between average pulses parameters values and mean parameters values wasn't so satisfactory.

Once again, for the *PWV* from two pulses values the results were not encouraging. The relation between average pulse values and mean values wasn't verified (see, for example, Figure 63 of chapter 7).

COMPARISON RESULTS

Since *AIx* and *PWV* are related with arterial stiffness, they are expected to show some correlation, i.e. if an individual shows high *PWV* values it should also present high *AIx* values.

In fact, a very good correlation between *AIx* and *PWV* from a single pulse was verified, especially with the deconvolution method (see Figures 65 and 66, of chapter 7). Besides that, and despite the unlikable results obtained for the *PWV* from two pulses, this parameter also shows some correlation with the two others. This last result suggests that maybe the method isn't so erroneous and perhaps more studies or different approaches could give rise to better results.

8.2 HRV and Respiration Signal

The study of *HRV* and respiration required long acquisition signals but lower time resolution. Thus, a 5 minutes period at a 1KSpss rate was selected for the acquisition task.

Global analysis of the *PuScope* software (see chapter 6), was used in this study in order to determine *HRV* in the time and frequency domains; and also make the same calculations for the respiratory signal.

It was previously known from the literature that the respiration and *HRV* show an inverse direct relation, so it could be useful to analyze both signals, especially in the frequency domain. In fact, determining the *FFT* of the *HRV* signal could be inefficient since this signal resolution is low, however, since it was proven that the respiration signal was related with the *HRV* it could be used the first signal to fulfill this analysis (once the respiration signal resolution is quite higher). By other hand, the time domain analysis should give very coincident results for both signals. Besides that, great disagreements between time domain *HRV* and respiration values could be related with respiratory or cardiac dysfunctions.

TIME DOMAIN ANALYSIS

To analyze *HRV* and respiration signal in time domain the standard deviation, *STD*, of both signals was computed. Results showed some coincidence between both signals (see Figure 67 of chapter 7). Nevertheless rather different *STD* values for *HRV* and respiration were verified, the latter yielding higher values. Besides that, in these cases, it was achieved a very regular respiration signal, which gave rise to higher than normal *STD* values. Analyzing all the *HRV* values for both signals it is

realized that it has a mean value about 7% for this population. This suggests that the deviations do not correspond to correct values. Besides, it is known that the *HRV* signal isn't as regular as the respiration signal could be. That's why it was possible to found great deviations between both *STD* values, great *STD* for respiration signal and lower for the *HRV* signal, in these cases. On the other hand, when the respiration signal was poor, i.e. very irregular, it gave rise to lower-than-normal *STD* values than those obtained for the *HRV* signal.

The study suggests that an accurate *HRV* time domain analysis should preferentially use the *STD* values of the *HRV* signal. The respiration signal *STD* could be used to detect cardiac or respiratory dysfunctions if several signals from the same person were analyzed.

FREQUENCY DOMAIN ANALYSIS

The frequency domain analysis of *HRV* revealed that the use of the respiration signal should be preferred to *HRV*. Despite the results (Figures 68 and 69, of chapter 7) show higher correlation between the frequency values of both signals, it was difficult to determine the exact *HF* and *LF* from the *HRV* signal. Generally it was verified, that for the respiration signal both frequencies were quite identifiable. On the other hand, for the *HRV* signal it was, for the most of the cases, difficult to identify which frequency corresponds to the characteristic *HF* and *LF*, especially for the *HF* determination.

It can be concluded that the *HRV* determination requires both, *HRV* and respiration signals, since one can compensate the other.

8.3 HR

The *HR* frequency is a basic and simple to compute hemodynamic parameter. However it is also essential for global hemodynamic evaluation. The *HR* frequency assessment requires also long acquisition signals but doesn't require high resolution. In this way, the same signals as the ones used for the *HRV* assessment were used to study this parameter.

The results obtained by *PulScope* were compared with the *HR* values from the pressure device happy life® and a good correlation was verified (see Figure 70, of chapter 7). However the study should be repeated using a more accurate pressure device. Despite this, the values exhibit a good agreement and should represent the real *HR*.

CHAPTER 9

CONCLUSIONS

Since the discussion of results has been made in the previous chapter, the ingoing chapter simply plots generic and summarized conclusions.

Foremost, the obtained results and the entire analysis show that the developed acquisition system, i.e. the new *PZ* probe and the *PuScope* software, are appropriate tools for a global hemodynamic assessment. The main advantages of the developed system are the simplicity of the acquisition procedure, which requires only one operator, the *PuScope* friendly usage and the low cost of the hardware.

AIx and *PWV* assessment from a single pulse yielded steady results that agree with the values reported in the literature. It was also observed a good correlation between both parameters. The values determined for *PWV* from two pulses weren't consistent, although some degree of correlation was detected with both, *AIx* and *PWV* from a single pulse values.

HRV and respiration signals show a strait correlation and reliable results. The respiration signal analysis suggests it can provide an auxiliary means of analysis for *HRV*.

HR didn't rose significant problems and the obtained values show a good agreement with the HR obtained by a pressure device (happy life®).

The integration and deconvolution methods for arterial pulse, generally yielded good results; besides, a straight correlation between the results obtained by these two methods was also shown. However, the deconvolution method shows better accuracy and consistency, especially when applied to signals with poor signal-to-noise ratio.

The usage of an average pulse to obtain hemodynamic parameters, instead of calculating the mean hemodynamic parameters of several individual pulses, shows truthful and reliable results, especially when used with the deconvolution method.

The presented *PZ* probe calibration produced interesting results, showing a possible new approach for a *PZ* sensor calibration. This issue needs further study and confirmation.

FUTURE WORK

A one year Project spent on this research has shown the feasibility and versatility of the *PZ* sensors in the assessment of some hemodynamic parameters. Even instrumentation and software require more advance, the obtained results present a satisfying accuracy when compared with the parameters normal values from the literature.

Obviously there is still much work to do in order to achieve a strong enough and reliable hemodynamic system (instrumentation and software application) able to reach clinical acceptance and eventually used for medical applications in this area.

Since this work is to be continued, it is interesting and maybe helpful to point out the main steps to be implemented next, in order to improve what has been done so far and to achieve the ultimate goal (system for medical application). In general, an improvement of the instrumentation, a software expansion and clinical tests will be required.

10.1 Instrument Optimization

The hardware improvement could be done in two different ways: by constructing other types *PZ* probes and by modifying the acquisition unit.

10.1.1 Piezoelectric Probes

Some misconceptions of the *PZ* probes that originate in their shape/format construction were verified.

In the early stages of this work, the carotid signal was hard to capture and this operation normally took several minutes and a great deal of skill/expertise was required from the operator to manipulate the *PZ* probes. The *PZ* ring size was thought to be very large and a smaller area was tried out to permit a more rapid capture of the carotid signal. On the other hand, the contact area goes beyond the *PZ* ring, up to the whole surface of the *PZ* probe, which is about 2cm per 1cm. In this way the contact area may be too large and it is possible that it can suppress the artery throbbing activity preventing the full arterial pulse to activate the sensing area of the probe. Actually, this fact was proven by comparison with other *PZ* probes, used in a different Project running in our Center (*PWV* assessment), in which smaller contact areas are used. Figure 71 schematically represents these probes.

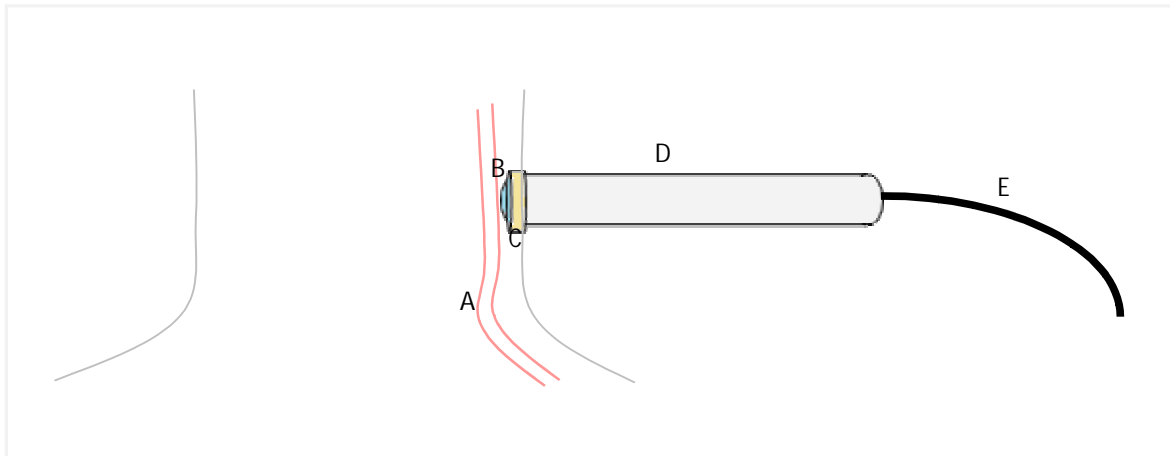


Figure 71. Schematic of the PZ probe used in the PWV assessment project.
 A – left common carotid; B – silicone rubber; C – PZ ring; D – metal tube; E – coaxial cable. The operator holds the probe by the metal tube.

Besides that, it was shown that it is fundamental that the operator holds the PZ probe against the artery with an as much as possible constant load. Otherwise the signal will exhibit amplitude variations which could strongly affect some parameters. To avoid this drawback it is necessary to build a PZ probe which can be applied in the neck without the operator holding it. In addition, solving this problem frees the operator and lets him pay more attention to data recording. A possible PZ probe with these characteristics could be a semi-ring collar in plastic material with the PZ sensor in one of its extremities (Figure 72).

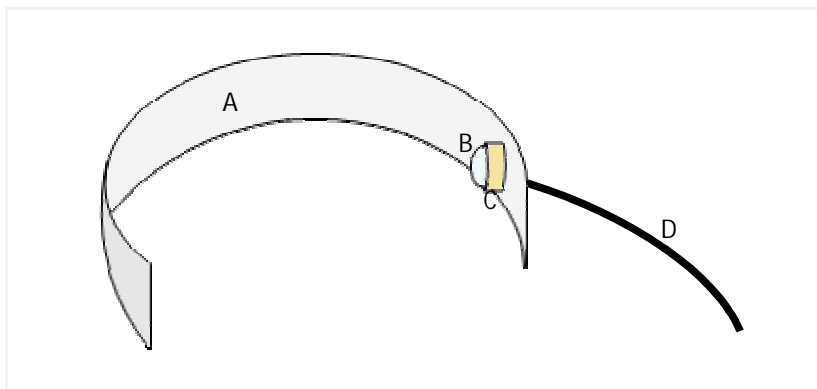


Figure 72. Schematic of a semi-ring PZ Probe (example).
 A – plastic semi-ring; B – silicone rubber; C – PZ ring; D – coaxial cable. The plastic semi-ring is placed around the neck and pressures the PZ sensor against the carotid artery.

This configuration can be extended to another application if another *PZ* sensor is placed at the other extremity making it possible to simultaneously assess the right and left carotid signals, to investigate the arterial pulse differences between the two carotid arteries.

10.1.2 Acquisition Unit

The acquisition unit, which employs the NI USB-6210© module, has some limitations, related to the reduced real time capacities and software inflexibility. An interesting modification consists in using a late generation microcontroller which will permit real time arterial pulse processing. This device can be programmed to integrate or deconvolve the *PZ* signal as the same time the system records it, in order to acquire arterial pressure/displacement pulses. To achieve this, a new electronic platform has to be designed and tested, and the acquisition philosophy modified.

Other possible improvement, although not so much necessary, is to use a standard RF communication protocol (Bluetooth, Zigbee, Wi-Fi...) to communicate with the computer, instead of an USB connection. This will mostly permit a higher degree of portability and flexibility.

10.2 Software Optimization

The improvement of the existent software tool can be done either by optimizing the existing routines or by creating new ones, which may determine other hemodynamic parameters (flow, for instance) or assess the same parameters using different approaches.

In fact, there is still much to develop in order to have self-understanding more user friendly software, even considering that it is intended for the skilled user in a research environment.

If the intention switches to building a complete software pack for medical/clinical use it is essential to use an interactive mouse-driven interface as well as an efficient help tool. A number of errors resulting from inadequate software procedures also have to be revised and eliminated.

10.3 Clinical Tests

It is really imperative to testify the developed instrumentation in a medically controlled clinical environment.

The developed system was only put to test with healthy subjects and without medical supervision. Assessing the same hemodynamic parameters in subjects with heart disease, especially hypertension, is vital to prove the usefulness of the results. At least one cardiologist is needed to monitor the whole process, which was not possible this year. One or more systems should be placed in

clinical/medical offices not only for building a signal data base but also for the follow-up of patients under medication/treatment.

It is also necessary that the parameters determined by the developed system are compared with the same parameters obtained with standard systems, like the Sphygmocor® for the *PWV* assessment and the HEM 9000ai® for *Aix*.

Only these actions can provide the full validation of the system under development.

REFERENCES

- [1] <http://science.jrank.org/pages/1228/Cardiac-Cycle.html>
- [2] <http://www.scienceclarified.com/Ga-He/Heart.html>
- [3] <http://www.makku.com/index.php/23/lub-dub-lub-dub-ye...>
- [4] <http://www.biosbcc.net/b100cardio/htm/heartant.htm>
- [5] <http://en.wikipedia.org/wiki/Pulse>
- [6] Parker, K. H. and Jones, C. J. H. - *Forward and Backward Running Waves in the Arteries: Analysis Using the Method of Characteristics* - Imperial College of Science, Technology and Medicine, London, *Journal of Biomechanical Engineering*, August 1999
- [7] <http://www.peb.ufrj.br/modules.php?name=Lib&pa=showpage&pid=16>
- [8] O'Rourke, Michael F.; Pauca, Alfredo and Jiang, Xiong-Jin, *Pulse Wave Analysis*, St Vincent's Clinic, Sydney, Winston-Salem and 3Fu Wai Hospital, Beijing (China), *Blackwell Science Ltd*, March 2001
- [9] <http://www.drashirleydecampos.com.br/noticias/13183>
- [10] <http://www.medis-de.com/en/ipg.html>
- [11] <http://circ.ahajournals.org/cgi/reprint/111/25/3384.pdf>
- [12] <http://www.scielo.br/pdf/abc/v86n3/a02v86n3.pdf>
- [13] Meckenzie, I.S.; Wilkinson, I.B. and Cockcroft, J.R. - *Assessment of Arterial Stiffness in Clinical Practice* – University of Cambridge, Cambridge (UK), *QJM*, 2002
- [14] Rogers, Walter J. *et al* - *Age-Associated Changes in Regional Aortic Pulse Wave Velocity* – Pittsburgh (Pennsylvania) and Charlottesville (Virginia), *Journal of American College of Cardiology*, 2001
- [15] Laurent, S. *et al* – *Expert Consensus Document on Arterial Stiffness: Methodological Issues and Clinical Applications* – Special article, *European Heart Journal*, volume 27, number 21, pp. 2588-2605, September 2006
- [16] <http://herkules.oulu.fi/isbn951426973X/html/x957.html>
- [17] Safar, M. *et al* – *Aortic Pulse Wave Velocity: an Independent Marker of Cardiovascular Risk* – *Geriatr Cardiol*, 11, pp. 295-298, 2002
- [18] <http://departamentos.cardiol.br/dha/revista/13-1/14-velocidade-onda.pdf>
- [19] Nichols, W.W. and O'Rourke, M.F. – *McDonald's Blood Flow in Arteries: Theoretical Experimental and Clinical Principles* – 5th ed., pp. 92, *Hodder Arnold*, London, 2005
- [20] <http://www.pmsinstruments.co.uk/Complior%20SP.htm>

- [21] <http://atcormedical.com/sphygmocor.html>
- [22] Koh, Tat W. *et al* – *Analysis of Wave Reflections in the Arterial System using Wave Intensity: a novel method for predicting the timing and amplitude of reflected waves* – Imperial College of Science, London (UK), *Heart and Vessels*, December 1998
- [23] Yasmin and Brown, M.J. – *Similarities and Differences between Augmentation Index and Pulse Wave Velocity in the Assessment of Arterial Stiffness* – University of Cambridge, Cambridge (UK), *QJ Med*, July 1999
- [24] <http://www.atcormedical.com/pdf/TN8%20-%20Reference%20Values%20for%20SphygmoCor%20Px.pdf>
- [25] <http://www.patentstorm.us/patents/6786872/description.html>
- [26] <http://www.omronhealthcare.com/product/default.asp?t=211>
- [27] *Heart Rate Variability: Standards of Measurement, Physiological Interpretation, and Clinical Use* – Department of Cardiological Science, London (UK), *American Heart Association Inc.*, 1996, <http://circ.ahajournals.org/cgi/content/full/93/5/1043>
- [28] MacArthur, John D. and Catherine – *Heart Rate Variability* – University of California (San Francisco), 1997, <http://www.macses.ucsf.edu/Research/Allostatic/notebook/heart.rate.html>
- [29] *Coherence Newsletter*, May 2007, <http://circ.ahajournals.org/cgi/content/full/93/5/1043>
- [30] Huikuri, Heikki V. *et al* – *Measurement of Heart Rate Variability: a clinical tool or a research toy?* – University of Miami (Florida, USA), September 1999, <http://content.onlinejacc.org/cgi/content/full/34/7/1878>
- [31] <http://www.nymc.edu/fhp/centers/syncope/heart%20rate%20variability,%20blood%20pressure%20variability%20and%20the%20baroreflex.htm>
- [32] <http://www.biocomtech.com/products/hrvl>
- [33] <http://soundlab.cs.princeton.edu/learning/tutorials/sensors/node7.html>
- [34] *Introduction to Piezoelectric Sensors – Piezocryst website*, http://www.piezocryst.com/piezoelectric_sensors.php
- [35] *Interfacing Piezo Film to Electronics – Measurement Specialties website* (March 2006), <http://www.meas-spec.com/myMeas/download/pdf/english/piezo/Interfacing%20to%20Electronics.pdf>
- [36] http://en.wikipedia.org/wiki/Piezoelectric_sensor
- [37] *NI website*, <http://sine.ni.com/nips/cds/view/p/lang/en/nid/203189>
- [38] Sugawara, Motoaki *et al* – *Relationship between the Pressure and Diameter of the Carotid Artery in Humans* – University of School Medicine, Tokyo (Japan), *Heart Vessels*, April 2000
- [39] O'Haver T. – *Intro to Signal Processing: Deconvolution* – University of Maryland at College Park, August 2007, <http://www.wam.umd.edu/~toh/spectrum/Deconvolution.html>

[40] World Health Organization Publication,
<http://www.who.int/mediacentre/factsheets/fs317/en/index.html>

[41] *Aging, Vascular Stiffness, and Cardiovascular Function* – Volume 24, Number 24, National Institute on Aging, June 1995, <http://grants.nih.gov/grants/guide/pa-files/PA-95-074.html>

[42] Tsui, Po-Hsiang *et al* – *Arterial Pulse Waveform Analysis by the Probability Distribution of Amplitude* – National Taiwan University, Taipei (Taiwan), *Physiological Measurement*, May 2007

[43] Wilkinson, Ian B. *et al* – *The Influence of Heart Rate in Augmentation Index and Central Arterial Pressure in Humans* – University of Edinburgh, Edinburgh (UK), *Journal of Physiology*, May 2008, <http://jp.physoc.org/cgi/content/full/525/1/263>

[44] <http://www.cvphysiology.com/Arrhythmias/A009.htm>

[45] Searle R., Norman *et al* – *Assessment of the Arterial Tonometer (N-CAT) for the Continuous Blood Pressure Measurement in Rapid Atrial Fibrillation* –, Montreal Heart Institute, Montreal (Canada), December 1992, <http://www.cja-jca.org/cgi/reprint/40/4/388.pdf>

